

Mimetic Covariant Discretization of Connections over Curvilinear Domains

MSc Thesis

by

Yashasvi Giridhar

Student number: 4749219
Project duration: April 28, 2019 – November 27, 2020
Thesis committee: Dr. ir. M. I. Gerritsma, TU Delft, Supervisor
Dr. ir. M. Möller, TU Delft
Dr. ir. B. Chen, TU Delft
Mr. ir. Y. Zhang, TU Delft

ॐ असतो मा सद्गमय ।
तमसो मा ज्योतिर्गमय ।
मृत्योर्मा अमृतं गमय ।
ॐ शान्तिः शान्तिः शान्तिः॥

– बृहदारण्यक उपनिषद् (१.३.२८)

Om, from falsehood lead me to truth,
From darkness lead me to the light,
From death lead me to immortality,
Om peace peace peace!

– Brihadaranyaka Upanishad (I.III. XXVIII)

Preface

As the mathematician Steven Strogatz puts it, “Calculus has a penchant for peddling useful fiction”. My discovery of this truth came through my research work on this thesis project. The desire to work in computational sciences, that too with an emphasis on modelling and simulation, grew within me during my undergraduate studies in India. The reason was not very profound, it was simply the ability to study a varied number of sciences without any expensive equipment, just a laptop and a programming compiler. This humble origin of my motivation is what prevents me from appropriating the noble intents of great physicists and mathematicians to my work when writing this report. However, my interest in simulations grew many-fold after I attended Prof. Gerritsma’s course on Discretization Schemes during my graduate programme at TU Delft.

The coursework assignment opened my mind to the many exciting possibilities in this field. To imagine that such a realization can dawn upon an examination of something as abstract and dry as a mesh discretization scheme is an indication to how misled my understanding of this field was. What was even more surprising was the understanding of how flawed and simplistic the pedagogy of tensor and vector calculus taught to every freshman undergraduate, really is. The stark difference between what is taught and what ought to be, is enough to turn any engineer into a rebel (of sorts). It was appropriate, I suppose, that my introduction to the theory of differential geometry came through William Burke’s *Samizdat* (a Russian word for any banned dissident literature) on Applied Differential Geometry. Though a cumbersome book for sure, the revelations, when they strike you, are truly amazing.

Coming back to the useful fictions—by the early beginning of my research, it was clear to me that the craft of devising computational schemes were hopelessly flawed without any representation of the structure of the differential equations they aimed to model. And, to borrow from a British phrase, the tradition of modeling true geometric-structure of governing equations was a custom more honored in the breach when it came to many computational methods. As far the scope of my work was concerned, the serial offenders were the finite element methods, closely followed by their less sophisticated cousins, the volume and difference schemes.

My work through this thesis project is part of a broader, concerted research effort to address this gap in the synthesis mechanism of numerical schemes. Following from the early doctoral work of Jasper Kreeft, the Mimetic Spectral Element Methods (MSEM) have undergone several iterations, increasing its scope and applications. The latest addition to this iteration came through the work of Joël Fisser by achieving pointwise-exact mass and momentum conservation on orthogonal grids using a hybrid MSEM. My task was to implement an extension of this method to curvilinear meshes with no loss of the pointwise exact conservation. Though this was a fairly well-defined aim for my research, I also had the opportunity to learn from my colleagues in the research group, specially Wessel Niek Weijers and Sebastiaan van Schie. The possible areas of future extension of my research work has certainly informed my approach to engineering solutions for implementation problems.

Apart from addressing gaps in the applied mathematical methods, working with Prof. Gerritsma as my supervisor, meant that I always had something new to learn from him. His curious and energetic approach to his own research did have a spillover effect on me as it allowed me to dabble in the realm of pure mathematics. This came about through a progression

of meetings where he was kind enough to educate me on the intricacies of functional analyses and the rigors of proving the theoretical soundness of our numerical approach. I would amiss if I were not to acknowledge Jeremy Budd, a doctoral student at the Applied Mathematics department, for his lucid and eye-opening explanation of the abstractions of metric and linear topological spaces.

I highly doubt if my education would have taken the turn for such rarefied domains of mathematical enquiry if it were not for this thesis opportunity. For that I am grateful to Prof. Gerritsma, that he accepted me as a student for his supervision and aided me through this process. Throughout the period of my association with him, I have had the blessed opportunity to know him as a kind, caring and generous human being as well as a supportive and nurturing academician.

Continuing with the list of people I am thankful to, I must extend my gratitude towards my fellow graduate students, especially —Amey Vasulkar, Bishwadeep Das, Sukanya Walaskar and Chinmay Pathak for their constant support and help throughout this project both personal and professional. There were also other kindred spirits that kept me company for the last couple of years in this foreign land: Devendra Kulkarni, Rajesh Rajwade, Shreyas Nikte, Kunal Kanawade, Palash Patole, Sharad Rajampeta, Sneha Gokhale, and Sharayu Kore.

I am thankful to my creator for my family. My brother and his wife, have been a source of constant support and encouragement throughout this endeavor. My parents, on the other hand, have indebted me unending gratitude through their lifetime of dogged efforts to nurture me and their iron-will to see me succeed in life. No amount of acknowledgement to them would suffice in the stead of what I have had the good fortune of receiving from them. Finally, I would like to dedicate this work to my grandmother Smt. K. Parvati, who I lost during the course of my graduation studies and one who had for long remained my mentor in matters of personal philosophy.

Finally, in a lighter vein, should the diatribe on the applied mathematical sciences of numerical methods above appear harsh, I apologize. It is just that I have had a good company of visionaries such as Cantor, Cartán, Grassman, Whitney, Tonti and many more for the past few months and I have been influenced by them greatly. I quote from Emerson's *Society and Solitude* :

there are books . . . which take rank in our life with parents and lovers and passionate experiences, so medicinal, so stringent, so revolutionary, so authoritative, — books which are the work and the proof of faculties so comprehensive, so nearly equal to the world which they paint, that though one shuts them with meaner ones, he feels his exclusion from them to accuse his way of living.

Yashasvi Giridhar
Delft, January 2020

Abstract

The present research aims at establishing a numerical technique that allows for simple discretization of curved domains. The method of implementation features use of covariant exterior derivatives that are used alongside structure preserving mixed mimetic spectral methods, that is primal and algebraic dual polynomials. A single element implementation is used to demonstrate the applicability of the method over two diffeomorphisms, a horizontal shear with non-linear skew and a modified polar coordinate transformation, for 0-forms and 1-forms. Finally, an extension of this framework towards continuum mechanics is discussed with a discussion over a co-vector valued stress and elasticity formulation.

Contents

List of Figures	ix
1 Introduction	1
1.1 Background	1
1.1.1 Geometric Intuition in Computational Methods	2
1.1.2 A Differential Geometry Perspective	3
1.1.3 A Case in Point!	4
1.2 Aim and Scope	4
1.3 Overview of this Report	5
2 Understanding the Geometry of Physics	7
2.1 Basics, Terminology and Notations	7
2.2 Reimagining Mathematical Physics: Mimetic Approach to CFD	16
2.2.1 Pressing the ‘Reset’ Button: Applied Differential Geometry	16
2.2.2 Similarities in Physical Theories	17
2.3 Tools for Investigation: Operators and Cohomologies	21
2.3.1 Algebraic Topology	21
2.3.2 Differential Geometry	24
2.4 What next?	25
3 Background to Mimetic Spectral Element Methods	27
3.1 Introduction	27
3.1.1 Mimetic Applications of Mixed FEM	28
3.2 Development History at TU Delft	29
3.2.1 The DeRahm Cohomology Revisited	29
3.2.2 Reconstruction and Reduction	30
3.3 Mimetic Spectral Element Framework	31
3.3.1 Notation	31
3.3.2 Grid Construction	31
3.3.3 Primal Basis Functions	32
3.3.4 Dual Basis Functions	33
3.3.5 Reduction and Reconstruction	36
3.3.6 Error Computations	37
4 How to Handle Curvature?	39
4.1 Curvature over Manifolds	39
4.1.1 Covariant Derivatives	41
4.1.2 Lie Derivatives	42
4.2 Which derivative to choose?	43
4.3 Commutativity of the Exterior Derivative	44
4.4 Deriving Function Space with Curvatures	45
4.4.1 Mapping from physical domains	45
4.4.2 Example transformation: non-linear bulk shear parallel to the horizontal axis	46
4.4.3 Example transformation: polar transformation (without origin)	60

4.5	Application towards stress tensors	76
5	Conclusions and Future Scope	77
5.1	Summary of Work Done	77
5.2	Conclusions	77
5.3	Future Scope of Research	77
	Appendices	79
A	Covariant Divergence of Stress Tensor	81
	Bibliography	83

List of Figures

- 1.1 An example of linear transformation of vectors, in this case—reflection. The coordinate plane x-y has a vector located from the origin O to the point P (in black color) whereas its reflection about a mirror plane yields a vector O'P (as shown in green) 2
- 2.1 The continuously invertible chart $\varphi : C \rightarrow \mathbb{R}^m$ takes in values from the open topological space C (known as a *cover*) on the manifold space M and maps them to a real number space \mathbb{R}^m . Thus, this chart operation allows us to work in a locally \mathbb{R}^m space on a manifold. Similarly, a function $f : C \rightarrow \mathbb{R}$ maps the set C onto a real space \mathbb{R} [6]. 9
- 2.2 Tangent vectors defined over a spherical manifold (left) and two ‘free’ vectors in Euclidian \mathbb{R}^2 space (right) 10
- 2.3 (Left) Tangent vectors $W_{\gamma(t)}$ over a flow $\gamma(t)$ evaluated at two different points 0 and p; (Right) The pullback defined over the manifold points allows re-mapping of the tangent space $W_{\gamma(t)}$ over the vector field V [57] 12
- 2.4 Basic classification of physical variables of a theory [69] 18
- 2.5 Cell complex for (a) \mathbb{R}^1 , (b) \mathbb{R}^2 and (c) \mathbb{R}^3 [69] 19
- 2.6 Classification of basic geometrical elements of a cell complex K and its dual \hat{K} in \mathbb{R}^3 [69] 19
- 2.7 Inner orientation of p-cells [69] 20
- 2.8 Outer orientation of p-cells [69] 21
- 2.9 Construction of a coboundary from a p-chain [69] 23
- 2.10 Chains on primal and dual cell complexes for $n = 3$ 23
- 3.1 Primal basis functions for $p=5$ 33
- 3.2 Dual basis functions for $p=5$ 35
- 4.1 Tangent vectors defined over a spherical manifold. 40
- 4.2 A bundle $\pi: E \rightarrow M(S^1)$ 40
- 4.3 Illustration of parallel transport of a tangent vector over a spherical manifold (TS²) [6, p. 232]. 42
- 4.4 A case of non-commutativity of v and w, $[v, w] \neq 0$ [6]. 43
- 4.5 Discrete mesh systems in different domains with positive directions for flow assigned 47
- 4.6 Reconstructed function $f^h(x, y)$ computed as a result of a pullback $(\varphi_k^*)^{-1}[\bar{f}] = \bar{f} \circ \varphi_k^{-1}$ interpolated with primal and algebraic dual nodal functions (left) and exact function $f(x, y)$ (right). The results are plotted over the shear deformed domain Ω_k . Polynomial order, $p = 15$ 48
- 4.7 Reconstructed function $\bar{f}^h(\xi, \eta)$ interpolated with primal and algebraic dual nodal functions (left) and exact function $\bar{f}(\xi, \eta)$ (right). This reconstruction over the reference element is created through a mix of primal and dual nodal polynomials. Polynomial order, $p = 15$ 49

- 4.8 Exact function $\frac{\partial f}{\partial x}(x,y)$ (left), reconstructed function $\frac{\partial f^h}{\partial \xi}(\xi,\eta)$ without transformation φ_k (center), and reconstructed function $\frac{\partial f^h}{\partial x}(x,y)$ transformed using $\frac{\partial f^h}{\partial \xi}(\xi,\eta)$ and φ_k (right). This reconstruction over the reference element is created through a mix of primal and dual nodal polynomials. Polynomial order, $p = 15$ 50
- 4.9 Exact function $\frac{\partial f}{\partial y}(x,y)$ (left), reconstructed function $\frac{\partial f^h}{\partial \eta}(\xi,\eta)$ without transformation φ_k (center), and reconstructed function $\frac{\partial f^h}{\partial y}(x,y)$ transformed using $\frac{\partial f^h}{\partial \eta}(\xi,\eta)$, $\frac{\partial f^h}{\partial \xi}(\xi,\eta)$ and φ_k (right). This reconstruction over the reference element is created through a mix of primal and dual nodal polynomials. Polynomial order, $p = 15$ 51
- 4.10 Spectral or p-refinement result for the scalar function reconstruction for the function $\bar{f}(\xi,\eta)$ 51
- 4.11 Error distribution over reference element for polynomial order, $p = 20$ 52
- 4.12 Vector field $\mathbf{u}(x,y)$ displayed over the physical domain Ω_k with a quiver plot, polynomial order of 15 55
- 4.13 Analytical distribution of co-vector field $\mathbf{u}(x,y)$ over both reference domain K as well as physical domain Ω_k 56
- 4.14 Exact function $u_x(x,y)$ (left) and reconstructed function $u_x^h(x,y)$ computed as a result of a pullback $(\varphi_k^*)^{-1}[\bar{u}_\xi^h, \bar{u}_\eta^h]^T = \bar{u}_\xi^h \circ \varphi_k^{-1}$ interpolated with primal and algebraic dual nodal functions (right). The results are plotted over the shear deformed domain Ω_k . Polynomial order, $p = 9$ 57
- 4.15 Exact function $u_y(x,y)$ (left) and reconstructed function $u_y^h(x,y)$ computed as a result of a pullback $(\varphi_k^*)^{-1}[\bar{u}_\xi^h, \bar{u}_\eta^h]^T = -0.1(3+\eta)\bar{u}_\xi^h \circ \varphi_k^{-1}$ interpolated with primal and algebraic dual nodal functions (right). The results are plotted over the shear deformed domain Ω_k . Polynomial order, $p = 9$ 57
- 4.16 Exact function $\frac{\partial u_x}{\partial x}(x,y)$ (left) and reconstructed function $\frac{\partial u_x^h}{\partial x}(x,y)$ computed as a result of a pullback $(\varphi_k^*)^{-1}[\frac{\partial \bar{u}_\xi^h}{\partial \xi}, \frac{\partial \bar{u}_\eta^h}{\partial \eta}]^T = \frac{\partial \bar{u}_\xi^h}{\partial \xi} \circ \varphi_k^{-1}$ interpolated with primal and algebraic dual nodal functions (right). The results are plotted over the shear deformed domain Ω_k . Polynomial order, $p = 9$ 58
- 4.17 Exact function $\frac{\partial u_x}{\partial y}(x,y)$ (left) and reconstructed function $\frac{\partial u_x^h}{\partial y}(x,y)$ computed as a result of a pullback $(\varphi_k^*)^{-1}[\frac{\partial \bar{u}_\xi^h}{\partial \xi}, \frac{\partial \bar{u}_\eta^h}{\partial \eta}]^T = [\frac{\partial \bar{u}_\xi}{\partial \eta} - 0.1(3+\eta)\frac{\partial \bar{u}_\xi}{\partial \xi}] \circ \varphi_k^{-1}$ interpolated with primal and algebraic dual nodal functions (right). The results are plotted over the shear deformed domain Ω_k . Polynomial order, $p = 9$ 58
- 4.18 Exact function $\frac{\partial u_y}{\partial x}(x,y)$ (left) and reconstructed function $\frac{\partial u_y^h}{\partial x}(x,y)$ computed as a result of a pullback $(\varphi_k^*)^{-1}[\frac{\partial \bar{u}_\xi^h}{\partial \xi}, \frac{\partial \bar{u}_\eta^h}{\partial \eta}]^T = [-0.1(3+\eta)\frac{\partial \bar{u}_\xi^h}{\partial \xi}] \circ \varphi_k^{-1}$ interpolated with primal and algebraic dual nodal functions (right). The results are plotted over the shear deformed domain Ω_k . Polynomial order, $p = 9$ 59
- 4.19 Exact function $\frac{\partial u_y}{\partial y}(x,y)$ (left) and reconstructed function $\frac{\partial u_y^h}{\partial y}(x,y)$ computed as a result of a pullback $(\varphi_k^*)^{-1}[\frac{\partial \bar{u}_\xi^h}{\partial \xi}, \frac{\partial \bar{u}_\eta^h}{\partial \eta}]^T$ interpolated with primal and algebraic dual nodal functions (right). The results are plotted over the shear deformed domain Ω_k . Polynomial order, $p = 9$ 59
- 4.20 Spectral or p-refinement result for the covector field reconstruction $\mathbf{u}(x,y)$. . . 60

- 4.21 A transfinite mapping from Cartesian coordinate system to a modified Polar coordinate system as defined in equation 4.33. 60
- 4.22 Discrete mesh systems in different coordinate systems with positive directions for flow assigned 61
- 4.23 Exact function \bar{u}_ξ (right) and reconstructed function \bar{u}_ξ^h , using mixed basis functions, interpolated with primal and algebraic dual nodal functions (left). The results are plotted over the reference domain K. Polynomial order, $p = 9$. . . 65
- 4.24 Exact function $\frac{\partial \bar{u}_\xi}{\partial \xi}$ (right) and reconstructed function $\frac{\partial \bar{u}_\xi^h}{\partial \xi}$ using mixed basis functions, interpolated with primal and algebraic dual nodal functions (left). The results are plotted over the reference domain K. Polynomial order, $p = 9$. . . 65
- 4.25 Exact function $u_\xi(r, \theta)$ (left) and reconstructed function $u_\xi^h(r, \theta)$ computed as a result of a pullback $(\varphi_k^*)^{-1}[\bar{u}_\xi^h, \bar{u}_\eta^h]^T = \frac{(r_2-r_1)}{2}\bar{u}_\xi^h \circ \varphi_k^{-1}$ interpolated with primal and algebraic dual nodal functions (right). The results are plotted over the modified polar domain Ω_k . Polynomial order, $p = 9$ 66
- 4.26 Exact function $\frac{\partial u_r}{\partial r}(r, \theta)$ (left) and reconstructed function $\frac{\partial u_r^h}{\partial r}(r, \theta)$ computed as a result of a pullback $(\varphi_k^*)^{-1}[\frac{\partial u_\xi^h}{\partial \xi}, \frac{\partial u_\eta^h}{\partial \eta}]^T = \frac{\partial u_\xi^h}{\partial \xi} \circ \varphi_k^{-1}$ interpolated with primal and algebraic dual nodal functions (right). The results are plotted over the modified polar domain Ω_k . Polynomial order, $p = 9$ 66
- 4.27 Velocity field over the modified polar domain Ω_k showing radially outward flow emanating from a unit strength line source, computed from the reconstructed solution (after transformation) for a polynomial order = 9. 67
- 4.28 Exact function \bar{u}_η (right) and reconstructed function \bar{u}_η^h using mixed basis functions, interpolated with primal and algebraic dual nodal functions (left). The results are plotted over the reference domain K. Polynomial order, $p = 9$ 69
- 4.29 Exact function $\frac{\partial \bar{u}_\eta}{\partial \xi}$ (right) and reconstructed function $\frac{\partial \bar{u}_\eta^h}{\partial \xi}$ using mixed basis functions, interpolated with primal and algebraic dual nodal functions (left). The results are plotted over the reference domain K. Polynomial order, $p = 9$. . . 69
- 4.30 Exact function $\frac{\partial \bar{u}_\eta}{\partial \eta}$ (right) and reconstructed function $\frac{\partial \bar{u}_\eta^h}{\partial \eta}$ using mixed basis functions, interpolated with primal and algebraic dual nodal functions (left). The results are plotted over the reference domain K. Polynomial order, $p = 9$. . . 70
- 4.31 Exact function $u(r, \theta)$ (left) and reconstructed function $u^h(r, \theta)$ computed as a result of a pullback $(\varphi_k^*)^{-1}[\bar{u}_\xi^h, \bar{u}_\eta^h]^T = \frac{2}{(r_2-r_1)}\bar{u}_\eta^h \circ \varphi_k^{-1}$ interpolated with primal and algebraic dual nodal functions (right). The results are plotted over the shear deformed domain Ω_k . Polynomial order, $p = 9$ 70
- 4.32 Exact function $\frac{\partial u_\theta}{\partial r}$ (left) and reconstructed function $\frac{\partial u_\theta^h}{\partial r}$ computed as a result of a pullback $(\varphi_k^*)^{-1}[\bar{u}_\xi^h, \bar{u}_\eta^h]^T = \frac{2}{(r_2-r_1)}\bar{u}_\eta^h \circ \varphi_k^{-1}$ interpolated with primal and algebraic dual nodal functions (right). The results are plotted over the shear deformed domain Ω_k . Polynomial order, $p = 9$ 71
- 4.33 Reconstructed function $\frac{\partial u_\theta^h}{\partial \theta} = \frac{\partial \bar{u}_\eta^h}{\partial \eta} - \frac{u_\theta}{c} \cos \alpha \sin \alpha$ computed as a result of a pullback $(\varphi_k^*)^{-1}[\bar{u}_\xi^h, \bar{u}_\eta^h]^T = \frac{2}{(r_2-r_1)}\bar{u}_\eta^h \circ \varphi_k^{-1}$ interpolated with primal and algebraic dual nodal functions. The results are plotted over the shear deformed domain Ω_k . Note that as polynomial order increases and accuracy of approximation increases this distribution should vanish. Plotted with a low polynomial order, $p = 5$ 71

4.34	Velocity field over the modified polar domain Ω_k showing rotational flow emanating from a unit strength line vortex, computed from the reconstructed solution (after transformation) for a polynomial order = 9.	72
4.35	Spectral or p-refinement result for the covector field reconstruction $\mathbf{u}(x,y)$. . .	73
4.36	Spectral or p-refinement result for the covector field reconstruction $\mathbf{u}(x,y)$. . .	73
4.37	Error distribution over physical element for polynomial order, $p = 20$	74
4.38	Error distribution over physical element for polynomial order, $p = 20$	75

Introduction

1.1. Background

The present document aims to capture the research efforts put towards obtaining a covariant discretization of the connection coefficients over curvilinear geometries using a class of mimetic methods. There is a quite a lot to unpack in this sentence. The present chapter aims to do just that —provide an overview, and perhaps a context as well, towards the non-traditional approach of computational mathematics —*mimetic methods*.

This begins by as we trace over a period of the past fifty years, the emergence of a particularly persuasive philosophy of thought in the community of mathematicians and engineers as they attempt to model and simulate complex natural phenomena using modern and sophisticated numerical techniques. This school of philosophy, as we shall explore further, primarily aims to inform the craft of computational sciences with an intuitiveness already present in its progenitors —theoretical mathematics and physics. Interestingly, even as an offspring of these highly intuitive sciences, this sense of ‘intuition’ has been missing when it comes to the study and synthesis of numerical methods.

Our discussion is quite limited as we attempt a survey of a particular family of numerical methods that came into existence during the later half of the last century —Finite Element Methods (FEM). For instance, the first coherent expression of FEM as a tool was to aid the design of dams and bridges [19, 37], and it remained as a primarily tool for structural engineering and computational mechanics. On the other hand, the highly non-linear systems of fluid mechanics developed a similar branch of Computational Fluid Dynamics (CFD) with aims of tackling linearized problems through simple mathematical tools such as potential flows and conformal transformations [60] for instance.

Today however, FEM is not only restricted to structural and mechanical engineering applications and finds its uses in aerospace, marine, oil & gas industries. Simultaneously, aided by the leapfrog advances in computational capacities of the modern computing systems, these highly sophisticated methods are becoming more affordable tools for CFD prediction and analysis. This is because, the computational costs incurred due the mathematical complexities involved have reduced significantly while the results are far more accurate than those offered by their simpler numerical counterparts. However, despite these progresses, the lack of geometric intuition has been a consistent feature of most FEM schemes being used. Thus, it becomes pertinent to discuss the importance of this geometric nature of numerical schemes and what does a method gain by addressing issues related to the lack of this feature.

Having established this background of the class of Finite Element Methods, we now begin an illustration of the nature of the methods that can be grouped as broadly as two sub-classes in the FEM family tree —the *geometry-aware* and the *metric-dependent* methods. The need for this distinction will, it is hoped, become clear as we begin our examination into the nature of the construction of these methods and identify the underlying geometric intuition (or lack of it) modeling discrete physical quantities when devising a numerical scheme.

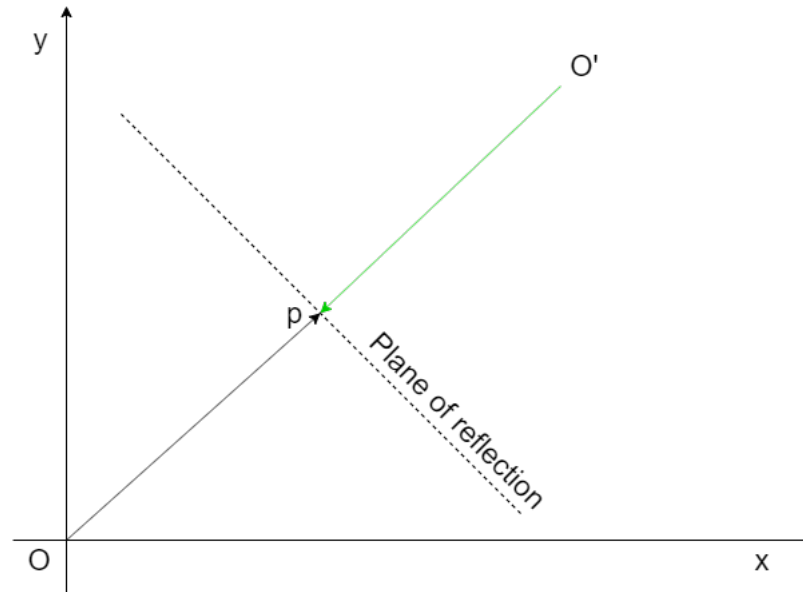


Figure 1.1: An example of linear transformation of vectors, in this case—reflection. The coordinate plane x - y has a vector located from the origin O to the point P (in black color) whereas its reflection about a mirror plane yields a vector $O'P$ (as shown in green)

1.1.1. Geometric Intuition in Computational Methods

We begin with the assertion that physical entities such as pressure, velocity, linear and angular momentum *etc* have geometric associations in space-time. The implications of this quite simple statement are far-reaching, in that, they call into question the ‘mainstream’ understanding of how these entities behave in a system. This is best reflected in the mathematical models of physical systems, where such geometric associations are merely secondary constructs. On the other hand, the dry and uncaring metric and algebraic relationships take priority over the geometric structure of constitutive and governing equations that help model the behavior of a system.

On a whole, computational science has featured methods that adopt a ‘brute-force approach’ as described by Gerritsma [34, p. 48] where the objective is morphed into a minimization of the residual or of the truncation error instead of the idea of approximating the original governing equations. As a response to this rather consistent irreverence towards the geometrical association of variables and entities within any given differential equation, quite a bit of work has been done in exploring the structure of these entities with a more rigorous understanding of the equations involved.

For instance, in his works, Burke [18] sought to replace the dominant mathematical formulations of tensor and vector calculus with the principles of differential geometry in an attempt to establish the foundational principles of a geometry-aware mathematical tradition.

Should the reader wish to understand the fundamental difference that Burke argued for, we consider the following example. General modeling approaches consider the quantities such as the force, velocity, and displacement as vector quantities, however principles of differential geometry and topology would disagree. A curious property of vectors is that they are invariant under linear transformations, this would include operations such as reflection about an axis, displacement or scaling with respect to a coordinate system. True vectors such as that of the position vector exhibit this property, in that if the coordinate system where the position vector lies is transformed linearly, the position vector would still serve the same purpose and point the correct position. On the other hand, the so-called vector quantities such as force,

velocity or displacement would not remain invariant under such a transformation and convey a different meaning altogether—they show inversion of intended action and thus convey a different physical meaning (see figure 1.1).

The author would like to stress here that these are not trivial obsessions about mathematical details. As we shall discover further, such subtle yet significant observations lead to the identification and conclusively, inclusion of the more appropriate and mathematically correct entities in the CFD model and discretization which shows remarkable changes downstream. Infact, several unresolved fluid flow behaviors that appear in CFD simulations may be attributed to this absence of geometric information encoded into the solver settings [1, 58, 65]. For instance, Desbrun et al [63, p. 443] attribute the findings in the works of Thomas et al [58] to ‘a loss of Lagrangian structures’ and identify them as a major impediment of the current generation of numerical methods.

1.1.2. A Differential Geometry Perspective

Having briefly underscored the importance of the ‘geometric-content’ of a numerical scheme, we proceed towards understanding the eccentricities of our *mimetic approach*. It is true, that many of the traditional methods mischaracterize a set of physical quantities as vectors, whereas on deeper inspection, they belie their assumed nature. It is for these sets of quantities we introduce a sibling notation, namely—the *co-vector*.

Details of this entity will be discussed in sufficient details in the following chapters, but for the moment, it would be enough to emphasize the utility of its existence. Unlike a vector, a covector (or alternatively, a one-form) does infact change under linear transformation such as reflection. Armed with this realization, a revision of the basis of geometric characterization of quantities would lead to the classification of velocities, mometum, and force among others as co-vectors. This reevaluation leads to other reflections, of which an important one is of recognizing geometric stress from the classical solid mechanics as a *covector-valued differential two-form* [47].

This characterization of geometric stress fundamentally revises the numerical representation of the classical solid mechanical theories of stress. A key revision here is the reformulation of balance laws, among other fundamental laws, using a new operator—the *covariant* derivative. This is necessitated due to the principle of energy balance for a solid deformation process where a change of system state is expressed through a transformation of the space coordinate system. The covariant derivative then helps formulate the change of this coordinate basis through a curvilinear transformation to a deformed solid state.

An excellent example of this application is the work of Kanso et.al. [47] where the second order stress tensors, namely the Cauchy stress tensor (\mathbf{s}) and the two-point Piola-Kirchhoff stress tensor (\mathbf{P}), are rewritten as covector valued two-forms. Thus, when a *deformation* mapping (φ) is applied to a Euclidian three-space \mathbb{R}^3 , a covariant derivative can be used to compose the metric component of the differentiation operator \mathfrak{d} so that transformed stress fields can be obtained under deformation φ [47, p. 849].

What is the benefit of implementing this rigour? To begin with, this approach yields a more natural formulation—of stress tensors, in this paper—even generally. Furthermore, as we shall see later, this improves our modelling approach since many of the characteristics falsely assumed to be metric-dependent and implemented as constitutive relationships can be instituted as topological features, thus removing a component of modelling and truncation error. This means, increase in accuracy and potentially fewer iterations to converge, given a complete reformulation of the mathematical expression.

1.1.3. A Case in Point!

The tradition of devising geometry-aware numerical schemes, though relatively new, has a sizable number of adherents and as expected there exists a respectable body of work to illustrate the benefits of this approach. Select cases have been highlighted here to showcase potential use and application of this system of inquiry to revise traditional mathematical formulations. The reader will be introduced to a short survey of these methods and associated narratives would be presented in the following chapters. However, at the moment, in order to establish relevance to the scope of this work, we identify our association with an existing line of inquiry into the class of Mimetic Spectral Element Methods (MSEM) (see chapter 3) introduced by Kreeft and Gerritsma [34, 49] at the TU Delft, Netherlands.

Recent works by TU Delft on the applications of MSEM [35, 45, 46, 48] illustrate the evolution of this method towards implementing pointwise exact mass and momentum conservation over orthogonal meshes [29]. The next step, then would naturally be towards introducing compatibility of this method to curvilinear meshes so that curvature can be effectively discretized while preserving mass and momentum conservation seen over orthogonal meshes. This is also important since, establishing these conservation properties over curved geometries as well, allows inquiry into elasticity and its modeling through the implementation of MSEM. The recent work by Fisser [29] also proposed a novel formulation of linear elasticity using mixed mimetic methods for applications of pointwise conservation of mass, linear momentum and angular momentum. This implementation however, remained restricted to orthogonal meshes with the use of Lagrange multipliers to enforce conservation in case of curved geometries. This limitation, can be overcome through an application of these mixed methods over curvatures using connection coefficients. The difficulty however, lies in discretizing these coefficients over complicated transformations within the mimetic methods framework. This gap forms the core interest of this thesis work.

1.2. Aim and Scope

The main purpose of this project is to propose and implement a mixed mimetic simulation solver with extended capabilities of discretization on curvilinear meshes in addition to the present orthogonal mesh features. In order to do this, we explore a different approach towards discretizing differential operators, namely the exterior derivative. The manner of approach towards this goal, however, is not direct. It depends in fact on developing a method of discretizing the computational mesh and its discrete differential operator analogues over its curvilinear domains using covariant derivatives that preserve invariance under general coordinate transformations. This is achieved through the Christoffel coefficients of the covariant derivative [32], which determines how quantities change with the curvature of a manifold. As the mimetic computational capabilities exist for orthogonal grids (where these coefficients are zero), the challenge then becomes to identify and discretize these coefficients (and thus the effect of curvature on the computational space) and implement an extensible mimetic framework.

The research question, thus, becomes:

“How to implement a mixed mimetic spectral method which extends to the curvilinear meshes using the covariant exterior derivative?”

Keeping with this question in mind, we formulate the following aims and objectives:

1. Identify covariant derivatives as a tool that allows commutativity of the exterior derivative with the transformations
2. Establish a mixed mimetic implementation with a covariant exterior derivative that commutes with transformation of frames

3. Develop a programming framework in Python and Matlab with basis function implementations , grid generation, reduction and reconstruction schemes
4. Develop and implement test cases where different problem cases can be solved and compare results with previous implementations such as manufactured field solutions that change under modification of the space curvature.
5. Document code structure, centralize a repository, and prepare review reports

1.3. Overview of this Report

This report is structured to give the reader a brief overview into the relevant subject matter before proceeding to the core technical subject at hand. Towards this end, the listing of the subsequent chapters is as follows: chapter 2 introduces basic terminology and mathematical structures that support the understanding of mathematical physics and its relevance to the mimetic methods as implemented in this thesis work. The reader is introduced to concepts of differential geometry, algebraic topology and the Hodge operator as a tool within the MSEM implementation theory. Chapter 3 provides a literature survey of the class of mimetic methods known to be similar to the MSEM at least in principle. Emphasis is given on the discussions of mixed mimetic methods as a framework to model phenomena. Later on, basic construction principles of basis functions, algebraic dual functions and its applications are explained. Chapter 4 deals with the application of a covariant exterior derivative within the mixed mimetic method framework with example applications to scalar fields (0-forms) and covector (1-form) fields. Finally a brief discussion into the extensibility of the covariant derivative for stress tensors is placed. This is then followed by chapter 5 with summarizes the work done and reflects on possible recommendations for the future.

Understanding the Geometry of Physics

Following the previous chapter, where an introduction towards the notion of geometric content of a mathematical structure was made, we now delve a bit deeper into the nature of this geometry and how it molds our physical models. As such, this chapter serves as a brief overview into the development of mathematical physics as we envision it today. These developments span over nearly three centuries (*ca.* 1700 AD) of research in mathematical sciences ranging from the allied areas of discrete and algebraic topology to the remote and abstract domains of set theory and theorems of symmetries. Clearly, these broad areas of development are too wide-ranging to explain within the scope of this work. Thus, a narrative of developments pertaining to the current application is constructed and presented.

Towards the end of this chapter, the reader will be familiarized in the concepts of topological spaces, vector fields, tangent and cotangent spaces, Hodge operators and dual spaces. With this it is intended that a foundational vocabulary is built that can help navigate the mathematical descriptions of curvature on topological manifolds and implementation of MSEM over these spaces.

2.1. Basics, Terminology and Notations

Having established the importance of the geometric content in CFD modeling and discretizations (in the previous chapter), we now attempt at drawing contours around the extent and nature of the mathematical relationships that enable the expression of this geometry with rigour. This undertaking, as will be seen further, leads to an intersection of various pure mathematical fields, namely that of — algebraic topologies, metric and topological spaces (functional analysis) and differential geometry.

What is interesting is that these intersections are not happenstance, but are in fact the natural consequence of the fundamental logic governing each of these silos of mathematics. The ideas expressed within the realm of algebraic topologies find a neat parallel in the domains of functional analyses as well as in differential geometry. This convergence signifies, at least qualitatively, the universal nature of geometry as a consideration for the synthesis of numerical schemes, particularly FEM based CFD methods.

Although the exact nature of these convergences will be revealed in the successive chapters, a qualitative assessment of their roles and impact is made here. As has been noted previously, the basic idea dictating our considerations here, is that entities that describe a physical system have geometric associations. For example, consider the scalar quantity, temperature T and material density ρ at a point in a field. Despite both being scalars, their geometric association differ—a pointwise association for the former and a volume association for the latter. Similarly, for vector quantities, it is easy to identify examples where the geometric associations are different. For instance, the velocity vector is defined along curves or line segments whereas mass flux is defined across a surface element (two different geometric classes).

To express these subtle associations, a framework provided by differential geometry is used. We fashion differential forms as a tool to express these associations in generalized dimensions.

Additionally, creating this abstract framework also helps identify structures that appear to have some geometric association when mired in simple vector calculus formulations, but in fact turn out to be independent of geometries. This is in reference to the set of operators familiar to the vector calculus framework: $\text{grad}(\vec{\nabla})$, $\text{div}(\nabla \cdot)$ and $\text{curl}(\vec{\nabla} \times)$. Realizing the applications of differential geometry presents a generalized differential operator which when applied to elements of varying geometric associations, appears to take on new operator forms. This realization allows us to write a generalized Stokes' theorem.

Furthermore, since these operators do not depend on the geometry of the domain, but can be generalized to higher dimension spaces, we refer to them as being metric-independent. To help explain this concept, the idea of a *metric* is now considered. It is understood to be a mathematical structure imposed on a space that allows the measure of the distance between two points within that space. The consideration of this concept allows for a segue into the nature of space when viewed through the lens of differential geometry, algebraic topology and functional analysis. We begin with defining the basic algebraic structure known as a *topological space* using the concepts of open sets [32, p. 12].

Definition 2.1. A **topological space** is a set M with a distinguished collection of *open sets*, that satisfy the following conditions:

1. Both M and the null set \varnothing are open
2. If U and V are open sets, then the intersection $U \cap V$ is open as well
3. The union of any number of open sets is open

The idea of a topological space is fundamental to all future endeavors considered in this document. This mathematical structure allows for the introduction of concepts such as continuity, convergence and thus, completeness of a space [[6]]. These ideas shall be successively introduced as it pertains to the current scope of enquiry. The immediate application of this definition is that it allows us to identify *manifold* and *metric spaces*.

We begin by submitting the idea of a manifold, which can be understood to be a generalized space in n -dimensions. The traditional space where mathematicians and engineers make their considerations takes place within a locality of this manifold. Put more formally, an n -dimensional manifold M^n is a topological space that is locally \mathbb{R}^n [32, p. 13]¹. The structure of a manifold space is liberating for a student of Euclidean geometry as it admits into itself possibilities of generalized coordinate systems and the behavior of differential forms over these generalized spaces.

It may be noted here, that a manifold space² is simply a specialization of a topological space with extra constraints applied over it. Just for purposes of completeness we also mention that in our studies, a manifold is assumed to be smooth which implies 'paracompact' and 'Hausdorff' conditions are satisfied [6]. A manifold can be covered with a number of open sets of topological spaces and mappings known as 'charts' can be defined on them which transform the local set space into a real numbered space (see 2.1).

Consider a function $f: C \rightarrow \mathbb{R}$ which lives on the topological space C . Coupling the two maps $\varphi^{-1} \circ f$ (the mapping φ is continuously invertible), is termed as a *transition function* as it transforms the kernel domain and image domain into $\mathbb{R}^m \rightarrow \mathbb{R}$. When these transition

¹We avoid the more technical, rigorous and complicated definition of a manifold that includes ideas of compactness and Hausdorff spaces, among others. The intention of supplying these definitions here is simply to make intuitive sense into the nature of the survey conducted and not to provide a comprehensive view into the subject matter

²Although not mentioned explicitly, we deal with differential manifold space in our research work. This implies an extra constraint of differentiability of the local coordinate patches over the general manifold space [32, p. 20]

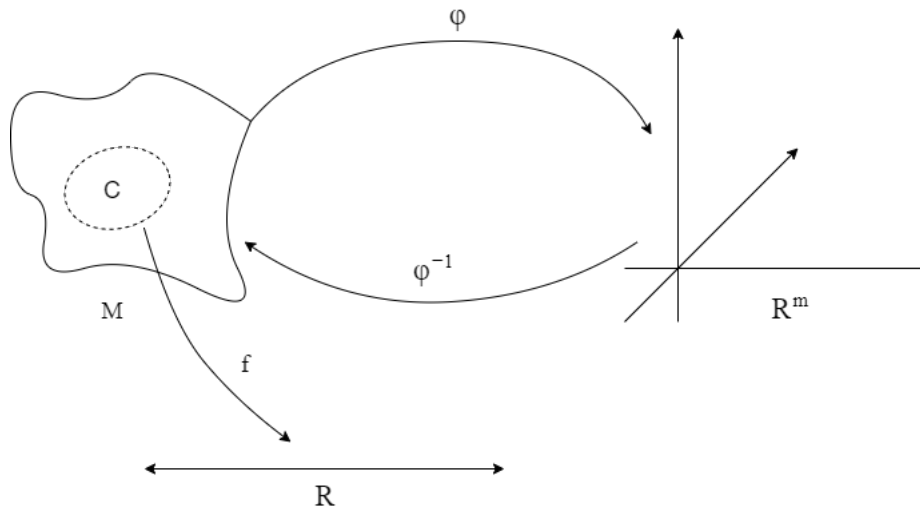


Figure 2.1: The continuously invertible chart $\varphi : C \rightarrow \mathbb{R}^m$ takes in values from the open topological space C (known as a *cover*) on the manifold space M and maps them to a real number space \mathbb{R}^m . Thus, this chart operation allows us to work in a locally \mathbb{R}^m space on a manifold. Similarly, a function $f : C \rightarrow \mathbb{R}$ maps the set C onto a real space \mathbb{R} [6].

functions are continuous as well, the manifold is known as a *topological manifold*³. It should be noted that the description of manifolds and topological spaces thus far have been general enough to capture an understanding of these concepts both within functional analysis as well as in differential geometry perspectives. Deeper inspection of these concepts involve different points-of-view of examination of these structures, however they parallel each other conceptually (in absence of a metric structure).

Vector fields on a manifold: tangents, flows and Lie bracket

There are two kinds of entities that live on a manifold, namely —vector fields and differential forms. We turn our focus to the former. The essential idea here is to generalize the concept of a vector field as defined on a real numbered space (say, \mathbb{R}^3) which is probably familiar to the reader. The purpose of introducing these vector fields to manifolds, however, is less phenomenological than is normally the case. This is to say, that these vector fields do not necessarily hold any real physical significance and are mostly thought of as a tool to differentiate functions defined on a manifold [6].

Definition 2.2. A **vector field** v on a manifold M is defined as a function from the space of infinitely differentiable functions C^∞ to another C^∞ , such that for all $f, g \in C^\infty(M)$ and $\alpha \in \mathbb{R}$:

1. $v(f + g) = v(f) + v(g)$
2. $v(\alpha f) = \alpha v(f)$
3. $v(fg) = v(f)g + fv(g)$,

Conceptualizing a vector field over a smooth manifold allows several possibilities of analyzing functions defined over the manifold. This is done through generalizing the concept of *directional derivatives*. Any physicist or engineer has familiarity with these ideas working in the common Euclidian space where the *basis* of the reference system are all orthogonal and

³Differential manifolds are topological manifolds equipped with a ‘differential structure’

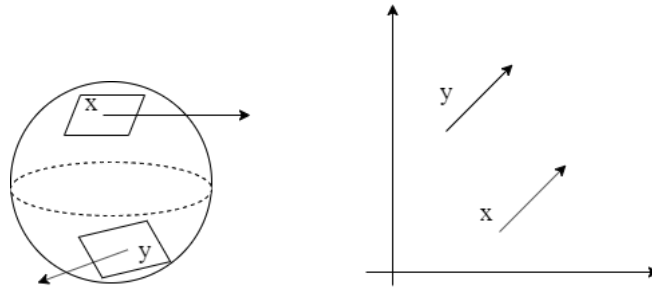


Figure 2.2: Tangent vectors defined over a spherical manifold (left) and two ‘free’ vectors in Euclidian \mathbb{R}^2 space (right)

every *tangent vector* belongs to the same space. For instance, consider the Euclidian space \mathbb{R}^3 , where a function f and a vector field v are defined. Then the directional derivative of the function over this space is given by vf . If deconstructed into component terms, this expression can be expressed as:

$$v(f) = v^p \partial_p f, \quad (2.1)$$

In a Euclidian space, the basis vectors $\partial_p f$ are also a member of the space \mathbb{R}^3 , similar to the vector components v^p . This however, is not true for manifolds all the time. To understand this deviation from the common understanding, a brief introduction of *tangent vectors*⁴ is now provided.

Definition 2.3. A **tangent vector** (v_p) over a manifold M at a point p defines a vector field such that the directional derivative of the function $f \in C^\infty(M)$ is given as $v_p : C^\infty \rightarrow \mathbb{R}$. Furthermore, the following properties hold true:

1. $v_p(f + g) = v_p(f) + v_p(g)$
2. $v_p(\alpha f) = \alpha v_p(f)$
3. $v_p(fg) = v_p(f)g(p) + f(p)v_p(g)$,

The properties to be satisfied by the tangent vectors follow directly from the Definition 2.2. The space spanned by the tangent vectors at a point p is in fact a vector space $T_p M$. A related concept of a *tangent bundle* is that it is a disjoint union of the tangent spaces at all points over the manifold M and is denoted as TM [57].

We now return to the original assertion that led to this digression. Consider the Figure 2.2 (left), where the tangent vectors are shown at two different points x and y . To compare these two tangent vectors is not possible since they belong to different vector spaces. This is counter-intuitive since the common understanding of vector equality is built on a Euclidian space such as the \mathbb{R}^2 shown in Figure 2.2 (right) where the two *free* vectors at point x and y can be compared since their basis vectors belong to the same vector space⁵.

Having introduced the concepts of tangent fields (which are vector fields over a manifold in their own right), it becomes easier to introduce another class of concepts —flows and the Lie bracket. To motivate the need for these ideas in an already overcrowded idea space, we note

⁴For reasons of simplicity, the exposition of tangent vectors is kept simple and no distinction is made between the class of geometric tangent vectors and the broader and more abstract notion of tangent vectors. Consequently, the bridging concept of a *pushforward* is avoided as well. For more information the reader is encouraged to refer to [57]

⁵To enable this comparison of two tangent vectors originating at two different points, the concept of *parallel transport* is needed. This theory will be utilized subsequently.

that the vector fields defined over a manifold enable the differentiation of a function defined over that manifold. Introducing Lie brackets as a tool to generate the vector field themselves and consequently provides a framework for the computing the derivative of a vector field with respect to another field.

Definition 2.4. A **flow** $\{\varphi_t\}$ is defined as a set of all maps or integrable curves defined for a vector field $v(M)$ at a point $p \in M$.

The concept of flow formalizes the notion of vector fields that one encounters in physical examinations such as a velocity field over a manifold. Consider the vector field $v(M)$ over the manifold M . At some point $p \in M$ we trace the particle motion through a curve $\gamma(t)$ such that $\gamma(0) = p$. For this curve to be considered for set membership into a flow over this vector field, we require this curve to be integrable over the manifold domain. That is, the integral curve $\gamma(t)$ should be defined for all time t . Finally, in order to compute this curve, we assume that $\gamma'(t) = v_{\gamma(t)}$.

Given these flows over a manifold, the Lie bracket is an operator that measures the failure of these flows to commute over different vector fields. This is possible since the Lie Bracket acts as a *commutator* of vector fields and as such is used to get new vector fields from old ones.

Definition 2.5. Given $v, w \in Vect(M)$, the **Lie Bracket** is defined as:

$$[v, w](f) = v(w(f)) - w(v(f)),$$

for all $f \in C^\infty(M)$. In short, this is written as,

$$[v, w] = vw - wv$$

In the definition above, it can be seen that for a pair of vector fields that represent mixed directional derivatives, their failure to commute is given by the Lie Bracket. For the ordinary mixed partial derivative we know beforehand, this commutation does not fail [6]. These geometrical interpretation are made palatable to a student of traditional Euclidian spaces with the help of the *Lie derivatives*. As mentioned previously, the idea of a vector field over a manifold is explained as an instrument to differentiate a function over the manifold. A Lie derivative enables the differentiation of a vector field with respect to another field.

The need for a distinct operator such as the Lie derivative is illustrated in the Figure 2.3. When evaluated over two different points over a flow $\gamma(t)$, the tangent vectors over the vector fields at these two points belong to two tangent different spaces. In order to find the directional derivatives over this flow, the spaces must be reconciled. This is done through the ‘pullback’ operator $d(\gamma_{-t})$ marked in blue. In this manner, the tangent vector for point $\gamma(t)$ is obtained within the tangent vector space at $\gamma(0)$ as $d(\gamma_{-t})_{\gamma_0} W_{\gamma_t}$.

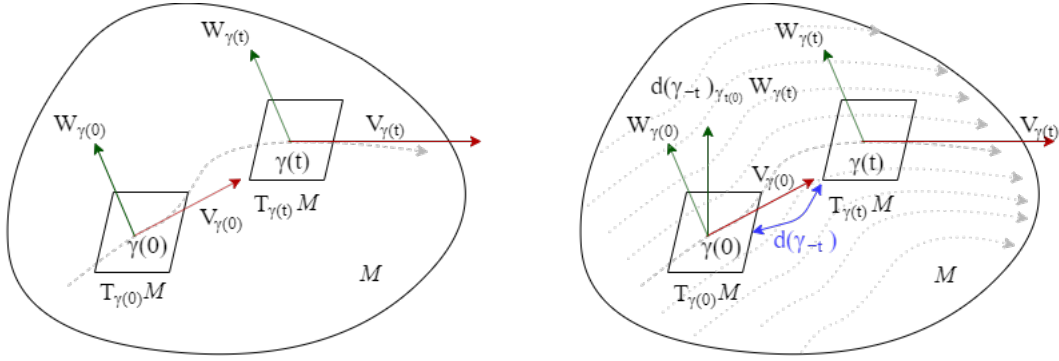


Figure 2.3: (Left) Tangent vectors $W_{\gamma(t)}$ over a flow $\gamma(t)$ evaluated at two different points 0 and p; (Right) The pullback defined over the manifold points allows re-mapping of the tangent space $W_{\gamma(t)}$ over the vector field V [57]

The Dual: covectors, contravariance and the differential of a function

Before the discussion here proceeds to the entities known as the differential forms, a brief detour towards the concepts of the *dual* is required. Furthermore, the pullback operator (mentioned above) is also discussed. As the reader has thus far been introduced to the vector spaces, the dual can be defined as the space of linear functionals that operate on the members of this vector space such that the image lies in the space of real numbers.

Definition 2.6. The **dual space** (V^*) of the vector space V is defined as:

$$V^* = \{f \mid \text{such that, } f : V \rightarrow \mathbb{R} \text{ or } f(v) \in \mathbb{R}, \text{ where } v \in V\}$$

The dual space of a vector space, is again a vector space in itself. Thus the algebra applicable to the primal vector space also applies here. Furthermore, the elements of this space of linear functionals to the space of vectors are referred to as covectors. Recall as an example of a covector, consider the entity known in physics as the ‘force vector’ (it has been relegated to the class of vectors due to a fundamental misreading of the very concepts being discussed here). The work done on a system W is given as:

$$W = F \vec{d}$$

where, this work done is derived within the space of real-numbers (*i.e.* $W \in \mathbb{R}$) using the displacement vector (\vec{d}) and the force functional (F) acting over this vector. As it has been observed already that for curves over a manifold, the tangent vectors provide a coordinate independent representation of their derivatives; similarly, a tangent covector serves to represent the derivatives of real-valued functions over a manifold [57].

Recall from equation 2.1 that a directional derivative of a function can be expressed using the basis of a vector field over that manifold. In a similar fashion, the elements of the covector space can be constructed using a set of basis known as the *dual basis*. For any finite dimensional vector space V , the primal basis $\{E_j\} \in V$ holds the following relationship with the dual basis $\{\varepsilon^i\} \in V^*$,

$$\varepsilon^i(E_j) = \delta_j^i,$$

where δ_j^i is the symbol for the Kronecker delta matrix. A natural consequence of this relationship is also that $\dim V^* = \dim V$. The careful reader might observe the distinction made between the notations of the dual and primal basis vectors —the former uses superscript indices whereas the latter uses subscripts. The reason for these differences are not merely for convenience. Instead, they also denote a natural property observed within the elements

of these spaces. This difference is in terms of how these elements in space relate with the manifold over which our consideration takes place. Specifically, these properties (of *covariance* and *contravariance*) describe how the elements in the primal and dual spaces transform with a transformation of their coordinate systems⁶.

Differential forms and exterior algebra

Recall that there are two types of entities that live over a manifold, the vector fields were described above. The other entity is known as a differential form. For the purposes of mathematical physics, it is perhaps sufficient to describe these differential forms in the fashion Flanders put it: "the things that occur under the integral sign" [30]. In order to provide some rigour to this definition, we consider a vector field v over a manifold M . A realization of the usefulness of differential forms occurs when we try to generalize the gradient of a function f over this space.

For the Euclidean space \mathbb{R}^n , the directional derivative along the vector gives the gradient of the function in that direction, as the dot product of ∇f with v :

$$\nabla f \cdot v = v f$$

On a manifold however, the structures that provide the mechanism to take such dot products are not available. This is accomplished through another concept known as the *metric*, which will be introduced later. For now, it is sufficient to know, that differential forms (for this example, 1-form) allows us to make this generalization without explicitly choosing an arbitrary metric structure. For instance, a 1-form ω is defined as a linear map between the spaces $\text{Vect}(M)$ and $C^\infty(M)$:

$$\omega: v \mapsto \nabla f \cdot v$$

with the following properties,

$$\begin{aligned}\omega(v + w) &= \omega(v) + \omega(w), \\ \omega(gv) &= g\omega(v)\end{aligned}$$

where, v and w are any two vector fields over the manifold M and g is any smooth function on \mathbb{R}^n . Furthermore, consider any manifold space and let $\Omega^1(M)$ represent the space of all 1-forms on M . Then for any smooth function f on M there is a 1-form df defined as:

$$df(v) = v f.$$

This 1-form is called the *differential* of f or the *exterior derivative* of f . This is the generalization of the function gradient that we set out to obtain. Of course, for the time being this provides the working definition of what a differential form might look like or what it might be used for. However, it is a good exercise to delve deeper into these concepts. The reader is now taken to a slight detour to another concept known as *cotangent vector*.

Definition 2.7. Given a manifold M and a point $p \in M$, a **cotangent vector** ω at p is defined as the linear map that takes in elements from the tangent space over M , $T_p M$ and maps them onto the real numbered space, \mathbb{R} . The set of these elements is denoted by, $T_p^* M$.

$$\omega_p(v_p) = \omega(v)(p)$$

where the 'function' $\omega(v)$ is evaluated at the point p .

⁶ Amazingly, this behavior is also explained through algebraic topologies using the concepts of orientations, as will be discussed shortly hereafter.

The notations used in the definition above should serve as a hint for the fact that the cotangent vectors are just the dual space to that of the tangent vectors. The need for this definition will become clearer as our exploration draws closer to that of p-forms. To motivate the need for these entities (similar to that of 1-forms), consider the product of vector entities⁷. In vector mathematics, the product of two vectors is taken to represent the surface area of a parallelogram that lies in the same plane as that of the two vectors. Thus a product operation creates an association between the line elements (vectors) and a surface element (the parallelogram). Similarly, consider the ‘right-hand rule’ applied in the computation of the cross product between two vectors. However, if one were to compute a cross product for four-dimensional vectors, there exists no such guiding principle (with geometric intuition included). Differential forms allow this generalization to take place. This means not working with the vectors themselves, but working with the p-forms instead. Consequently, the directional entities (with a tangible geometric interpretation) are no longer tangent vectors but cotangent vectors instead⁸.

This undertaking then requires some assembly, which comes in the form of what is known as *exterior algebra*. The rules and structure of this algebra degenerate to the known vector mathematics we know in the Euclidian three dimensions. For instance, exterior algebra defines an operation known as the *exterior product* or *wedge product* (denoted by \wedge). This operator is the generalization of the cross product (\times) operator familiar in 3-D vector mathematics.

$$\begin{aligned} \text{for any two vectors, we have: } \vec{v} \times \vec{w} &= -\vec{w} \times \vec{v} \\ \Rightarrow \text{this can be generalized as: } v \wedge w &= -w \wedge v \end{aligned}$$

Also, here $v, w \in V$. Similar to how the product of a cross product of two vectors is also a vector (and thus lies in the same vector space), the wedge product admits the output of the product into its own space. Thus, for any vector space V , the subspace $\wedge^p V$ is defined to be the subspace of $\wedge V$ consisting of the linear combinations of the “p-fold” products of vectors in V , that is, $v_1 \wedge v_2 \cdots \wedge v_p$. The elements of this subspace are said to have a *degree* of p .

The extension of this structure induced due to this operation over a manifold mapping between the smooth functions $C^\infty(M)$ and the space of 1-forms $\Omega^1(M)$ ⁹. Thus, *differential forms* $\Omega(M)$ are then defined as the ‘algebra’ generated over $C^\infty(M)$ by $\Omega^1(M)$ as shown:

$$\omega \wedge \mu = -\mu \wedge \omega \quad \forall \omega, \mu \in \Omega^1(M).$$

Combining p such products, one obtains what is called a *p-form*. Another important concept related to the world of exterior algebra is that of the exterior derivative (d). This operator takes in a p -form and produces a $(p+1)$ -form:

$$d: \Omega^p(M) \rightarrow \Omega^{p+1}(M).$$

The importance of this operator along with all the previous concepts of exterior algebra is reflected in the derivation of the generalized Stokes theorem. This is done through the realization that the differential operators are all different versions of the same operator:

⁷These examples are drawn from the excellent book by Baez and Munian [6].

⁸Another reason to qualitatively validate the utility of working with cotangent vectors is that this approach leads to the generalized Stokes theorem, where the differential operators: grad, div and curl are revealed to be different versions of the same differential operator.

⁹As opposed to the earlier construction that involved a mapping from a real-numbered space to that of a vector space.

$$\begin{aligned}
\text{Gradient: } & d: \Omega^0(\mathbb{R}^3) \rightarrow \Omega^1(\mathbb{R}^3) \\
\text{Curl: } & d: \Omega^1(\mathbb{R}^3) \rightarrow \Omega^2(\mathbb{R}^3) \\
\text{Divergence: } & d: \Omega^2(\mathbb{R}^3) \rightarrow \Omega^3(\mathbb{R}^3)
\end{aligned}$$

Furthermore, there is also a parallel to the Poincaré relationship in the form of: $d(d\omega) = 0$ ¹⁰.

The metric structure and Hodge operator

When further constraints of a metric are imposed on this space, we obtain what is known as a metric space. This metric allows induction of a topology on a set. In the more familiar terms of vector mathematics, a metric allows for the computation of the inner product between two vectors. Thus, the metric enables us to “compute” values in the real numbered space for some of the topological operations that take place in the world of differential geometry.

An interesting observation to be made here is how the use of metric and the implementation of that concept in the form of the Hodge operator (\star) is implicit in the classical vector calculus where the mathematics takes place in the Euclidean \mathbb{R}^3 . Recall the notation of $\wedge^p V$ as the subspace of the “p-fold” products of vectors in V . Baez [6] notes that the wedge product of two vectors in V lies in the space $\wedge^2 V$. in the 3-dimensional case however, the dimensions of the spaces $\wedge^2 V$ and V are equal. This allows for the common error (although this works!) of considering the cross product of two vectors to be vector. However, in any other space where the dimension is not three, this is not true.

In other dimensions, as mentioned previously, this transformation from one subspace to another is done through the Hodge operator (\star). For the three dimensions, where the basis are dx , dy , dz the following mapping holds:

$$\begin{aligned}
\star: dx \wedge dy &\rightarrow dz \\
\star: dy \wedge dz &\rightarrow dx \\
\star: dz \wedge dx &\rightarrow dy
\end{aligned}$$

To generalize, the star operator, referred to as the **Hodge operator** (\star) is a unique mapping on the oriented n-dimensional semi-Riemannian (that is, with a metric structure) manifold M , such that:

$$\star: \Omega^p(M) \rightarrow \Omega^{n-p}(M)$$

where for any two p forms ω and μ on M ,

$$\omega \wedge \star\mu = \langle \omega, \mu \rangle \text{ vol} \quad \omega, \mu \in \Omega^p(M)$$

where the term ‘vol’ represents a volume form (see [6, p. 82]). The application of the star operator on μ creates the *dual* of the p form in the $n-p$ space. The angle brackets represent the inner product defined over the manifold M as a result of imposing a metric on it.

Having explained these concepts of differential geometry and the extended concepts of space, the nature of space through this perspective it becomes clear to understand that the convergences with the manner and practice of traditional vector calculus is arbitrary in many respects. In fact, adopting this generalized approach has its uses in many forms other than rigour and logical consistency. We will build on these very ideas going forward, in order to develop a geometry-aware numerical scheme in order to mimetically discretize a curved mesh.

¹⁰Applies to coboundary operator in algebraic topology

2.2. Reimagining Mathematical Physics: Mimetic Approach to CFD

The developments in Computational Fluid Dynamics (CFD) as an approach to explore and investigate have been ongoing for little over half a century now, with new stimulus in the twin forms of increased computational power as well as improved numerical algorithms. While these developments in themselves are of great interest, each of them occur over a different time scale: computational hardware capabilities that limited computational power has made significant strides in a shorter time span of the last thirty years, whereas the mathematical logic governing numerical algorithms has steadily built an inventory of methods to tackle different mathematical systems. Our investigations here deal within the scope of the latter.

Interestingly, over this long period of development behind the rise of CFD as a respectable avenue for scientific inquiry, the concepts governing mathematical analysis and construction of numerical schemes have largely remained monolithic. With a large emphasis on discretization techniques, time-stepping methods and solver algorithms for matrix systems, the core logic behind these disciplines has seldom engaged in adventurism. This core logic refers to the system of vector calculus and integration theory that serves as the basis for most discretization techniques and formulation of the differential equations to be solved. As discussed previously, a large number of methods that descend from this school of formulation feature very similar recipes of what Gerritsma refers to as *brute force* approaches. Essentially, this involves excluding the *geometric content* embedded into the mathematical expressions we work with and instead indiscriminately discretizing entities over an abstract domain with an aim to *minimize the truncation error or the residual*.

On the other hand, the related disciplines of Computer Aided Geometric Design (CAGD) and Computer Graphics (CG) have managed to diversify into several families of approaches with very many philosophies dictating the modeling and the subsequent computational preferences. Perhaps, the author would suggest that, the lack of any predetermined mathematical models for representation real world object geometries served as a reason for a broad based system of inquiry into mathematics. Our inspiration here is one that finds common cause especially with the CAGD and CG community among others, namely —differential geometry and topology.

The pantheon of methods that have sprung into existence with links to differential geometry are several and varied such as Discrete Exterior Calculus (DEC) method, Discrete Differential Geometry (DDG), Finite Element Exterior Calculus (FEEC) method, structure/physics/symmetry-preserving discretization methods, mimetic discretization methods, compatible discretization methods, to name a few. These concepts of differential geometry, algebraic topologies and their applications to physical problems as we know them today found utterance in the later half of the twentieth century. It is these concepts which build the foundations of the work presented in this report. However as noted above, these were preceded by the slow churn of mathematics throughout the previous two centuries. Our current examination of the underlying history is rooted in this context.

2.2.1. Pressing the ‘Reset’ Button: Applied Differential Geometry

Equipped with a rudimentary understanding of differential geometric principles, we now attempt here to outline the ingress of these concepts into the realms of integration theory and subsequently, CFD applications. It is not the intention of our exploration here to be a comprehensive deep dive into the concepts since that would be out of the scope of this report. Although the developments in topology and geometry was picking pace up until the nineteenth century with the emergence of calculus in the works of Leibniz and the Reimann’s work on algebraic geometry, the dominant narrative over geometry and topology was driven by Euclidian principles and the modern concepts of linear algebra, topological spaces and differential

geometry were absent.

In his *Collected Works*, published between 1894-1911, Hermann Grassman put forward the ideas of *linear algebra* and *vector spaces*. This was preceded by his publication, *Die Lineale Ausdehnungslehre* (in 1844), wherein he proposed the ‘theory of extension’ (*Ausdehnungslehre*). Effectively, he argued for the extension of spatial dimension where the number of such dimensions are not restricted to three (as was dictated by the conventional wisdom). Though, revolutionary for his time, his work mostly argued for philosophical mathematical innovations but failed to motivate and provide sufficient rigour for his theories to be taken seriously [28]. In his works, he introduced geometry and algebra as intertwined entities as opposed to the previous interpretation of algebra was a simple paradigm that conveyed magnitudes. This was ofcourse, inline with Leibniz’s efforts (before him) to establish a universal algebra (*geometria situs* and *analysis situs*) as the intellectual predecessor to what we refer to as ‘topology’.

A big momentum to the inclusion of geometry into algebra and the related developments in functional analysis alongside algebraic topology was provided by Henri Poincaré, whose work titled ‘Analysis Situs’[66] laid way for the formalization of several topological as they exist today. This was a big shift from the Euclidian conception of geometry which limited understanding of the true nature of algebra and the nature of space. Finally, it was Hermann Weyl in 1920 (himself building on the work of the Italian mathematician, Giuseppe Peano [64]) who formalized the axiomatic definitions of the fundamentals such as vector spaces, topological groups, Lie groups and other geometric foundations of manifolds. This was also the time when the new ideas of *metric spaces* and *compactness* had entered the mathematical imagination through the dissertation work of Maurice Fréchet [33]¹¹.

The history of these developments, though interesting in their own right, are presented here simply to motivate the understanding of the novelty of these domains and their subsequent applications to mathematical and computational physics. Furthermore, having been previously acquainted with the basic concepts of differential geometry and algebraic topology, the reader is now introduced to advanced and much more related concepts in the following sections. First the reader is introduced to the concepts of geometric associations in mathematical physics, followed by an overview of the analysis tools used to utilize these geometric similarities —algebraic topology and differential geometry.

2.2.2. Similarities in Physical Theories

The Italian mathematician, Enzo Tonti first proposed a mathematical concept that sought to identify the similarities in the equations governing seemingly different fields of physical systems such as classical mechanics and electromagnetics [69, 70]. Here, he identified a different classification scheme for physical variables used to model physical systems.

Recall that in the previously we encountered examples of physical variables having different geometrical associations, such as with point, lines, surfaces and volumes. However, there are other approaches to construct these associations, such as the ones proposed by Tonti. He classified field variables into three categories —source variables, configuration variables and energy variables. This variable classification helps us identify the role each of them plays in any phenomenological or topological equation (conservation laws, constitutive equations, interaction equations etc.). For instance, the configuration variables can be thought of as entities that help identify the ‘configuration’ of any system. In classical mechanics, this variable can be identified as the position vector. Its complement in cases of field functions can be identified as a *potential* term such as temperature, electric or gravitational potential.

As a consequence, the family of variables that stem from these configuration variables

¹¹This was also the period where other major discoveries were being led by several noted mathematicians such as Darboux and Cartan. Due to limited scope of this report, these are not mentioned.

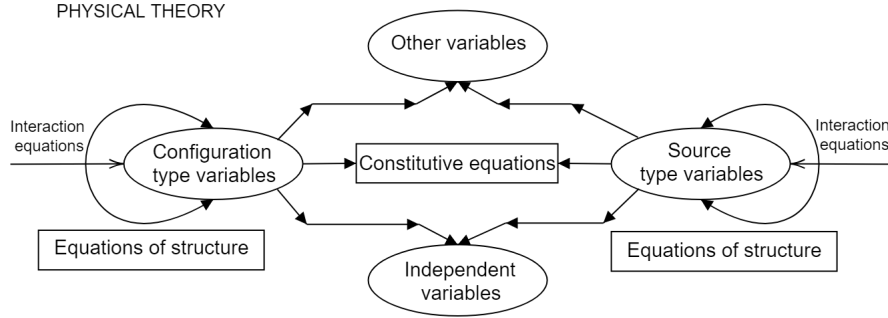


Figure 2.4: Basic classification of physical variables of a theory [69]

through operations such as sum or difference, total or partial derivatives —without any intervention from independent quantities such as physical constants, material properties, phenomenological constraints etc are referred to as *configuration-type* variables. In classical continuum mechanics, examples include displacement, velocity, strain, deformation gradient etc.

Source variables, on the other hand, are the basic entities that capture the *force concept*. They represent the source of change of the configuration of the system under consideration. Examples for these variables include force (in classical mechanics), mass (gravitation), electric charge (electrostatics or electrodynamics) etc. Furthermore, extending the concept of derived variables, *source-type* variables can be defined, for instance body force, body couple, momentum, stream functions etc. Energy variables can simply be defined as those that are derived as a product of source and configuration variables. Examples include work, power, kinetic energy, heat energy etc. These ideas are represented in the Figure 2.4 with the manner of interaction between the different classes of variables and their corresponding phenomenological equations.

Cell complexes, space and time elements

In this section, the associations of the physical quantities with the basic geometric and chronometric elements are considered, given a region Ω in the space \mathbb{R}^n . Accordingly, based on their geometric associations —some variables may be associated with surfaces ($n=2$) whereas others may associate with points ($n=0$) —and their chronometric counterparts —time instance ($n=0$) or time interval ($n=1$) —the classification discussed previously is developed further.

As an overview of possible quantity association with these elements the following examples may be considered. Flux variables, such as magnetic flux, electric flux, vortex flux, are associated with a surface geometry, by definition. On the other hand, variables that are expressed as a line intergral such as velocity circulation, electromotive forces etc. make reference to a line element. Interestingly, material based quantities *i.e.* energy, mass, entropy etc. associate with volumes. Certain source variables such as electric potential, velocity potential and temperature are quantified on points.

In order to study this further, a *n-dimensional cell* concept is introduced. Each three-dimensional cell (3-cell) is composed of vertices, edges and faces that, in themselves comprise 0-cells, 1-cells and 2-cells respectively:

0-cell: point, time-instant, event: P

1-cell: line segment, time interval: L

2-cell: surface segment, line segment \times time interval: S

3-cell: volume, surface segment \times time interval: V

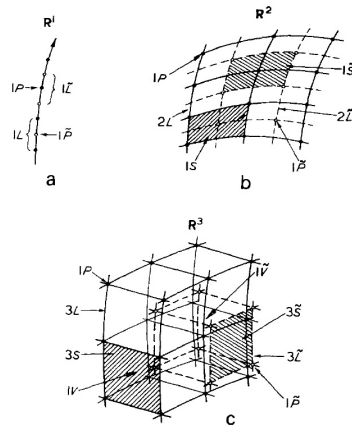


Figure 2.5: Cell complex for (a) \mathbb{R}^1 , (b) \mathbb{R}^2 and (c) \mathbb{R}^3 [69]

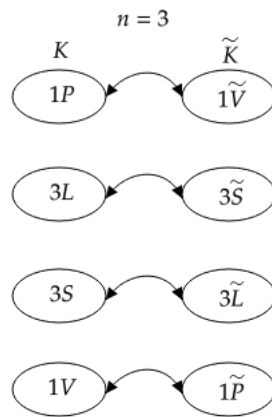


Figure 2.6: Classification of basic geometrical elements of a cell complex K and its dual \tilde{K} in \mathbb{R}^3 [69]

4-cell: hypervolume, volume \times time interval: H

Consider a volume V (3-cell) in the \mathbb{R}^3 space. For every point P (0-cell) in V , there are 3 coordinate lines (1-cells) and 3 coordinate surfaces (2-cells) that pass through it. Thus, it can be seen that any p -cell family groups within itself several $(p-1)$ -cells continuing upto 0-cells. Such a set of all the cells of various orders is called a *cell complex*, K in algebraic topology.

Once the concept of cell complex is introduced, a complementary concept of *dual* cell complex (\tilde{K}) also follows. In the present case, a dual cell complex becomes relevant as pressure-velocity collocation is attempted to solve the incompressible Navier-Stokes equation. Furthermore, it should be noted that for every p -cell of K there corresponds a $(n-p)$ cell of \tilde{K} and *vice versa*. Complexes (and duals) for one to three dimensional spaces are shown in the Figure 2.5. It can be seen that duals of complexes occupy the same \mathbb{R}^n space but with the center of gravity of the primal volume elements (V) as their point elements (\tilde{P}). In this manner a primal-dual association can be shown in the following manner (see Figure 2.6):

Orientation of p-cells and incidence matrices

The concept of *orientation* of a p -cell can be defined using permutations of the ordered set of vertices defining a geometry. To clarify this further, consider the simplest geometrical polygons (or polyhedrons) in \mathbb{R}^n spaces. For two-dimensional spaces, the simplest polygon, or *simplex*,

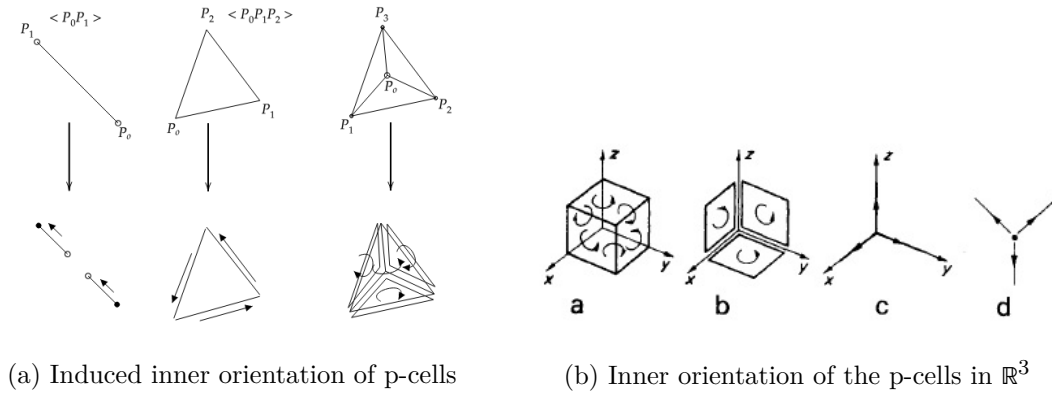


Figure 2.7: Inner orientation of p-cells [69]

would be a triangle. Similarly for a three-dimensional space the simplex object would be a tetrahedron. In this manner, if a simplex object in \mathbb{R}^n is considered, it can be represented by the following notation:

$$\langle P_0, P_1, P_2, \dots, P_n \rangle$$

The given arrangement along with anyone of the categories can be collectively called the *inner orientation* of the cell whereas the remaining category arrangements can be called the opposite orientation. Through this treatment, it becomes clear that this concept relates to a order through which the ‘perimeter’ of an object is traversed. This is shown in the Figure 2.7.

Furthermore, since any p-cell complex groups within itself a number of $(p-1)$ cells —all of whom are connected topologically to one another —simply choosing an inner orientation category for a simplex structure at the 1-cell level naturally induces inner orientations to all the following elements. This cascading of inner orientation is then referred to as the *induced* inner orientation. This is depicted in the Figure 2.7a.

This suggests a natural manner or algorithm for the assignment of inner orientation to a p-cell in n-dimensional spaces. This is as follows:

1. divide the p-cell into p-simplexes,
2. orient one simplex and propagate the orientation to adjacent simplexes,
3. orient all p-cells of the same family (lying on the same coordinate manifold)

Once this system of inner orientation has been defined, it can be extended to the dual (\mathbb{K}) counterparts of these primal cell complexes (\mathbb{K}). Continuing in this manner, it is to be noted that every p-cell of the primary cell complex in \mathbb{K} is crossed by a $(n-p)$ cell of \mathbb{K} . Thus this inner orientation of the dual complex is associated to the geometrical elements in the primal cells as well. For this reason, the dual orientation is named as the *outer* orientation of the p-cell. Naturally, this orientation gets induced as well as is shown in the Figure 2.8.

As mentioned previously, the propagation or induction of orientation from lower order cell complexes within a family to its higher order complexes follows topological laws (such as the Möbius Law of Edges); these induced orientations depend on the basic convention used. However, in the case that different orientation conventions are employed at every p-cell within a family, the propagation will not follow. In order to resolve this issue, a ‘bookmarking’ idea

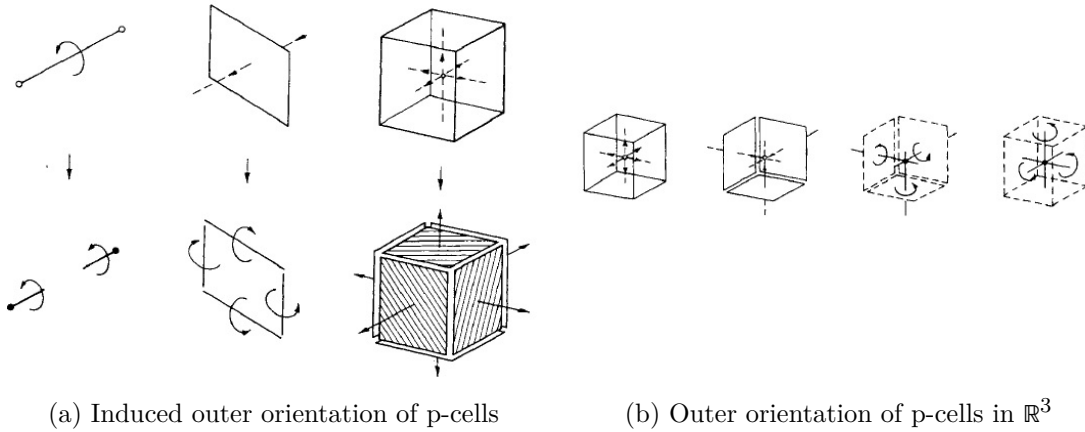


Figure 2.8: Outer orientation of p-cells [69]

is implemented in the form of *incidence numbers* (e):

$$e_{rs}^{(p-1,p)} = \begin{cases} + 1, & \text{induced orientation} = \text{assigned orientation} \\ 0, & \text{not a face of higher order cell} \\ - 1, & \text{induced orientation} \neq \text{assigned orientation} \end{cases}$$

where r is the index of the p -cell and s is the index of any $(p-1)$ cell grouped within the family. In case, the s^{th} $(p-1)$ -cell is not a face of the r^{th} p -cell, then the incidence number assigned to the pair (r,s) is null. On the other hand, if the pair are related to one another then their orientation compatibility is compared. In case these orientations are same, then a value of $+1$ is assigned whereas opposite orientations leads to a value of -1 to the (r,s) pair.

These incidence numbers can then be collated within an *incidence matrix* ($\mathbb{E}^{p,(p-1)}$) for all combinations of (r,s) . Thus, in case of \mathbb{R}^3 , three different incidence matrices are possible: $\mathbb{E}^{3,2}$, $\mathbb{E}^{2,1}$ and $\mathbb{E}^{1,0}$. A possible interpretation of these matrices is that of a connectivity matrix that reflect the output of combinatorial pairing of cells within the complex.

2.3. Tools for Investigation: Operators and Cohomologies

2.3.1. Algebraic Topology

In this section, the associations of physical quantities with space and time elements as discussed previously are considered while making use of the concepts of oriented cell complexes introduced already. This is relevant since using these oriented complexes will allow for the development of mathematical associations to the physical quantities as they appear in the equations describing a physical phenomena. In this regard, the framework employed to utilize the topological concepts involved with cell complexes and associated variables is a mapping known as a *chain*.

A p -chain is one such mapping between between the oriented p -cell complex and the elements of a set \mathbf{S} containing quantities of interest. Specifically, it helps define the operations that are characteristic of physical quantities (such as operations for scalars, vectors, tensors etc.) as a function of their associated cell complexes. In order to understand how this is accomplished, the following example can be considered.

In the case of fluid dynamics, specifically for the formulation of Navier Stokes equation, a parallelepiped fluid element is considered over which forces are balanced. In such a case, contact forces are considered acting over a face of the fluid element, or in a topological terminology, these forces are transmitted through a oriented 2-cell. It is important to note here that the outer orientation of this 2-cell is implicitly used while determining the nature of the force being applied *i.e.* compression or tensile. Accordingly, the contact forces which operate on a point

become associated to the center of gravity of the face —dual complex point elements —and its derived quantity —normal stress —gets associated with the surface element on the primal 2-cell.

The resulting deformations in the fluid element as a consequence of these forces are modeled through the displacement of the vertices of the fluid element, or in other words, the 0-cell of the primal complex. It should be noted here that there is deeper pattern to be identified here, *i.e.* the source variables (here, force) associates itself primarily with the dual complex \mathbb{K} whereas the configuration variables (here, displacement) make these associations with the primal cell complex \mathbb{K} . This is also true across many other physical systems and is generally taken as ‘rule of thumb’.

Mathematically, this association of force is represented through a 2-chain, wherefore each oriented 2-cell complex is described by assigning to it a vector as a measure of the distribution of the force. Then these vectors are referred to as the ‘coefficients’ ($\in \mathbf{S} = \mathbb{R}^3$) of the 2-chain constructed. Of the many 2-cells over which the force vector may act, consider the s^{th} 2-cell and the force vector itself as \vec{f}_s , then the 2-chain is represented as:

$$f^{(2)} = (\vec{f}_1, \vec{f}_2, \dots, \vec{f}_\alpha)$$

where, α is the number of 2-cells of the cell complex. Note that these chains are not only limited to geometrical (or space) elements alone and can be applied to quantities that are associated with time elements (0-cell or 1-cell).

In order to appropriately analyze the structural and phenomenological equations, another homology concept of *coboundary* is now introduced. It is a process that takes in a p -chain and produces a $(p+1)$ -chain. Essentially, this new chain is constructed by propagating the connectivity relation of an arbitrary p -cell and all of the $(p+1)$ cells of \mathbb{K} that are incident upon it. These incident cells are *cofaces* on the p -cell.

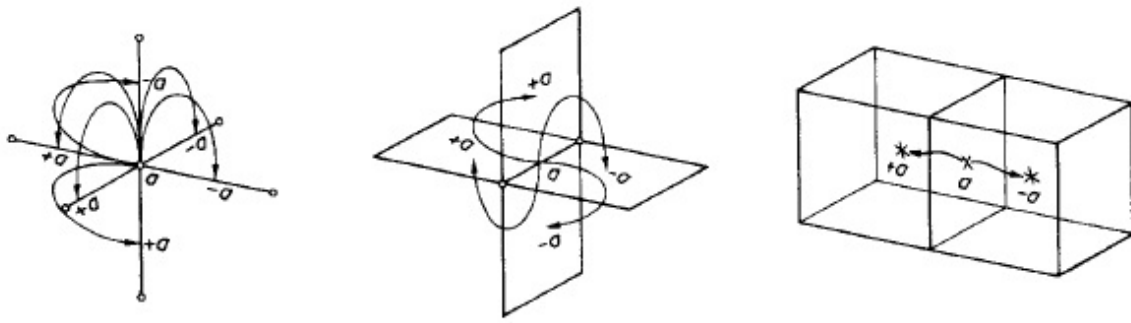
As with every chain a mapping to an element \mathbf{S} is required. Consider a mathematical entity β associated with every p -cell. Constructing the $(p+1)$ chain requires ‘transferring’ this value to each of the p -cell’s cofaces with the same or opposite sign depending on the associated incidence numbers. Thus, in this manner there are $(p+1)$ multiples of β each belonging to one of the cofaces. In order to compute the value associated with the $(p+1)$ cell all of the multiples of β are summed up. In this way, $(p+1)$ chain maps onto another element of \mathbf{S} . This $(p+1)$ -chain is known as the coboundary of the given p -chain. Mathematically this entire coboundary process can be represented in the form of a linear coboundary operator (δ):

$$b^{(p+1)} = \delta\beta^{(p)}$$

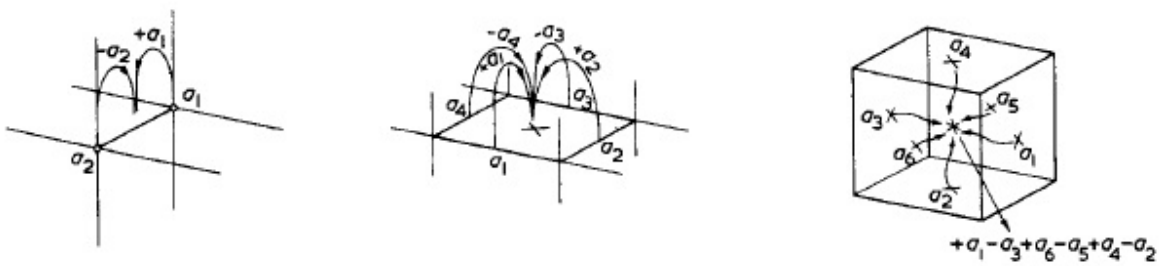
where, $b^{p+1} = (b_1, b_2, \dots, b_{\alpha_{p+1}})$ and $\beta^p = (\beta_1, \beta_2, \dots, \beta_{\alpha_p})$. This concept is demonstrated in the Figure 2.9. Furthermore, the complete classification scheme of a primal and dual cell complex is shown in the Figure 2.10. In this figure α_k denotes the number of p -cells of \mathbb{K} whereas γ_j denotes the number of p -cells of \mathbb{K} . Here the p -chains at every cell level are represented by $\{a^{(0)}, b^{(1)}, c^{(2)}, d^{(3)}\}$ for the primal cells in \mathbb{K} and whereas $\{e^{(0)}, f^{(1)}, g^{(2)}, h^{(3)}\}$ for the dual cells in \mathbb{K} . Also, $\mathbb{E}^{(p+1,p)}$ and $\mathbb{A}^{(p+1,p)}$ are the incidence matrices on the primal and dual cells respectively. Finally, it should be noted that the same coboundary operator δ is used throughout the chains on both cell spaces in order to construct higher-order chains.

An example of the use of coboundary processes in physical systems can be seen in the gradient operator. Consider a scalar quantity φ at every point \mathbf{P} , then the corresponding gradient depends on the difference between their values at different points (\mathbf{P}_i and \mathbf{P}_j):

$$\sigma_s = (+1)\varphi_j + (-1)\varphi_i$$



(a) Transferring β values to incident co-faces



(b) Summing assigned β multiples over every co-face

Figure 2.9: Construction of a coboundary from a p-chain [69]

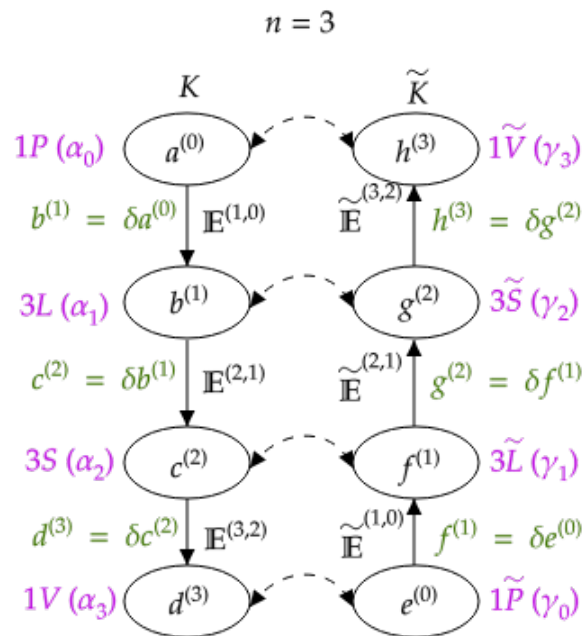


Figure 2.10: Chains on primal and dual cell complexes for $n = 3$

since this difference is associated with the line element, the corresponding incidence expression can be written as:

$$\sigma_s = \Sigma_h e_{sh}^{(1,0)} \varphi_h$$

or, simply,

$$\sigma^{(1)} = \delta\varphi^{(0)}$$

thus, in this case, the gradient is simply the coboundary construction of a 0-chain. This realization can be extended towards most structural and phenomenological equations (such as constitutive, circuital, balance, conservation equations)—that the $(p+1)$ -chain is the coboundary of the p -chain.

2.3.2. Differential Geometry

In this section, we briefly revisit the some concepts of differential geometry that were covered previously, however with a focus on vector calculus. We begin with differential forms. Flanders [30, p. 1] describes them as “the things which occur integral signs”. These forms are by definition independent of any metric, since that concept requires an algebraic structure imposed upon the ambient space, which is not present on manifolds by default (hence the generalization). Working with these items allows association with entities that have a geometrical relationship. An example of a differential form, here a 1-form, is as follows:

$$\lambda^{(1)} = A(x, y, z)dx + B(x, y, z)dy + C(x, y, z)dz, \quad (2.2)$$

here, the superscript (1) indicates that the expression is that of a 1-form. The identifying feature here is two-fold: first, the coefficients $A(x, y, z), B(x, y, z), C(x, y, z)$ are known as the *vector proxies* of this 1-form, it is these entities that largely feature in traditional vector calculus. What is ignored, on the other hand, is the second feature, which are the basis vectors for the space of vectors where this 1-form lives, dx, dy, dz . It is through these basis vectors, that the geometrical association of this 1-form can be made to the family of one-dimensional objects. Thus, the integration of this 1-form occurs over one-dimensional, smooth curves \mathcal{C} ,

$$\int_{\mathcal{C}} \lambda^{(1)} = \int_{\mathcal{C}} A(x, y, z)dx + B(x, y, z)dy + C(x, y, z)dz \quad (2.3)$$

Similarly, this idea can be extended to higher dimensions. For instance, consider a 2-form:

$$\gamma^{(2)} = A(x, y, z)dxdy + B(x, y, z)dydz + C(x, y, z)dzdx, \quad (2.4)$$

This entity again consists of a combination of vector proxies— $A(x, y, z), B(x, y, z), C(x, y, z)$, as well as the basis vectors. The 2-form is associated to surfaces or two-dimensional manifolds similar to 1-form association with one-dimensional objects. This association can also be expressed in the form of a *duality pairing*:

$$\langle \lambda^{(1)}, \mathcal{C} \rangle := \int_{\mathcal{C}} \lambda^{(1)}, \quad (2.5)$$

$$\langle \eta^{(2)}, \mathcal{S} \rangle := \int_{\mathcal{S}} \eta^{(2)}, \quad (2.6)$$

Notice, however, the different basis which is similar to the product of the 1-form basis vectors. In fact, this product is known as a *wedge product*: $dx \wedge dy \equiv dxdy$. This product takes in a k -form and a n -form defined over a space Ω and gives back a $(n+k)$ -form:

$$\wedge : \wedge^k(\Omega) \times \wedge^l(\Omega) \rightarrow \wedge^{k+l}(\Omega) \quad (2.7)$$

This multi-linear product operator is associative. Furthermore, as an anti-symmetric product, the following relationship holds:

$$dx \wedge dy = -dy \wedge dx \quad (2.8)$$

thus, we get the equations:

$$dx \wedge dx = dy \wedge dy = dz \wedge dz \equiv 0 \quad (2.9)$$

Another operation, known as *exterior derivatives*, is now discussed. This operation, when applied to k -forms transforms k -forms into $(k+1)$ -forms. Furthermore, consecutive application of this operator transforms a k -form into $0^{(k+2)}$ which is a zero $(k+2)$ -form.

Equipped with these tools, an expression of the generalized Stokes theorem is possible. The purpose of this expression is to provide the generalization of the differential operators —**grad**, **curl** and **div** in the form of the exterior derivative operator. Given a k -form η^k from the space \wedge^k holds the following relationship over a $(k+1)$ -dimensional manifold \mathcal{M} :

$$\int_{\mathcal{M}} d\eta^{(k)} = \int_{\partial\mathcal{M}} \eta^{(k)} \quad (2.10)$$

here, the manifold boundary is represented by $\partial\mathcal{M}$. This translates to the duality pairing in the following form:

$$\langle d\eta^{(k)}, \mathcal{M} \rangle = \langle \eta^{(k)}, \partial\mathcal{M} \rangle \quad (2.11)$$

The different values for $k=0,1,2$ in this case, will translate this generalized Stokes theorem into the gradient integral theorem, the classical Stokes theorem and the divergence theorem respectively [34, p. 55]. It should be noted here that, all of the entities discussed thus far, occur in a space with no metric structure imposed, thus their discrete implementation can be made exactly.

2.4. What next?

Thus far we have identified the basic concepts of topological spaces, vector fields as a means to differentiate quantities, flows and visualized these functional concepts with the flesh and bones of algebraic topology. Doing so also allowed a visually accessible discussion of chains and orientation and how the dual of a space can be identified physically in \mathbb{R}^3 . Note here that the discussion thus far has remained to real-valued chain complexes and their use in differential geometry. For our purposes however, it is more relevant to understand (co-)vector-valued chain complexes and thus build them into the mimetic framework. The reason for this change is the idea that traditional continuum mechanical approaches identify all kinematic and kinetic quantities using vector and tensor fields. Although this research and its predecessors, have also explored co-vector valued fields (reasons discussed in Chapter 4), the shift from real-valued chains becomes important.

We let this discussion rest here for the moment. The conversation over MSEM and its applications over preserving strong mass-momentum conservation over curved meshes will be explored in the following chapters. Doing this will require an examination of curvature properties and how they delineate over a manifold with the help of gauge theory. This exercise will be undertaken in chapter 4. At this junction, we are quite ready to explore the development of MSEM as a mimetic method (in the next chapter).

Background to Mimetic Spectral Element Methods

3.1. Introduction

Although in literature it has been difficult to classify clear distinctions between the classes of finite element methods with certain modifications and those of mixed finite element methods. However, for clear exposition of the basic ideas, Durán's conception of mixed FEM is quite relevant [15]: "Finite Element Methods in which two spaces are used to approximate two different variables receive the general denomination of mixed methods".

The motivation for implementing a mixed formulation is usually the need for computing a second field variable that is either related through derivatives to the primary unknown quantity or due to some physical interest. For instance, for elasticity problems, stress and displacement would be the two field quantities that need to be estimated simultaneously on two different spaces. Another case would be where the two variables are not directly coupled to one another such as the case of incompressible flows where the pressure and velocity variables, instead pressure is used as a Lagrange multiplier to enforce the conservation of mass.

Historically speaking, the development of these methods and their subsequent analysis methods are credited to the works of Brezzi [16, 17], Babuška[5], Crouzeix and Raviart [20], Falk and Osborn [26], and Fortin [31]. An example¹ would perhaps be the best way to illustrate the application of this formulation. We consider the following system:

$$\begin{aligned} -\nabla \cdot (a \nabla p) &= f \quad \text{in } \Omega \\ p &= 0 \quad \text{on } \partial\Omega \end{aligned}$$

where $\Omega \subset \mathbb{R}^n$ is the domain of computation and $a = a(x_1, x_2, \dots, x_n)$ is a bounded function coefficient². The mixed approach of creating two spaces for solution to be obtained is done through 'decoupling' the second order system into first-order equation systems:

$$\mathbf{u} = -a \nabla p,$$

This leads to the following equations:

$$\begin{aligned} \mathbf{u} + a \nabla p &= 0 \quad \text{in } \Omega, \\ \operatorname{div} \mathbf{u} &= f \quad \text{in } \Omega, \\ p &= 0 \quad \text{on } \partial\Omega. \end{aligned}$$

This first order system can now be implemented within a weak formulation using the Hilbert spaces of the *div* operator:

$$H(\operatorname{div}, \Omega) = \{\mathbf{v} \in L^2(\Omega)^n : \operatorname{div} \mathbf{v} \in L^2(\Omega)\}$$

¹This example is sourced from [15, p. 8].

²Generally speaking, a is a tensor, however a restriction to function confines us to a diagonal tensor with the same scalar quantity on the diagonal.

where, the test functions \mathbf{v} are supplied from this test space $H(\text{div}, \Omega)$. Considering, $\mu(x) = 1/a(x)^3$, we can write the weak mixed formulation as:

$$\begin{aligned} \int_{\Omega} \mu \mathbf{u} \cdot \mathbf{v} dx - \int_{\Omega} p \text{div } \mathbf{v} dx &= 0 & \forall \mathbf{v} \in H(\text{div}, \Omega), \\ \int_{\Omega} q \text{div } \mathbf{u} dx &= \int_{\Omega} f q dx & \forall q \in L^2(\Omega). \end{aligned}$$

This formulation admits into itself the Dirichlet boundary condition (implicitly) whereas the Neumann conditions would have to be imposed over the space as essential conditions. Furthermore, this weak formulation involves divergence of the solution and the test space and avoids arbitrary first derivatives on both. This allows for more flexibility or greater search space when looking for a solution in $H(\text{div}, \Omega)$ instead of the smaller $H^1(\Omega)^n$.

The example above seeks to illustrate the formulation and mechanism used for simpler yet challenging differential equation systems. For more sophisticated problems, such as the elasticity equations, the weak formulation also features the use of Lagrangian multipliers to enforce coupling between the boundary conditions, field properties (such as divergence of the vector or tensor fields etc.) and the primary as well as the secondary equation systems.

3.1.1. Mimetic Applications of Mixed FEM

As can be seen above the mixed finite element method applications have general applications for different physical and mathematical considerations in differential equation systems. But for the current brief, we are interested in exploring applications of this formulation within a mimetic context. As such we now look upon some of the work that serves as a precursor for the in-house research work covered in the following section. Through this line of thought, it is hoped that headway can be made towards discussing the differential forms-based framework where plenty of different mimetic formulations are found.

To understand the need for a differential-forms based framework (apart from the need for more efficient geometry-aware schemes), the reader is suggested a reading of Arnold et.al. [2], where the performance indicators of a finite element formulation is delineated into three categories viz. the approximation error, the consistency error and the stability constant. The respective functions of these three quantities are as follows —the approximation error measures the error between the true solution of the system and our best approximation using finite element solution spaces; the consistency error on the other hand is the measure of the how much ‘continuity’ is preserved when selecting the finite element solution (from the finite element solution space) with that of the true solution space. The stability constant is an indicator of the well-posedness of the finite dimensional problem obtained from our discretization of the governing equations.

While the first two of the quantities are deemed manageable while synthesizing the numerical schemes, the stability constant is not very easy to control as it is quite sensitive to the method chosen. Tackling or more accurately keeping track of how this stability depends on the finite dimensional model requires knowledge of deeper mathematical principles of geometry, topology and algebra. Thus, the following discussion can be seen as an exercise to establish better controls over the numerical stability of schemes. The mimetic finite difference methods (as majorly discussed in the three phases previously) are alongside several other classes of ‘mimetic’ methods that seek to implement geometrical properties.

Examples of such methods are the covolume methods [62], Finite Element Exterior Calculus (FEEC) [2] and Discrete Exterior Calculus (DEC) [21]. Despite some similarities or rather convergences when applied to simpler cases, the differences between these methods emerge

³alternatively, for the matrix a , $\mu = a^{-1}$

when problems of complicated nature appear. For instance, the mimetic finite differences and DEC operate over simplicial meshes as opposed to the differential forms which lie at the core of FEEC. Furthermore while it is possible to establish a map between differential forms over a simplex to simplicial cochains (which induces an isomorphism on the cohomology) [2], it is rather difficult to devise a reverse map that takes in cochains and gives out differential forms.

This missing piece was provided by Whitney [72] with an inverse de Rham map that associated any k -cochain with a piecewise linear differential k -form. Using this theory, Bossavit [11] led the work in the field of electromagnetics. He combined Whitney forms with his work on low-order finite element spaces for applications in electromagnetic systems [12–14] and in his series of ‘Japanese papers’. In a manner of extension to the work of Bossavit (who identified applications for lower-order Whitney forms), Hiptmair [36] explored higher order forms based differential forms of higher polynomial degrees.

There was however another scope of research in these works, that is, since these formulations were limited to real-valued differential forms, they did not consider structures with vector-valued or covector-valued differential forms. On the other hand, DEC aimed to build applications of exterior calculus over simplicial complexes with the foundational theory which included differential forms and discrete vector fields. While some work had been carried out in incorporating vector-fields into a cochain based approach with the help of exterior calculus [61, 67], it ultimately did not involve dual cochains and thus, failed to encode critical physical-geometric information into its framework. DEC, on the other hand, implemented a dual mesh approach that accomodated physical quantities related to the dual quantities such as the flux across boundaries [21]. Applications of DEC framework have been quite successful and appear in discussions on the applications of mimetics in solid and fluid mechanics [47, 73].

3.2. Development History at TU Delft

With the background of mimetic implementation in its various forms having been covered, the work being carried out at TU Delft and its history can be detailed. A good starting point for this survey would be the article by Gerritsma [34], where he highlights the mimetic formulation for quadrilaterals using new basis functions referred to as *edge functions*⁴. The mimetic framework he employs makes use of differential forms as opposed to a primary/derived operator framework (DVTC). Following from the discussions on differential geometry from the previous chapter, applications are drawn for the exact modeling of the governing partial differential equations and its discrete counterparts that would require additional concepts of algebraic topology and chain complexes.

3.2.1. The DeRahm Cohomology Revisited

Similar to how the generalized Stokes theorem provides a single expression for the integral operations transforming quantities defined on n -dimensions to $(n+1)$ -dimensional objects in a continuous manner, the discrete geometric approach is to identify sequences that map elements of one set to another. Consider for instance, the following mapping from Gerritsma [34, p. 50]:

$$H_S \xrightarrow{\text{div}} H_V \quad (3.1)$$

where H_S is the space of quantities defined on surfaces ($n=2$) and H_V is the space of variables defined over volumes ($n=3$). The divergence operator in this case, acts as the mapping function between these two sets. Similary, other transformations can be identified as well, in a sequence

⁴Gerritsma refers to these edge functions as “the extension of the classical Whitney forms to quadrilaterals” [34, p. 49]

of mappings, infact giving us:

$$\mathbb{H}_P \xrightarrow{\mathbf{grad}} \mathbb{H}_L \xrightarrow{\mathbf{curl}} \mathbb{H}_S \xrightarrow{\mathbf{div}} \mathbb{H}_V \quad (3.2)$$

Equation 3.4, when observed, displays properties of exactness as noted by Gerritsma [34, p. 51], “in the sense that the range of one of these operators is contained in the null space of the next operator”

$$\mathcal{R}(\mathbf{grad}) \subset \mathcal{N}(\mathbf{curl}) \text{ and } \mathcal{R}(\mathbf{curl}) \subset \mathcal{N}(\mathbf{div}) \quad (3.3)$$

This exactness leads to the identification of this sequence as a De Rahm complex of the form:

$$\mathbb{R} \longrightarrow \mathbb{H}_P \xrightarrow{\mathbf{grad}} \mathbb{H}_L \xrightarrow{\mathbf{curl}} \mathbb{H}_S \xrightarrow{\mathbf{div}} \mathbb{H}_V \longrightarrow 0 \quad (3.4)$$

This sequence is appropriate for use in cases upto 3-dimensions (\mathbb{R}^3) as indicated by the 0 at the end of this chain. In terms of numerical implementation we refer to [34, p. 51]—“in finite element methods, the spaces $\mathbb{H}_P, \mathbb{H}_L, \mathbb{H}_S,$ and \mathbb{H}_V are generally associated with the function spaces $H^1(\Omega), H(\mathbf{curl};\Omega), H(\mathbf{div};\Omega),$ and $L^2(\Omega),$ respectively”.

Furthermore, following from general concepts of linear algebra, the dual of a space such as $\mathbb{H}_P, \mathbb{H}_L, \mathbb{H}_S,$ and \mathbb{H}_V (defined over a field of real numbers, \mathbb{R}) consists of linear functionals φ such that the image of these spaces is in the set of real numbers. That is, for $\mathbb{H}_L,$ the dual space is $\varphi_L : \mathbb{H}_L \rightarrow \mathbb{R}.$ This space containing $\varphi \in \varphi_L$ is itself a vector space similar to $\mathbb{H}_L.$ Furthermore, it should be noted here that the dual space of a vector space is also a vector space in itself, that is, the space spanned by the dual of $\mathbb{H}_P, \mathbb{H}_L, \mathbb{H}_S,$ and \mathbb{H}_V is in itself a vector space.

Thus, owing to the analogies with differential concepts presented thus far, the sequences can replace the representations for $\{\mathbb{H}_P, \mathbb{H}_L, \mathbb{H}_S,$ and $\mathbb{H}_V\}$ with $\{\Lambda^0(\Omega), \Lambda^1(\Omega), \Lambda^2(\Omega),$ and $\Lambda^3(\Omega)\}.$ And since, the current discussion is restricted upto three-dimensional objects (\mathbb{R}^3), the dual space for these k -dimensional spaces will have dimensions upto $(n-k)$ —the dual space will change from $\{\varphi_P, \varphi_L, \varphi_S,$ and $\varphi_V\}$ with $\{\Lambda^3(\Omega), \Lambda^2(\Omega), \Lambda^1(\Omega),$ and $\Lambda^0(\Omega)\}.$

Thus, identifying the functional spaces with their respective differential forms, the following De Rahm chain is obtained:

$$\mathbb{R} \longrightarrow \Lambda^0(\Omega) \xrightarrow{d} \Lambda^1(\Omega) \xrightarrow{d} \Lambda^2(\Omega) \xrightarrow{d} \Lambda^3(\Omega) \xrightarrow{d} 0 \quad (3.5)$$

3.2.2. Reconstruction and Reduction

From a continuous formulation of the differential equation system to a discrete version fit for computational implementation (*reduction*) and vice versa *reconstruction* of the discrete solution space, this pipeline is implemented through the reduction and reconstruction operator, respectively.

The Reduction Operator

For a n -dimensional manifold $\Omega,$ considered covered by a cell complex, we assume the p -chains as p -dimensional submanifolds of $\Omega.$ For any differential form $a^{(p)}$ over a sub-manifold $\Lambda^p(\Omega),$ the reduction operator is defined using a duality relationship as,

$$\langle \mathcal{R}a^{(p)}, C_{(p)} \rangle := \int_{C_{(p)}} a^{(p)},$$

where the object $\mathcal{R}a^{(p)}$ is a p -cochain acting on a p -chain, $C_{(p)}.$ The reduction operator \mathcal{R} thus, when applied to the differential p -form maps onto a p -cochain. Expanding the p -chain $C_{(p)}$ into the p -cells of the cell complex,

$$C_p = \sum_{i=1}^{n_p} m_{(p),i} c_{(p),i},$$

and since the duality relationship is linear in nature and the p-cells are considered disjoint [34, p. 59], we obtain,

$$\langle \mathcal{R}a^{(p)}, \sum_{i=1}^{n_p} m_{(p),i} c_{(p),i} \rangle = \sum_{i=1}^{n_p} m_{(p),i} \langle \mathcal{R}a^{(p)}, c_{(p),i} \rangle.$$

The reduction operator is thus evaluated over the entire range of p-cells through integration.

Furthermore, the reduction operation commutes with the exterior derivative operator (or the coboundary operator on the discrete level) as shown in the equation 3.6,

$$\begin{array}{ccc} \Lambda^k(\Omega) & \xrightarrow{d} & \Lambda^{k+1}(\Omega) \\ \uparrow \mathcal{R} & & \uparrow \mathcal{R} \\ C^{(k)} & \xrightarrow{\delta} & C^{(k+1)} \end{array} \quad (3.6)$$

The Reconstruction Operator

The reconstruction operator, denoted by \mathcal{I} is used to obtain the continuous formulations from the discrete solution space values. Thus, this operator maps p-cochains onto differential p-forms. The reduction operator when applied to the reconstructed p-forms should again give the original p-cochains. In this manner, these operations are inverse⁵ to one another [42]:

$$\mathcal{R} \circ \mathcal{I} = I$$

The example applications of this operator, similar to the reduction operator are illustrated well by Gerritsma [34, p. 60-61].

3.3. Mimetic Spectral Element Framework

3.3.1. Notation

Throughout this treatment and in the following chapter, we seek to introduce a consistent notation scheme to refer to relevant parameters, characterizing both their nature and function. For instance, a vector is marked in boldface typeface, for instance \mathbf{v} for a vector-valued field function, f for a scalar-valued field function and \underline{g} to denote a tensor field. The grid construction depends on two key parameters, the polynomial order p and the polynomial mesh density, measured in the number of nodes, N . The polynomial mesh density, needs to be at least $N = p+1$ in order to successfully reconstruct the function spaces reduced by the polynomial nodes.

The mesh grid density is also characterized by the element size used to discretize the domain shape in the problem statement. This element size is noted as h , where its measure is determined by the number of discretized elements in the grid, denoted as k . The k-forms, as they correlate with the number of element discretizations used, are denoted using a superscript k as in $\varphi^{(k)}$. The dual spaces corresponding to these forms are denoted with a prime symbol occupying the superscript notation, as in Ω' . The fields (vectors, scalars and tensors) are all denoted with a superscript h , referring to the mesh size of reconstruction.

3.3.2. Grid Construction

Basis functions are used for interpolation of the field variables within a grid constructed over the computational domain. Current implementations of the mimetic method features spectral mimetic basis functions as the primal functions and whose algebraic dual can be computed [35]. The calculation of this algebraic dual requires the primal grid points and the definition of the inner product as defined on the finite dimensional space. The treatment surveyed here

⁵ \mathcal{I} is a right inverse of \mathcal{R} , but only an approximate left inverse

only considers the latest applications since previous applications also made use of nodal spectral elements in combination with Galerkin (GSEM) or a least-squares formulation (LSSEM) [48, p. 285]. The choice of using mimetic spectral element interpolation was made in order to achieve a pointwise divergence-free solution for all mesh sizes (all while satisfying the Ladyshenskaya–Babuška–Brezzi (LBB) stability conditions). This was not possible with the previous choice of methods since GSEM resulted in only a weakly-divergence free solution thus the divergence converged to zero only for refined meshes. Whereas, the LSSEM resulted in poor mass conservation properties.

The grid construction follows the Gauss-Lobatto-Legendre (GLL) formulation [35], where the root locations of the following polynomial (φ_{GLL}) determine the grid locations:

$$\varphi_{\text{GLL}} = (1-\xi^2) \frac{dL_p(\xi)}{d\xi}$$

where, L_p is a Legendre polynomial of degree p . This polynomial in itself can be admitted as a solution to the following differential equation:

$$\frac{d}{d\xi} \left((1-\xi^2) \frac{dL_p(\xi)}{d\xi} \right) + p(p+1)L_p(\xi) = 0$$

3.3.3. Primal Basis Functions

Once these grid locations are defined, the primal basis functions may be defined. Fisser [29] provides an overview of this construction, himself sourcing the derivations from [35]. Given the nodal and edge degrees of freedom, \mathcal{N}_i^0 and \mathcal{N}_i^1 respectively, the differential 0-form ($\lambda^{(0)}$) and 1-form ($\lambda^{(1)}$) are given as:

$$\begin{aligned} \lambda^{(0)}(\xi) &= \sum_{i=1}^{p+1} \mathcal{N}_i^0(\lambda^{(0)}) h_i(\xi) \\ \lambda^{(1)}(\xi) &= \sum_{i=1}^p \mathcal{N}_i^1(\lambda^{(1)}) e_i(\xi) \end{aligned}$$

where h_i and e_i are the nodal and edge basis functions respectively. Further, considering the computational domain restricted in the closed space $[-1,1]$, such that, $-1 = \xi_1 \leq \xi_2 \cdots \leq \xi_{p+1} = 1$, the nodal and edge degrees of freedom can be expressed as the following linear functionals [45],

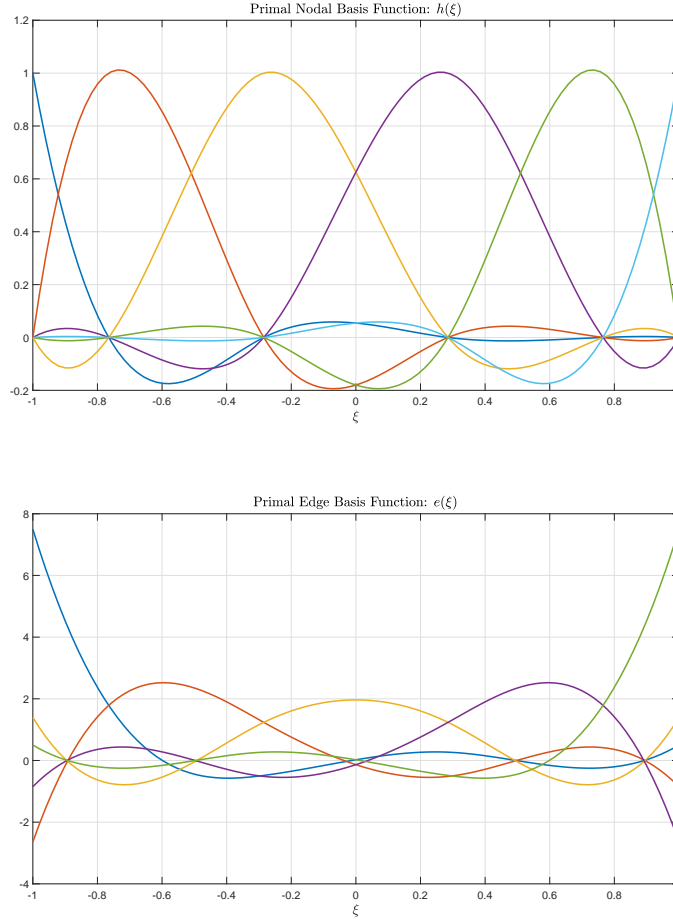
$$\begin{aligned} \mathcal{N}_i^0(\lambda^{(0)}) &\equiv \lambda^{(0)}(\xi_i) \\ \mathcal{N}_i^1(\lambda^{(1)}) &\equiv \int_{\xi_i}^{\xi_{i+1}} \lambda^{(1)}(\xi) \end{aligned}$$

The zero-form expansion includes the nodal expansion basis functions, h_i . These functions need to satisfy the following properties:

$$h_j(\xi_i) = \delta_{ij} = \begin{cases} 1, & \text{if } j = i \\ 0, & \text{if } j \neq i \end{cases}, \quad \forall i, j \in [1, p+1],$$

These properties are satisfied by the Lagrange polynomials constructed from $p+1$ data points. These nodal functions can then be defined as,

$$h_i(\xi) \equiv \prod_{k=1, k \neq i}^{p+1} \frac{\xi - \xi_k}{\xi_i - \xi_k},$$

Figure 3.1: Primal basis functions for $p=5$

Furthermore, the edge functions satisfy the following properties,

$$\int_{\xi_i}^{\xi_{i+1}} e_j = \delta_{ij} = \begin{cases} 1, & \text{if } j = i \\ 0, & \text{if } j \neq i \end{cases}, \quad \forall i, j \in [1, p].$$

The primal basis functions are shown in the Figure 3.1. The edge basis functions are related to the nodal basis functions over a GLL grid by,

$$e_j(\xi) = - \sum_{k=1}^j dh_k(\xi) \equiv - \sum_{k+1}^j \frac{dh_k(x)}{dx} dx = \varepsilon_j(x) dx.$$

3.3.4. Dual Basis Functions

Once these primal grid basis functions are determined, the algebraic dual basis are determined using mass matrices. The one dimensional mass matrix $\mathbb{M}_{1D}^{(0)}$ is given as,

$$\mathbb{M}_{1D}^{(0)} = \int_{\Omega} (\psi^0(\xi))^T \psi^0(\xi) d\Omega,$$

where the term $\psi^0(\xi)$ is the matrix representation of the primal nodal basis functions,

$$\psi^0(\xi) = [h_1(\xi), h_1(\xi), \dots, h_{p+1}(\xi)].$$

Consider the product of two 0-forms $\lambda^{(0)}(\xi)$ and $\pi^{(0)}(\xi)$, then the L^2 -inner product is given as,

$$(\lambda^{(0)}, \pi^{(0)})_{L^2(\Omega)} \equiv \int_{\Omega} \lambda^{(0)} \pi^{(0)} d\Omega = \int_{\Omega} (\mathcal{N}^0(\varphi))^T (\varphi^0(\xi))^T \varphi^0(\xi) \mathcal{N}^0(\pi)$$

where, the nodal degrees of freedom are represented in the matrix form as,

$$(\mathcal{N}^0(\varphi))^T = [\mathcal{N}_1^0(\varphi), \mathcal{N}_2^0(\varphi), \dots, \mathcal{N}_{p+1}^0(\varphi)],$$

the L^2 -inner product then becomes,

$$(\lambda^{(0)}, \pi^{(0)})_{L^2(\Omega)} = \int_{\Omega} (\mathcal{N}^0(\varphi))^T \mathbb{M}_{1D}^{(0)} \mathcal{N}^0(\pi),$$

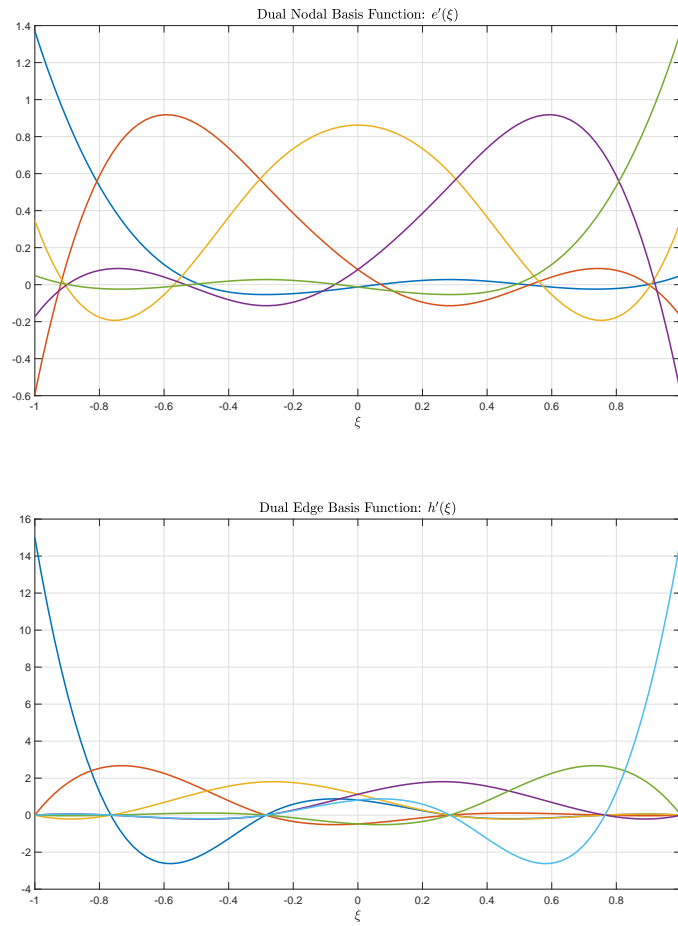
the dual basis function can then be defined as $\mathcal{N}'^1(\pi)$,

$$(\mathcal{N}^0(\varphi))^T \mathcal{N}'^1(\pi) \equiv (\mathcal{N}^0(\varphi))^T \underbrace{\mathbb{M}_{1D}^{(0)} \mathcal{N}^0(\pi)}_{\mathcal{N}'^1(\pi)},$$

and, similar to the functions on the primal basis functions, the dual basis functions $h'_j(\xi)$ obey the Kronecker-delta property such that $\mathcal{N}'^1(h'_j) = \delta_{ij}$. The dual nodal polynomials are then found to be:

$$\psi'^1(\xi) = \psi^0(\xi) (\mathbb{M}_{1D}^{(0)})^{-1}.$$

where, $\psi'^1(\xi) = [e'_1(\xi), e'_2(\xi), \dots, e'_{p+1}(\xi)]$. Similar expressions can be derived for the dual nodal polynomials corresponding to the one dimensional mass matrix $\mathbb{M}_{1D}^{(1)}$ [29, 35]. The dual algebraic polynomials are shown in the Figure 3.2.

Figure 3.2: Dual basis functions for $p=5$

3.3.5. Reduction and Reconstruction

We consider here, a purely mathematical exercise, that is the reduction and reconstruction of a scalar function over an unit square reference element Ω . We begin by illustrating the reduction operation followed by a reconstruction of the scalar field to the reference element numerically. For now, we consider a one-dimensional case, such that the element is given as $\xi = [-1, 1]$. Given the function $f(\xi)$, we *reduce* the function into coefficients or integration points through the discretization of the reference domain using $N+1$ Gauss-Lobatto Nodes, such that $-1 = \xi_0 < \xi_1 < \dots < \xi_N = 1$. These nodal points are then assigned an equal number of Lagrange basis polynomials (h) of the order N as discussed in the previous sections. Thus we may write the reconstruction as a result of the reduced point sets as:

$$f^h(\xi) = \sum_{i=0}^N f_i h_i(\xi), \quad \text{where, } f_i = f(\xi_i) d\xi \quad (3.7)$$

alternatively, the reduction can also be done using the primal edge basis functions. To achieve this, we assign to each of N edges created as a result of the discretization, N edge basis polynomials (e) of the order $(N-1)$ such that, we may write:

$$f^h(\xi) = \sum_{i=1}^N f_i e_i(\xi), \quad \text{where, } f_i = \int_{\xi_i}^{\xi_{i-1}} f(\xi) d\xi \quad (3.8)$$

Now we move towards the more interesting case of two-dimensional reduction and reconstruction operations. Assuming another scalar function $g(\xi, \eta)$ over the 2-D reference domain Ω , we write:

$$g_{kl} = \int_{\Omega} g(\xi, \eta) h_k(\xi) h_l'(\eta) d\Omega \quad (3.9)$$

Note here that mixed basis functions (a combination of the primal and dual Lagrange polynomials) have been used to compute the integration points for this function g . Once we obtain these integration points, we may reconstruct the numerical field distribution as shown:

$$g^h(\xi, \eta) = \sum_{i=1}^N \sum_{j=0}^N g_{ij} h_i'(\xi) h_j(\eta) \quad (3.10)$$

Since, we use the Lagrange polynomials over both the primal as well as dual function spaces, it becomes easier to compute the derivatives of these functions computed numerically. This is because upon differentiation, both dual as well as primal Lagrange polynomials yield their respective edge functions. Thus this mixture of Lagrangian polynomial based reduction and reconstruction is used in this research. Thus we say,

$$\begin{aligned} \frac{\partial g^h}{\partial \xi} &= \sum_{i=1}^{N+1} \sum_{j=0}^N [g_{i,j} - g_{i-1,j}] e_i'(\xi) h_j(\eta) \\ \frac{\partial g^h}{\partial \eta} &= \sum_{i=1}^N \sum_{j=1}^N [g_{i,j} - g_{i,j-1}] h_i'(\xi) e_j(\eta) \end{aligned} \quad (3.11)$$

note here that the boundary values for the integration points are supplied using additional information along the boundary $\partial\Omega$. We write that,

$$g_{0,j} = \int_{\partial\Omega} \sum_{j=0}^N g(\xi = -1, \eta) h_j'(\eta)$$

$$g_{N+1,j} = \int_{\partial\Omega} \sum_{j=0}^N g(\xi = 1, \eta) h_j'(\eta)$$

Reduction and reconstruction for vector fields can be computed using a similar procedure, such that, for a vector function $\mathbf{u} = [u(\xi, \eta), v(\xi, \eta)]^T$ we discretize the fields as follows

$$\int_{\Omega} u(\xi, \eta) h_k(\xi) h_l'(\eta) = u_{kl}$$

$$\int_{\Omega} v(\xi, \eta) h_k'(\xi) h_l(\eta) = v_{kl} \quad (3.12)$$

these integration points can then be used for the reconstruction of their respective component fields as:

$$u(\xi, \eta) = \sum_{i=1}^N \sum_{j=0}^N u_{ij} h_i'(\xi) h_j(\eta)$$

$$v(\xi, \eta) = \sum_{i=0}^N \sum_{j=1}^N v_{ij} h_i(\xi) h_j'(\eta) \quad (3.13)$$

such that the derivatives are computed as shown:

$$\frac{\partial u}{\partial \xi} = \sum_{i=1}^{N+1} \sum_{j=0}^N [u_{ij} - u_{i-1,j}] e_i'(\xi) h_j(\eta)$$

$$\frac{\partial u}{\partial \eta} = \sum_{i=1}^N \sum_{j=1}^N [u_{ij} - u_{i,j-1}] h_i'(\xi) e_j(\eta)$$

$$\frac{\partial v}{\partial \xi} = \sum_{i=1}^N \sum_{j=1}^N [v_{ij} - v_{i-1,j}] e_i(\xi) h_j'(\eta)$$

$$\frac{\partial v}{\partial \eta} = \sum_{i=1}^{N+1} \sum_{j=0}^N [v_{ij} - v_{i,j-1}] h_i(\xi) e_j'(\eta) \quad (3.14)$$

note again, that the boundary values are computed using similar approach as shown above, giving:

$$u_{0,j} = \int_{\partial\Omega} \sum_{j=0}^N g(\xi = -1) h_j'(\eta)$$

$$v_{i,0} = \int_{\partial\Omega} \sum_{i=0}^N v(\eta = -1) h_i'(\xi)$$

$$u_{N+1,j} = \int_{\partial\Omega} \sum_{j=0}^N g(\xi = 1) h_j'(\eta)$$

$$v_{N+1,i} = \int_{\partial\Omega} \sum_{i=0}^N v(\eta = 1) h_i'(\xi)$$

3.3.6. Error Computations

In this section, we discuss the numerical computation of the error in the reconstructed solutions when compared to the exact or analytical representations of the solutions. To do this, we in-

roduce the measures of errors considered in this research and used to measure the convergence properties of a finite element approximation ⁶.

Norms

The L^2 error norm is used in order to measure the error terms for different scalar as well as vector quantities. In order to do this, the space of square integrable functions over the domain Ω , $L^2(\Omega)$ is used, which is defined as [15]:

$$L^2(\Omega) = \left\{ f \mid \int_{\Omega} |f|^2 d\Omega = \|f\|_{L^2(\Omega)}^2 < \infty \right\}$$

when applied to scalar, say p , this error (between the exact value p^{ex} and the computed value p^{h}) is computed as:

$$\|\epsilon_p\|_{L^2(\Omega)}^2 = \int_{\Omega} (p^{\text{ex}}(\xi, \eta) - p^{\text{h}}(\xi, \eta))^2 d\Omega \quad (3.15)$$

which can be numerically computed as:

$$\|\epsilon_p\|_{L^2(\Omega)}^2 \approx \sum_r \sum_s (p^{\text{ex}}(\xi_r, \eta_s) - p^{\text{h}}(\xi_r, \eta_s))^2 w_r w_s \quad (3.16)$$

where w_r and w_s are the weights associated with a quadrature over a refined GLL mesh used to computed the integral of the squared-error difference.

Convergence

Following the error computations, understanding the convergence behavior of the approximation becomes important to conclude whether a superior accuracy of the approximation becomes possible upon refinement of numerical parameters. This is done through a relationship wherein, the error obtained above is related to the number of nodes used for refinement, $h = 1/K$, where K is the number of elements used,

$$\epsilon \propto h^{\alpha p}$$

where α is a positive, non-zero constant that indicates the optimality of the convergence with respect to a completely exponential convergence, p is polynomial order used in numerical computation. It is expected that for a linear increase in the polynomial order, there should be an exponential decrease in error. In this thesis only a single element implementation is shown, that is with $K=1$.

⁶In order to keep consistency, the description of errors and norms follows from [29]

How to Handle Curvature?

This chapter deals with the primary and core subject matter that this thesis aims to present, that is —discretization of curved geometries in numerical schemes. This is done by adapting the differential geometry treatment of the curvature in the fields over spacetime manifolds. This has downstream consequences over how the ideas of infinitesimals and derivatives over a generalized fields are computed. The sub-discipline of differential geometry that deals exclusively with this subject is that of *Gauge theory*. An excellent reference for this subject is the book by Baez and Muniain [6].

We begin with a brief overview of what does ‘curvature’ mean in the broader sense of the term when rooted in the context of differential geometry and how it can be analyzed over a spacetime manifold. A note is then presented on how mathematical physics of solid mechanics informs our choice of tools that are used in the analyses of function fields over these manifolds. Finally, a computational setup is presented where the methods of analysing the curvature effects are computed and the novelties that are introduced are explained.

4.1. Curvature over Manifolds

Gauge theory can be understood to be the generalization of the concepts of Lagrangian invariance (known as *Gauge invariance*) under transformations as was observed to be the case with Maxwell’s equations. As part of this generalization, key concepts of *bundles* and *connections* are needed. These ‘structures’ when imposed on a general field over the spacetime manifold, allows for the evaluation of the field values at different points of the manifold. To clarify the need for this structure, perhaps it is better to understand how our classical understanding of vector fields over an Euclidian space creates an illusion of a fixed vector space.

Consider a manifold M , where a simple field f can be imagined to exist:

$$f : M \rightarrow V$$

However, we immediately run into problems owing to the inadequate nature of this expression when applied globally to M . That is, this relationship, where points on M are mapped to a fixed vector space V , only holds for localized spaces (*charts*) on M . This is because, as opposed to the vector field that exists on M , this mapping acts on the tangent spaces of this vector field over a space. This implies that the values of the vector fields at different points on the manifold cannot be compared directly, since their vector spaces (where they ‘live’) are different (see Figure 4.1).

The consequences of this limitation imposes upon us another limitation when it comes to differentiating these vector fields (since that essentially requires differences over vector field values at different points). Structures proposed under the Gauge theory seek to remedy this situation. Essentially the different vector spaces over the manifold are sought to be consolidated under the notion of vector ‘bundles’ at each point in M . The vector fields, then become what are referred to as the ‘sections’ of these bundles. Consider the Figure 4.2 where this concept

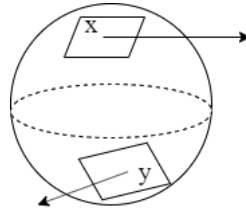
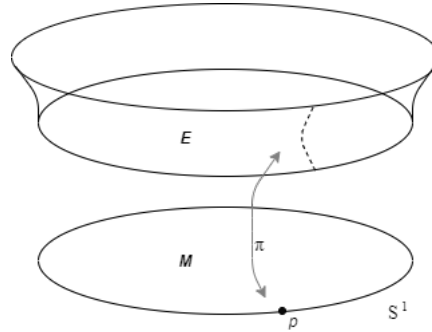


Figure 4.1: Tangent vectors defined over a spherical manifold.

Figure 4.2: A bundle $\pi: E \rightarrow M(S^1)$.

is illustrated. Here, the manifold space M is shown as a one-dimensional sphere S^1 or simply as a circle. This manifold is referred to as the *base space*, in the context of this bundle. The *projection* map π maps this base space to the *total space* E where the *fibres* over each point $p \in M$ are defined. For our purposes, it is sufficient to consider this total space to be the space of the tangent bundle over M . The total space then can be expressed simply as the totality of all the tangent bundle fibres over all the points in space:

$$TM = \bigcup_{p \in M} T_p M.$$

The projection, then can be written as: $\pi: TM \rightarrow M$. Here, π maps each tangent vector $v \in T_p M$ to the point $p \in M$. There are however, additional restrictions that can be placed on this basic idea such as that of being ‘locally trivial’ and that pertaining to ‘morphisms’. For the purposes of the present discussion, we assume all of the required qualifications to apply such that we approach the concept of a *real vector bundle*. Once this has been established, the concept of a *section* can be defined with an improved rigour. A section of a bundle $\pi: E \rightarrow M$ is a function $s: M \rightarrow E$ such that for any $p \in M$,

$$s(p) \in E_p.$$

thus, a section is an instrument that maps each point in the base space to a vector in the fibre over that point.

With these concepts introduced, it is perhaps appropriate to bring forth the idea of *connections*. Functionally, it is a mechanism that enables the differentiation of vector bundle sections. It is important to realize the need for this structure, since the differentiation operation requires addition (subtraction) between vector fibres over different points in the base space. A connection D on M then describes a mapping where each vector field v on M is assigned a function (or an operator) D_v within the spaces of sections of E , denoted as $\Gamma(E)$ [6]. With this, we are prepared for a segue into the concepts of *covariant differentiation* and *parallel transport*.

4.1.1. Covariant Derivatives

Continuing with the previous definition of a connection, we identify the function D_v with the following properties:

$$\begin{aligned} D_v(\alpha s) &= \alpha D_v s \\ D_v(s+t) &= D_v s + D_v t \\ D_v(fs) &= v(f)s + fD_v s \\ D_{v+w}(s) &= D_v s + D_w s \\ D_{fv}(s) &= fD_v s \end{aligned}$$

for all $v, w \in \text{Vect}(M)$, $s, t \in \Gamma(E)$, $f \in C^\infty(M)$ and all scalars α [6]. The reader should note here that the properties of this function are similar to that of a vector field and that the third property is just another version of the Leibniz law. This implies that the role of this function D_v is similar to that of differentiation. Thus, given any section s and a vector field v , the term $D_v s$ is called the *covariant derivative* of the section s in the direction v .

Principally, the covariant derivative is simply a reformulation of the notion of the *intrinsic derivative*¹ over a manifold. For a given tangent vector field \mathbf{v} to the manifold M , the tangent vector \mathbf{X} to M lies at p . Then the covariant derivative $\nabla_{\mathbf{X}}\mathbf{v}$ at p is then expressed in terms of the local coordinates as:

$$(\nabla_{\mathbf{X}}\mathbf{v})^\alpha = \left(\frac{\partial v^\alpha}{\partial u^\beta} + \Gamma_{\beta\gamma}^\alpha v^\gamma \right) X^\beta \quad (4.1)$$

In this equation, the terms Γ denote what are known as *Christoffel symbols*. Considering a coordinate frame², $\mathbf{e} = (\mathbf{e}_1, \dots, \mathbf{e}_n)$ in a region U . Then the vector field $\mathbf{X} = \mathbf{e}_j X^j$ in equation leads to the following:

$$\nabla_{\mathbf{X}}(\mathbf{e}_k \mathbf{v}^k) = X^j \mathbf{e}_i \omega_{jk}^i \mathbf{v}^k + X^j_j (\mathbf{v}^k) \mathbf{e}_k, \quad (4.2)$$

where the coefficients ω_{jk}^i are defined by,

$$\nabla_{\mathbf{e}_j}(\mathbf{e}_k) = \mathbf{e}_i \omega_{jk}^i. \quad (4.3)$$

It becomes pertinent to the discussion in this report, to consider the change of frames and the consequent effect on the covariant derivative and the associated Christoffel symbols. Consider the transformation matrix \mathbf{P} which is a non-singular $n \times n$ matrix function, which takes the coordinate space \mathbf{e} to $\mathbf{e}' = \mathbf{e}\mathbf{P}$. The vector \mathbf{v} then holds the following relationship:

$$\begin{aligned} \mathbf{v} &= \mathbf{e}\mathbf{v} = \mathbf{e}'\mathbf{v}' = \mathbf{e}\mathbf{P}\mathbf{v}', \\ \therefore \mathbf{v}' &= \mathbf{P}^{-1}\mathbf{v}. \end{aligned} \quad (4.4)$$

Furthermore, in order to evaluate the covariant derivative in a coordinate independent formulation, we need to define the transformational relationships between the change of frames. The dual σ of the coordinate basis also follows the transformation rules:

$$\mathbf{e}\sigma = \mathbf{I} = \mathbf{e}'\sigma' = \mathbf{e}\mathbf{P}\sigma'$$

¹The intrinsic derivative over a manifold is the projection of $d\mathbf{X}/dt$ into the tangent space ($\nabla\mathbf{X}/dt$) to M at any given point, where \mathbf{X} is a vector field defined over a curve C parameterized by t and is tangent to M .

²A *coordinate frame* is simply a special case of what is known as the *frame* of vector fields. A frame of vector fields consists of n linearly independent smooth vector fields $\mathbf{e} = (\mathbf{e}_1, \mathbf{e}_2, \dots, \mathbf{e}_n)$ in the region U . For a frame to qualify as a coordinate system, the vector fields $\mathbf{e}_i = \partial/\partial x^i$ are orthogonal to one another $[\mathbf{e}_i, \mathbf{e}_j] = [\partial_i, \partial_j] = 0$ [32, p. 243].

Furthermore, the differential operator ∇ transforms as shown:

$$\begin{aligned}\nabla \mathbf{e} &= \mathbf{e}\boldsymbol{\omega} \\ \text{and, } \nabla \mathbf{e}' &= \mathbf{e}'\boldsymbol{\omega}'\end{aligned}$$

The derivative over the transformed basis of the coordinate frames is then given as,

$$\nabla \mathbf{e}' = \nabla \mathbf{e}\mathbf{P} = (\nabla \mathbf{e})\mathbf{P} + \mathbf{e}d\mathbf{P} = \mathbf{e}\boldsymbol{\omega}\mathbf{P} + \mathbf{e}d\mathbf{P}$$

the Christoffel symbols in the transformed frame are given as,

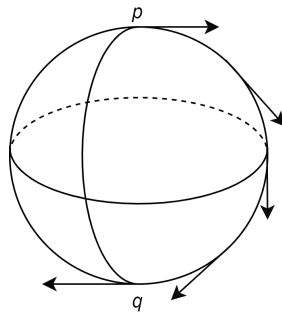
$$\boldsymbol{\omega}' = \mathbf{P}^{-1}\boldsymbol{\omega}\mathbf{P} + \mathbf{P}^{-1}d\mathbf{P}, \quad (4.5)$$

Considering the case for the basis coordinate frame (non-transformed grid) to orthogonal, we have that $\boldsymbol{\omega} = \mathbf{0}$. The new connection coefficients are then given as:

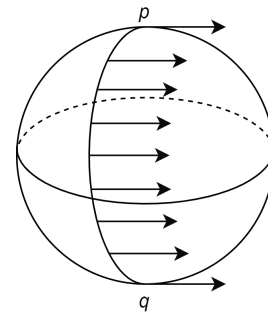
$$\boldsymbol{\omega}' = \mathbf{P}^{-1}d\mathbf{P}. \quad (4.6)$$

A Note on Parallel Transport

There is an important concept that is related to the discussion of connections over a curved manifold, known as *parallel transport*. The reader should recall that comparison of vectors lying in the fibres of a vector bundle over two different points p and q is not canonically possible. The construction of the connection structure allows for the differentiation of a section, however, there is an additional benefit to it. Consider a path γ between two points p and q and a connection over it. Parallel transport provides a canonical mechanism to ‘drag’ a vector over γ such that the vector over the fibre bundle p ends up at in the fibre bundle over q (see the Figure 4.3). If for a given path, the covariant derivative is obtained as zero, then the vector is said to have been “parallelly transported” along the path.



(a) Parallel translating a tangent vector along a path



(b) Parallel translating a tangent vector along another path

Figure 4.3: Illustration of parallel transport of a tangent vector over a spherical manifold (TS^2) [6, p. 232].

4.1.2. Lie Derivatives

In the above subsection, we identified a mechanism to generalize the notion of intrinsic derivative of a manifold space. This is loosely related to the idea of a directional derivative. However, a much more significant generalization of the directional derivative is given in the form of the *Lie derivative*. This subsection gives a brief overview of this idea, just for the sake of completeness of the subject matter being discussed at hand.

Similar to how the construct of connections were utilized to provide a framework for evaluating the curvature of a manifold through covariant differentiation, there are certain structures

that are required for the introduction of Lie derivatives over a manifold space. In previous chapters the reader was introduced to these structures, namely *flow* and the *Lie bracket*.

Effectively, the Lie bracket allows us to measure how much the commutativity of mixed directional derivatives over a manifold space ‘fails’ by. This is done by the operation known as the *commutator*, wherein for any two given vector fields a third vector field is generated. Given, $v, w \in \text{Vect}(M)$, the commutator or the Lie bracket $[v, w]$ is defined as:

$$[v, w](f) = v(w(f)) - w(v(f)), \quad (4.7)$$

for all $f \in C^\infty(M)$. Thus,

$$[v, w](f) = vw - wv.$$

For ordinary mixed partial derivatives, the vector fields commute and thus the Lie bracket is zero. However, for vector fields such as the one shown in Figure 4.4 below, the fields do not commute.

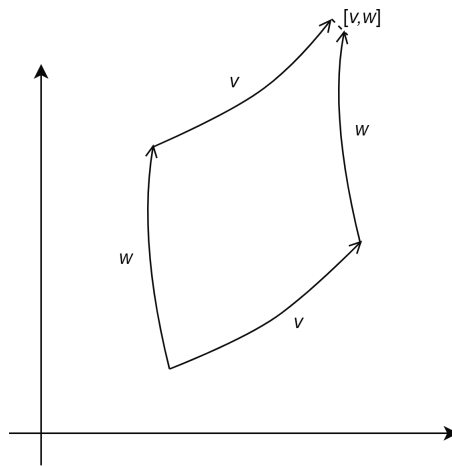


Figure 4.4: A case of non-commutativity of v and w , $[v, w] \neq 0$ [6].

Finally, the Lie derivative, built off of this idea, enables us to differentiate vector fields with respect to one another (similar to how the vector fields allow differentiation of functions defined on a manifold space). The need for a distinct operator such as the Lie derivative was illustrated in the Figure 2.3. When evaluated over two different points over a flow $\gamma(t)$, the tangent vectors over the vector fields at these two points belong to two different spaces. In order to find the directional derivatives over this flow, the spaces must be reconciled. This is done through the ‘pullback’ operator $d(\gamma_{-t})$ marked in blue. In this manner, the tangent vector for point $\gamma(t)$ is obtained within the tangent vector space at $\gamma(0)$ as $d(\gamma_{-t})_{\gamma_0} W_{\gamma_t}$. The Lie derivative, $\mathcal{L}_V W$ thus computes the directional derivative of the vector field W with respect to V .

$$(\mathcal{L}_V W)_p = \left. \frac{d}{dt} \right|_{t=0} d(\theta_{-t})_{\theta_t(p)} (W_{\theta_t(p)}) = \lim_{t \rightarrow 0} \frac{d(\theta_{-t})_{\theta_t(p)} (W_{\theta_t(p)} - W_p)}{t} \quad (4.8)$$

4.2. Which derivative to choose?

Having considered two derivatives on curved spaces, it becomes pertinent to identify the operator to be used for our purposes. The primary aim of the research presented here is to develop extensibility for the existing strongly conserved mass and momentum methods developed by

Fisser [29] over curved geometries, the due consideration of the choice of operator is made in this context.

While Lie derivatives allow the analysis of curved geometries by evaluating the derivatives of vector fields with respect to one another, they do not allow for parallel transport which is a necessity considering the Lagrangian formulation of many flow phenomena problems wherein conservation of properties in an element requires a comparison across a geodesic that is akin to parallel transport considerations. In their paper, Kanson et.al. [47] provided a mathematical formulation of the stress field in the classical theory of continuum mechanics where covector-valued differential two-forms were used. Furthermore, the balance laws along with the other fundamental laws were rewritten using covariant derivatives within the framework of energy balance. Our approach here, is somewhat informed by their approach along with Frankel's [32] treatment of solid mechanics where mechanical stress is treated as a vector-valued two-form.

This means, that in the (co-)vector framework of continuum mechanics, the standard stresses when replaced with the (n-1)-forms (in n -dimensional ambient space) represent a covariant derivation of balance laws and constitutive relations without taking the classical nature of stress as a two-tensor into account. This, the authors Kanson et.al believe reflects a more natural formulation of continuum mechanics. It is this consideration that pushes this research in the direction of covariant discretization of curvature so that this representation of mechanical stress may be utilized with the existing research of [29].

4.3. Commutativity of the Exterior Derivative

We now establish the commutative nature of the covariant exterior derivative, as this would be useful in situations of transformations which lead a change of frames.

We refer to Frankel [32, p. 253], in order to describe the operator ∇ applied to a vector field \mathbf{v} , such that ∇ is basis-free. For a given frame, with the basis \mathbf{e} , we write,

$$\mathbf{v} = \mathbf{e}v$$

such that, due a change of frame to \mathbf{e}' , we obtain,

$$\mathbf{v} = \mathbf{e}v = \mathbf{e}'v'$$

then we write,

$$\begin{aligned} \nabla \mathbf{v} &= \mathbf{e}(dv + \omega v) \\ \Rightarrow \nabla \mathbf{v} &= \mathbf{e}'P^{-1}(dv + \omega v), \quad (\text{from eqn. 4.4}) \end{aligned} \quad (4.9)$$

we know that from equation 4.4,

$$\begin{aligned} v &= Pv' \\ \Rightarrow dv &= (dP)v' + P(dv') \end{aligned}$$

using this in equation 4.9, we see that,

$$\begin{aligned} \nabla \mathbf{v} &= \mathbf{e}'P^{-1}[(dP)v' + P(dv') + \omega Pv'] \\ \Rightarrow \nabla \mathbf{v} &= \mathbf{e}'P^{-1}[(dP)v' + P(dv') + (P\omega' - dP)v'], \quad (\text{from eqn 4.5}) \\ \Rightarrow \nabla \mathbf{v} &= \mathbf{e}'P^{-1}[P(dv' + \omega'v')] \\ \Rightarrow \nabla \mathbf{v} &= \mathbf{e}'(dv' + \omega'v') = \nabla \mathbf{v}' \end{aligned} \quad (4.10)$$

Thus, we obtain the following commutativity between the change of coordinate systems ³:

$$\begin{array}{ccc} \mathbf{v}(x_1, x_2, \dots, x_i) & \xrightarrow{\nabla} & \nabla \mathbf{v}(x_1, x_2, \dots, x_i) \\ \uparrow \mathbf{P} & & \uparrow \mathbf{P} \\ \mathbf{v}(\xi_1, \xi_2, \dots, \xi_i) & \xrightarrow{\nabla} & \nabla \mathbf{v}(\xi_1, \xi_2, \dots, \xi_i) \end{array}$$

Having established the commutativity of the exterior derivative with transformations, we now look at specific examples and evaluate these terms analytically as well as computationally.

4.4. Deriving Function Space with Curvatures

4.4.1. Mapping from physical domains

In this section, we focus on deriving transformed function spaces that allow for conversion between our general reference element (\mathbf{K}) function spaces and those of the physical domain Ω_k . Thus, we denote through $\mathbf{K} := [-1, 1]^2$ the domain we constructed in the previous chapter and the arbitrary element, here referred to as the physical domain, as $\Omega_k \subset \mathbb{R}^2$ in two dimensions ⁴.

This transformation is obtained through the two element domains is obtained through a diffeomorphism in the fashion of a transfinite mapping φ_k , such that

$$\varphi_k : (\xi, \eta) \in \mathbf{K} \mapsto (x, y) \in \Omega_k \quad \text{and} \quad \mathbf{J} := \begin{bmatrix} \frac{\partial \varphi_k^x}{\partial \xi} & \frac{\partial \varphi_k^x}{\partial \eta} \\ \frac{\partial \varphi_k^y}{\partial \xi} & \frac{\partial \varphi_k^y}{\partial \eta} \end{bmatrix} \quad (4.11)$$

where, \mathbf{J} is the Jacobian tensor of the mapping φ_k . Furthermore, the transformation rules for scalar and vector-valued function spaces are defined in the following sub-sections.

Transforming a scalar-valued function space

Assume a pointwise scalar-valued function $\bar{f} \in C(\mathbf{K})$ on \mathbf{K} , we define the physical domain version of this function $f \in C(\Omega_k)$ on Ω_k as,

$$f := (\varphi_k^*)^{-1}[\bar{f}] = \bar{f} \circ \varphi_k^{-1}$$

where, φ_k^* is the pullback operator defined for this mapping. This leads to the following relation,

$$\bar{f} := (\varphi_k^*)[f] = f \circ \varphi_k$$

Finally, in the interest of completeness, we also write the rules of inner product of function spaces $f, g \in C(\Omega_k)$ as,

$$(f, g)_{\Omega_k} := \int_{\Omega_k} f g d\Omega = \int_{\varphi_k(\mathbf{K})} f g d\Omega = \int_{\mathbf{K}} \bar{f} \bar{g} \det(\mathbf{J}) d\mathbf{K}$$

Transforming a vector-valued function space

Similar to the section above and in keeping with [45], we define the transformation rules for a vector field $\bar{\mathbf{u}} \in D(\mathbf{K})$, such that this space maps onto the transformed vector field $\mathbf{u} \in D(\Omega_k)$, and is given by

$$\mathbf{u} := (\varphi_k^*)^{-1}[\bar{\mathbf{u}}] = \frac{1}{\det(\mathbf{J} \circ \varphi^{-1})} (\mathbf{J} \circ \varphi^{-1})(\bar{\mathbf{u}} \circ \varphi_k^{-1})$$

³Commutativity between different coordinate systems came up during a discussion with Marc Gerritsma, TU Delft.

⁴The notation used here and the treatment provided is similar to the work of Jain et.al. [45].

again, the pullback operator allows for the computation of the inverse of this transformation as:

$$\bar{\mathbf{u}} := \varphi_k^*[\mathbf{u}] = \det(\mathbf{J})\mathbf{J}^{-1}(\mathbf{u} \circ \varphi_k)$$

The inner product for the two vector fields, $\mathbf{u}, \mathbf{v} \in D(\Omega_k)$ on Ω_k is given as

$$(\mathbf{u}, \mathbf{v})_{\Omega_k} := \int_{\Omega_k} \mathbf{u}^T \mathbf{v} d\Omega = \int_K (\varphi_k^*[\mathbf{u}])^T \mathbf{J}^T \mathbf{J} \varphi_k^*[\mathbf{v}] \frac{1}{\det(\mathbf{J})} dK = \int_K \bar{\mathbf{u}}^T \mathbf{J}^T \mathbf{J} \bar{\mathbf{v}} \frac{1}{\det(\mathbf{J})} dK$$

4.4.2. Example transformation: non-linear bulk shear parallel to the horizontal axis

Following the blueprint of the transfinite mapping and its computations for vector and scalar valued functions, we consider an example of a mapping between the reference element $\mathbf{K} := [-1, 1]^2$ and the non-linear bulk shear domain $\Omega_k \subset \mathbb{R}^2$ (see Figure 4.5). The shear skewness is non-linear in η and linear in ξ , and is given by:

$$\begin{aligned} x &= \xi + 0.05(3 + \eta)^2; & -0.8 \leq x \leq 1.8 \\ y &= \eta + 2; & 1 \leq y \leq 3 \end{aligned} \quad (4.12)$$

The Jacobian for this transformation is then given as:

$$\mathbf{J} \circ \Phi_k = \begin{bmatrix} 1 & 0.1(3 + \eta) \\ 0 & 1 \end{bmatrix} \quad (4.13)$$

The Jacobian for the inverse of the transformation is then computed as:

$$\mathbf{J} \circ \Phi_k^{-1} := \begin{bmatrix} 1 & -0.1(1 + y) \\ 0 & 1 \end{bmatrix} \quad (4.14)$$

Furthermore, the determinant⁵ is:

$$\det(\mathbf{J} \circ \Phi_k^{-1}) := \det \begin{pmatrix} 1 & -0.1(1 + y) \\ 0 & 1 \end{pmatrix} = 1 \quad (4.15)$$

⁵Note that the equation 4.15 indicates that the volume of the domain is preserved and no dilation occurs during the deformation transformation since the determinant is found to be unity.

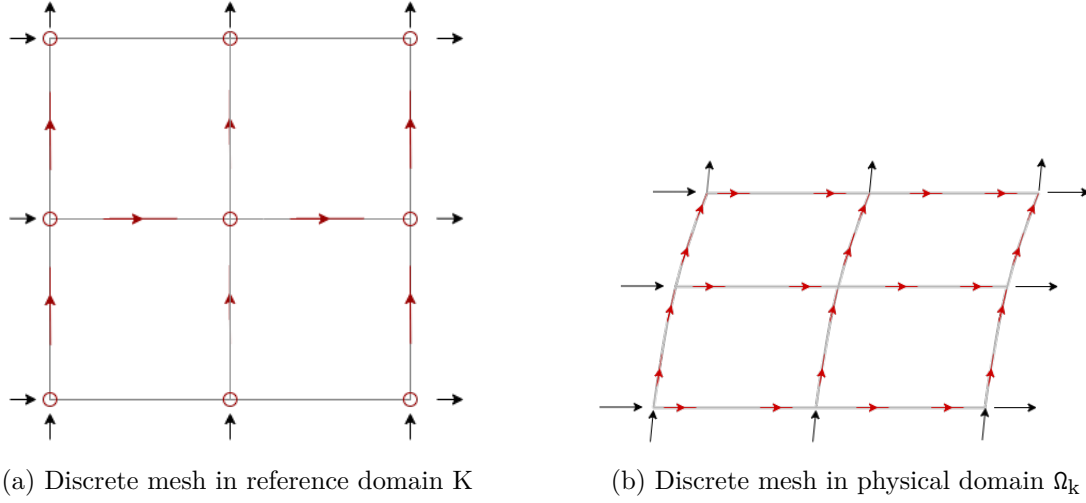


Figure 4.5: Discrete mesh systems in different domains with positive directions for flow assigned

Computing the Covariant Derivative

For the transformation in the equation 4.12, the following connections one-forms are obtained:

$$\begin{cases} \frac{\partial}{\partial x} = \frac{\partial}{\partial \xi} \frac{\partial \xi}{\partial x} + \frac{\partial}{\partial \eta} \frac{\partial \eta}{\partial x} = 1 \frac{\partial}{\partial \xi} + 0 \frac{\partial}{\partial \eta} \\ \frac{\partial}{\partial y} = \frac{\partial}{\partial \xi} \frac{\partial \xi}{\partial y} + \frac{\partial}{\partial \eta} \frac{\partial \eta}{\partial y} = -0.1(1+y) \frac{\partial}{\partial \xi} + 1 \frac{\partial}{\partial \eta} \end{cases} \quad (4.16)$$

therefore we write that the matrix P as,

$$\left(\frac{\partial}{\partial x}, \frac{\partial}{\partial y} \right) = \left(\frac{\partial}{\partial \xi}, \frac{\partial}{\partial \eta} \right) \underbrace{\begin{pmatrix} 1 & -0.1(1+y) \\ 0 & 1 \end{pmatrix}}_P \quad (4.17)$$

This then leads to the following terms,

$$\begin{aligned} P^{-1} &= \begin{pmatrix} 1 & 0.1(1+y) \\ 0 & 1 \end{pmatrix} \\ dP &= \begin{pmatrix} 0 & 0.1 dy \\ 0 & 0 \end{pmatrix} \\ \omega' &= P^{-1} dP = \begin{pmatrix} 0 & 0.1 dy \\ 0 & 0 \end{pmatrix} \end{aligned}$$

Transforming a scalar function

Consider the scalar-valued function \bar{f} defined over the points of the physical domain, Ω_k defined below,

$$f(x,y) = 2\pi \cos(\pi x) \sin(\pi y), \quad \text{where, } x, y \in \Omega_k \quad (4.18)$$

$$\begin{aligned} \frac{\partial f}{\partial x} &= -2\pi^2 \sin(\pi x) \sin(\pi y) \\ \frac{\partial f}{\partial y} &= 2\pi^2 \cos(\pi x) \cos(\pi y) \end{aligned} \quad (4.19)$$

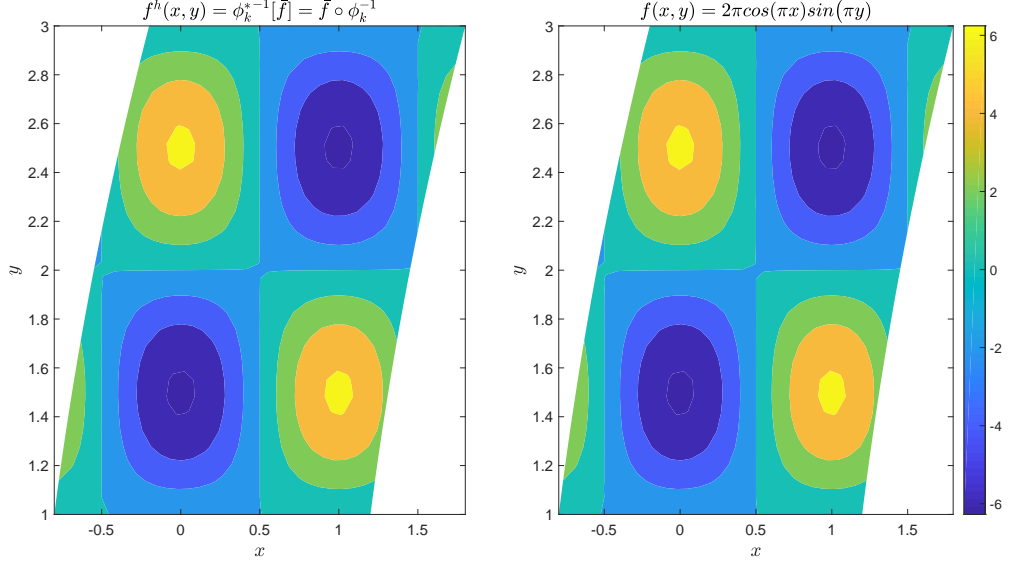


Figure 4.6: Reconstructed function $f^h(x,y)$ computed as a result of a pullback $(\varphi_k^*)^{-1}[\bar{f}] = \bar{f} \circ \varphi_k^{-1}$ interpolated with primal and algebraic dual nodal functions (left) and exact function $f(x,y)$ (right). The results are plotted over the shear deformed domain Ω_k . Polynomial order, $p = 15$.

Pullback into the reference element K , we obtain the transformed scalar function as,

$$\bar{f}(\xi, \eta) = 2\pi \cos[\pi(\xi + 0.05(3 + \eta)^2)] \sin[\pi(\eta + 2)], \quad \text{where, } \xi, \eta \in K \quad (4.20)$$

We begin to consider the derivatives of these functions on both domains, the reference or physical:

$$\begin{aligned} \frac{\partial \bar{f}}{\partial \xi} &= \frac{\partial f}{\partial x} \frac{\partial x}{\partial \xi} + \frac{\partial f}{\partial y} \frac{\partial y}{\partial \xi} \\ \frac{\partial \bar{f}}{\partial \eta} &= \frac{\partial f}{\partial x} \frac{\partial x}{\partial \eta} + \frac{\partial f}{\partial y} \frac{\partial y}{\partial \eta} \end{aligned} \quad (4.21)$$

computing the derivatives with respect to reference coordinates gives us,

$$\begin{aligned} \frac{\partial \bar{f}}{\partial \xi} &= -2\pi^2 \sin[\pi(\xi + 0.05(3 + \eta)^2)] \sin[\pi(\eta + 2)] \\ \frac{\partial \bar{f}}{\partial \eta} &= 2\pi^2 \cos[\pi(\xi + 0.05(3 + \eta)^2)] \cos[\pi(\eta + 2)] \\ &\quad - 0.02\pi^2(3 + \eta) \sin[\pi(\xi + 0.05(3 + \eta)^2)] \sin[\pi(\eta + 2)] \end{aligned} \quad (4.22)$$

Equations 4.20 and 4.18 are plotted over the respective domains $(\xi, \eta) \subset K$ in Figure 4.7 and $(x, y) \subset \Omega_k$ in Figure 4.6. The nature of the deformation in the shape of the domain is clearly visible. The curvature, thus introduced into the orthogonal nature of the Cartesian grid of K can be seen if one considers the mapping $\varphi_k^{-1} : (x, y) \in \Omega_k \mapsto (\xi, \eta) \in K$ acting over K .

We now turn our attention towards the computation of derivatives, as noted in the equations 4.19, 4.21 and 4.22. The challenge lies in computing the derivatives over the physical domain (grid) without performing discretization over this domain. Unlike the previous Figure 4.6 where

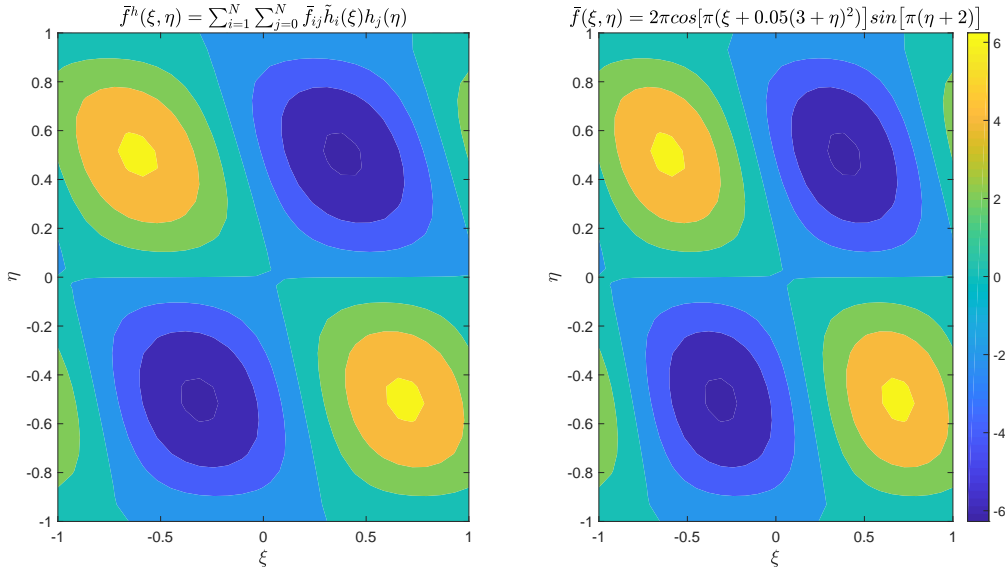


Figure 4.7: Reconstructed function $\bar{f}^h(\xi, \eta)$ interpolated with primal and algebraic dual nodal functions (left) and exact function $\bar{f}(\xi, \eta)$ (right). This reconstruction over the reference element is created through a mix of primal and dual nodal polynomials. Polynomial order, $p = 15$.

the scalar function was computed by simple exchange of coordinates themselves (application of the mapping function in the implementation), the computation of the derivatives relies upon the commutative property of the exterior derivative with the transformation as discussed in the section 4.3.

Let us now, consider how this commutative exterior derivative, when applied to the matrix of derivatives (over the reference element) leads to the computation of the derivatives over the physical domain. As seen in equation 4.19, we know that,

$$\begin{aligned}\frac{\partial \bar{f}}{\partial \xi} &= \frac{\partial f}{\partial x} \frac{\partial x}{\partial \xi} + \frac{\partial f}{\partial y} \frac{\partial y}{\partial \xi} \\ \frac{\partial \bar{f}}{\partial \eta} &= \frac{\partial f}{\partial x} \frac{\partial x}{\partial \eta} + \frac{\partial f}{\partial y} \frac{\partial y}{\partial \eta}\end{aligned}$$

alternatively, we can write,

$$\begin{aligned}\frac{\partial f}{\partial x} &= \frac{\partial \bar{f}}{\partial \xi} \frac{\partial \xi}{\partial x} + \frac{\partial \bar{f}}{\partial \eta} \frac{\partial \eta}{\partial x} \\ \frac{\partial f}{\partial y} &= \frac{\partial \bar{f}}{\partial \xi} \frac{\partial \xi}{\partial y} + \frac{\partial \bar{f}}{\partial \eta} \frac{\partial \eta}{\partial y}\end{aligned}$$

simplifying further, this gives,

$$\begin{bmatrix} \frac{\partial f}{\partial x} \\ \frac{\partial f}{\partial y} \end{bmatrix} = \underbrace{\begin{bmatrix} \frac{\partial \xi}{\partial x} & \frac{\partial \eta}{\partial x} \\ \frac{\partial \xi}{\partial y} & \frac{\partial \eta}{\partial y} \end{bmatrix}}_P \begin{bmatrix} \frac{\partial \bar{f}}{\partial \xi} \\ \frac{\partial \bar{f}}{\partial \eta} \end{bmatrix}$$

Thus, we are able to construct the field space of derivatives without actually performing the exterior derivation over the physical domain, as it commutes with the transformation matrix. Reader can verify that upon implementation of this matrix multiplication to the equation 4.19 does indeed produce 4.22. Using this principle, we can now plot the derivatives for the scalar function f over x and y .

Given the matrix P as in the equation 4.17, we can see that there is no difference in the derivative $\frac{\partial \bar{f}}{\partial x}$ and $\frac{\partial f}{\partial \xi}$ (since, $\frac{\partial \xi}{\partial x} = 1$ and $\frac{\partial \eta}{\partial x} = 0$). This is seen in the Figure 4.8, where the partial derivative for the field function does not vary at all. For the derivative $\frac{\partial \bar{f}}{\partial y}$ however, this is not the case (Figure 4.9). Upon application of the transformation correct (represented through the Jacobian), the exact derivative is reconstructed from the deformed derivative, reconstructed over a reference element.

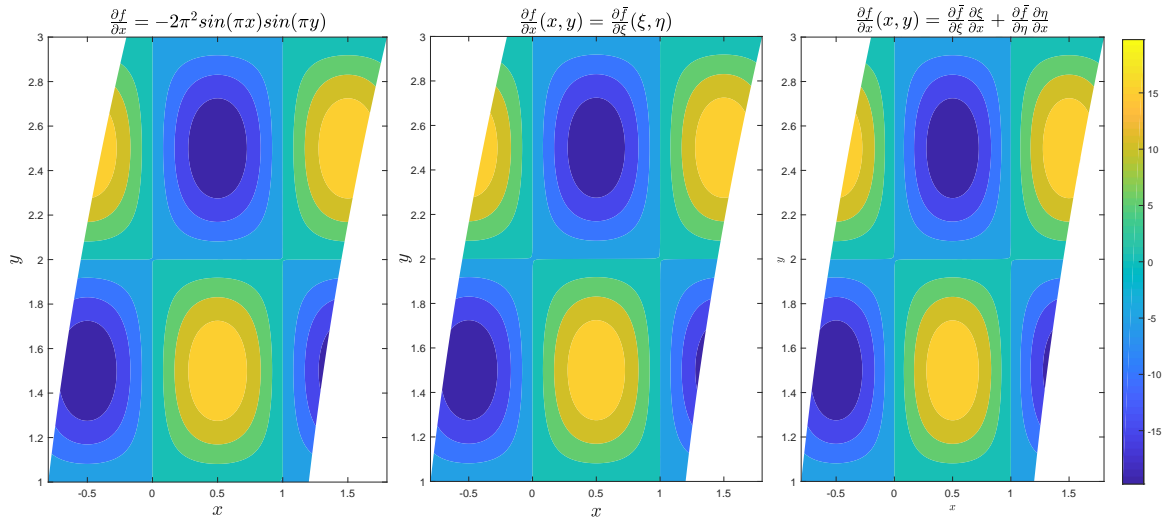


Figure 4.8: Exact function $\frac{\partial f}{\partial x}(x,y)$ (left), reconstructed function $\frac{\partial \bar{f}^h}{\partial \xi}(\xi,\eta)$ without transformation φ_k (center), and reconstructed function $\frac{\partial \bar{f}^h}{\partial x}(x,y)$ transformed using $\frac{\partial \bar{f}^h}{\partial \xi}(\xi,\eta)$ and φ_k (right). This reconstruction over the reference element is created through a mix of primal and dual nodal polynomials. Polynomial order, $p = 15$.

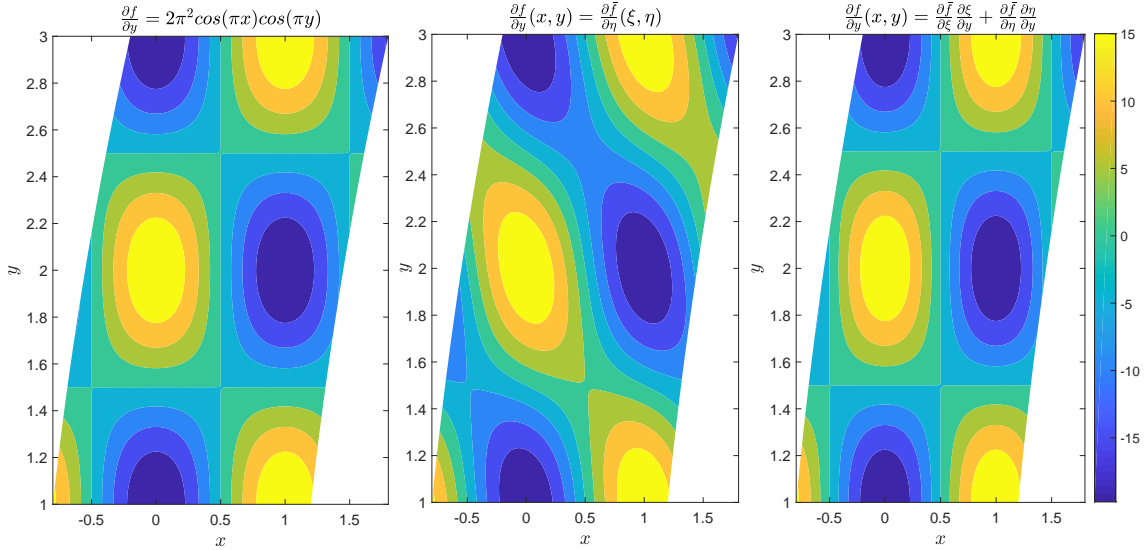


Figure 4.9: Exact function $\frac{\partial f}{\partial y}(x, y)$ (left), reconstructed function $\frac{\partial \bar{f}}{\partial \eta}(\xi, \eta)$ without transformation φ_k (center), and reconstructed function $\frac{\partial \bar{f}}{\partial y}(x, y)$ transformed using $\frac{\partial \bar{f}}{\partial \eta}(\xi, \eta)$, $\frac{\partial \bar{f}}{\partial \xi}(\xi, \eta)$ and φ_k (right). This reconstruction over the reference element is created through a mix of primal and dual nodal polynomials. Polynomial order, $p = 15$.

Error and convergence

We now compute the p-convergence behavior of this reconstruction for the scalar-valued field function \bar{f} . The semi-log plot of the error with respect to the polynomial order of interpolation is shown in figures 4.10. It can be seen that an exponential convergence is obtained, for a single element interpolation case. Note that this convergence behavior would increase if the number of elements were to be increased (convergence would then be achieved at a smaller polynomial order). Finally, to illustrate the error distribution for a sample case of interpolation error we can consider the figures shown in 4.11.

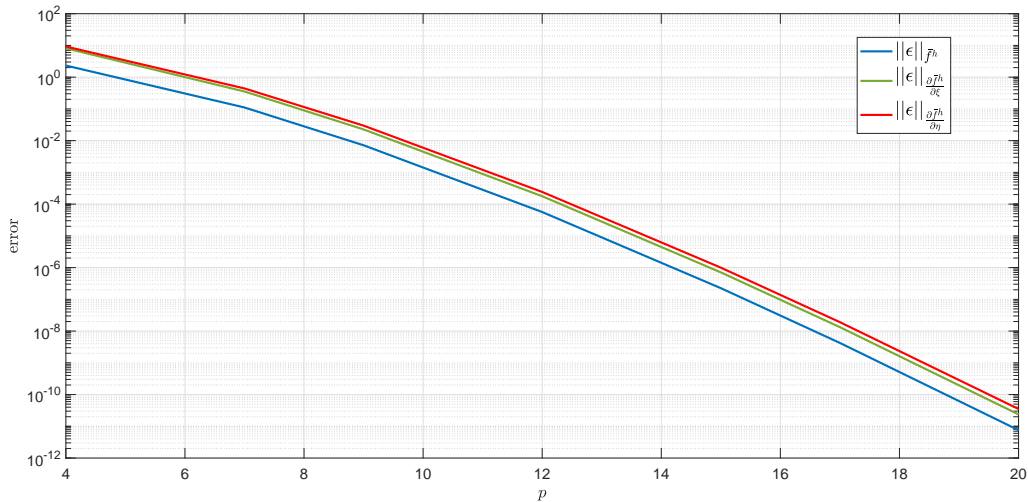
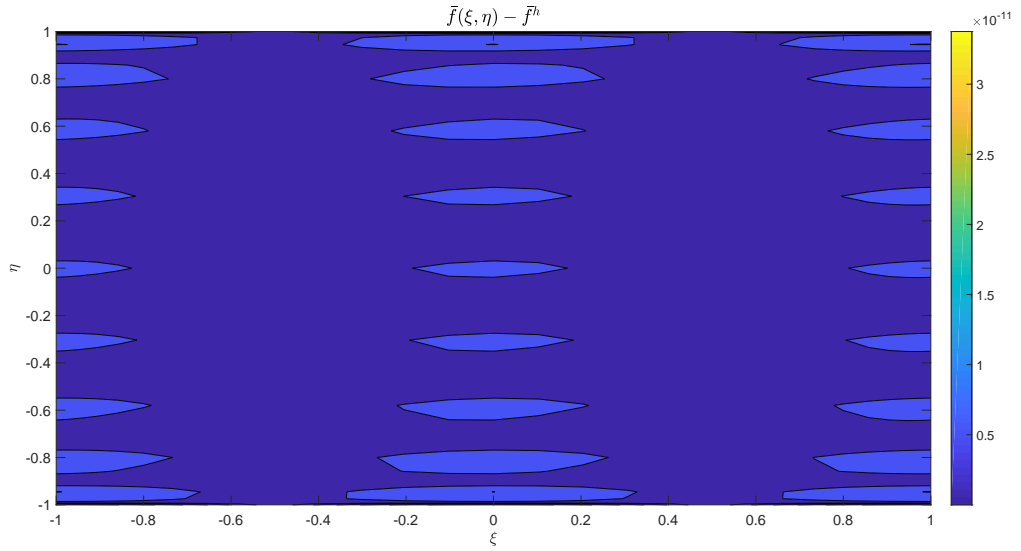
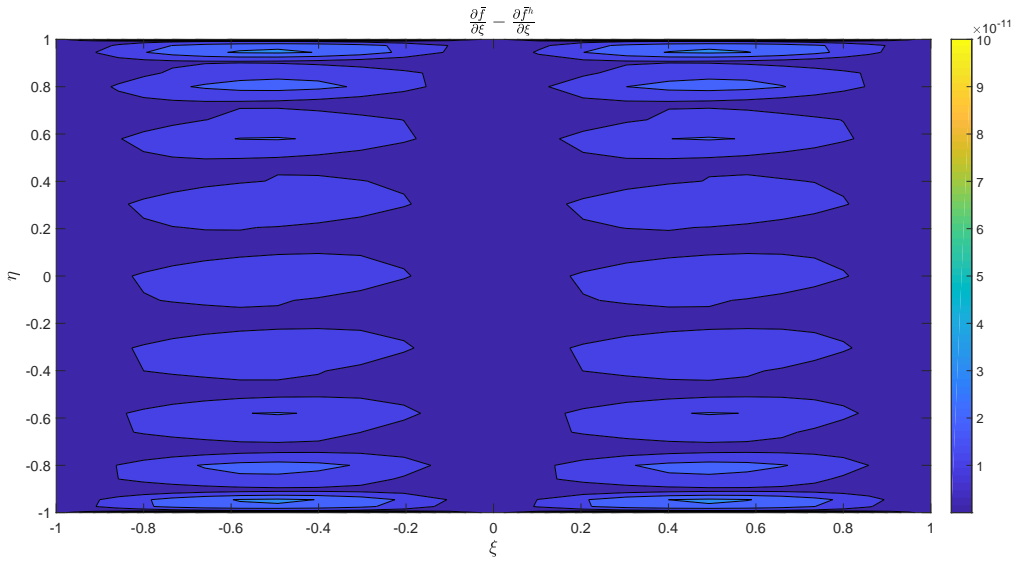


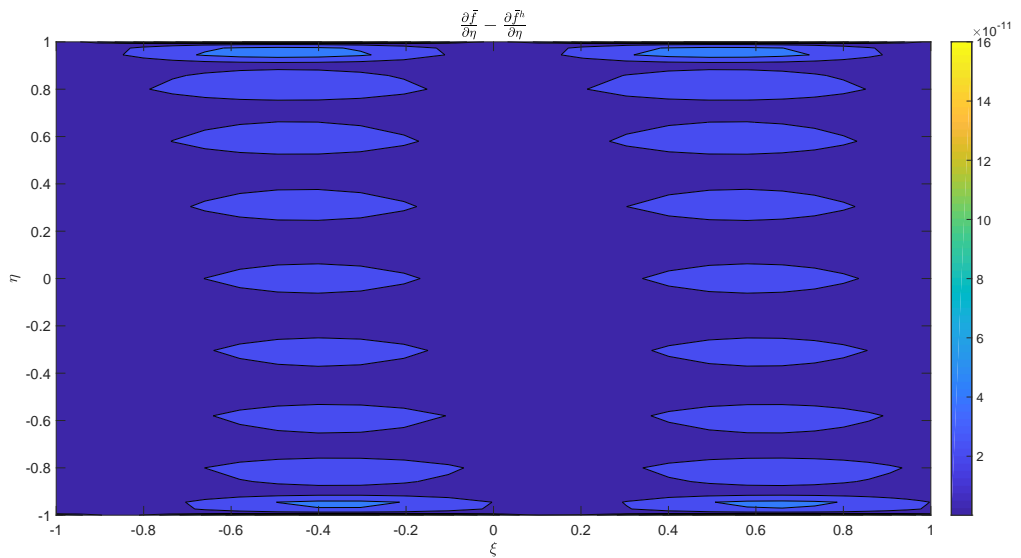
Figure 4.10: Spectral or p-refinement result for the scalar function reconstruction for the function $\bar{f}(\xi, \eta)$.



(a) Error on reference mesh $K := [-1, 1]^2$, polynomial order $p = 20$ for \bar{f}



(b) Error on reference mesh $K := [-1, 1]^2$, polynomial order $p = 20$ for $\frac{\partial \bar{f}}{\partial \xi}$



(c) Error on reference mesh $K := [-1, 1]^2$, polynomial order $p = 20$ for $\frac{\partial \bar{f}}{\partial \eta}$

Figure 4.11: Error distribution over reference element for polynomial order, $p = 20$

Transforming a co-vector field

In this example, we consider a co-vector field \mathbf{u} over the physical domain Ω_k as defined below,

$$\mathbf{u}(x, y) = u_x \mathbf{d}x + u_y \mathbf{d}y,$$

$$\text{that is, } \mathbf{u}(x, y) = \begin{Bmatrix} u_x \\ u_y \end{Bmatrix} = \begin{Bmatrix} 2\pi \cos(\pi x) \sin(\pi y) \\ -0.2(1+y)\pi \cos(\pi x) \sin(\pi y) \end{Bmatrix}, \quad \text{where, } x, y \in \Omega_k \quad (4.23)$$

For this co-vector field, it can be seen that,

$$\begin{aligned} \frac{\partial u_x}{\partial x} &= -2\pi^2 \sin(\pi x) \sin(\pi y) & \text{and} & & \frac{\partial u_y}{\partial x} &= 0.2(1+y)\pi^2 \sin(\pi x) \sin(\pi y) \\ \frac{\partial u_x}{\partial y} &= 2\pi^2 \cos(\pi x) \cos(\pi y) & & & \frac{\partial u_y}{\partial y} &= -0.2\pi \cos(\pi x) [\sin(\pi y) + (1+y)\pi \cos(\pi y)] \end{aligned} \quad (4.24)$$

Following the treatment for the scalar valued field function, we see that upon performing the pullback into the reference domain K , we obtain the following vector field,

$$\bar{\mathbf{u}}(\xi, \eta) = \bar{u}_\xi \mathbf{d}\xi + \bar{u}_\eta \mathbf{d}\eta$$

and since, we know from equation 4.12, we obtain the 1-forms $\mathbf{d}\xi$ and $\mathbf{d}\eta$ as,

$$\begin{aligned} \mathbf{d}x &= \mathbf{d}\xi + 0.1(3+\eta)\mathbf{d}\eta \\ \mathbf{d}y &= \mathbf{d}\eta \end{aligned}$$

upon transformation of the scalar components along with the 1-forms, we observe the elimination of one of the components of the vector field over the reference element K ,

$$\bar{\mathbf{u}}(\xi, \eta) = \begin{Bmatrix} \bar{u}_\xi \\ \bar{u}_\eta \end{Bmatrix} = \begin{Bmatrix} 2\pi \cos[\pi(\xi + 0.05(3+\eta)^2)] \sin[\pi(\eta + 2)] \\ 0 \end{Bmatrix}, \quad \text{where, } \xi, \eta \in K \quad (4.25)$$

computing the derivatives with respect to reference coordinates gives us,

$$\begin{aligned} \frac{\partial \bar{u}_\xi}{\partial \xi} &= -2\pi^2 \sin[\pi(\xi + 0.05(3+\eta)^2)] \sin[\pi(\eta + 2)] \\ \frac{\partial \bar{u}_\xi}{\partial \eta} &= 2\pi^2 \cos[\pi(\xi + 0.05(3+\eta)^2)] \cos[\pi(\eta + 2)] \\ &\quad - 0.2\pi^2(3+\eta) \sin[\pi(\xi + 0.05(3+\eta)^2)] \sin[\pi(\eta + 2)] \end{aligned} \quad (4.26)$$

$$\frac{\partial \bar{u}_\eta}{\partial \xi} = 0 \qquad \frac{\partial \bar{u}_\eta}{\partial \eta} = 0 \quad (4.27)$$

The careful reader might observe that the reconstruction of the derivative field over the physical domain using the reference co-vector fields and its derivatives, were it to be done, would require the use of only two sets of partial derivatives (equation 4.26) instead of the standard four (as the other two are eliminated as shown in equation 4.27).

This outcome is illustrated through the following equations: we write the covariant derivative in the physical domain as,

$$\nabla \mathbf{u} = \begin{pmatrix} \frac{\partial u_x}{\partial x} dx + \frac{\partial u_x}{\partial y} dy \\ \frac{\partial u_y}{\partial x} dx + \frac{\partial u_y}{\partial y} dy \end{pmatrix} \quad (4.28)$$

whereas, in the reference domain K , we have:

$$\nabla \bar{\mathbf{u}} = \begin{pmatrix} \frac{\partial \bar{u}_\xi}{\partial \xi} d\xi + \frac{\partial \bar{u}_\xi}{\partial \eta} d\eta \\ \frac{\partial \bar{u}_\eta}{\partial \xi} d\xi + \frac{\partial \bar{u}_\eta}{\partial \eta} d\eta \end{pmatrix} + \omega' \begin{pmatrix} \bar{u}_\xi \\ \bar{u}_\eta \end{pmatrix} \quad (4.29)$$

which gives,

$$\begin{aligned} \nabla \bar{\mathbf{u}} &= \begin{pmatrix} \frac{\partial \bar{u}_\xi}{\partial \xi} d\xi + \frac{\partial \bar{u}_\xi}{\partial \eta} d\eta \\ \frac{\partial \bar{u}_\eta}{\partial \xi} d\xi + \frac{\partial \bar{u}_\eta}{\partial \eta} d\eta \end{pmatrix} + \begin{bmatrix} 0 & 0 \\ 0.1 d\eta & 0 \end{bmatrix} \begin{pmatrix} \bar{u}_\xi \\ \bar{u}_\eta \end{pmatrix}, \quad \text{from equation 4.17} \\ \therefore \nabla \bar{\mathbf{u}} &= \begin{pmatrix} \frac{\partial \bar{u}_\xi}{\partial \xi} d\xi + \frac{\partial \bar{u}_\xi}{\partial \eta} d\eta \\ \frac{\partial \bar{u}_\eta}{\partial \xi} d\xi + \left(\frac{\partial \bar{u}_\eta}{\partial \eta} + 0.1 \bar{u}_\xi \right) d\eta \end{pmatrix} \end{aligned} \quad (4.30)$$

in order to reproduce $\nabla \mathbf{u}$ in equation 4.28 using $\nabla \bar{\mathbf{u}}$ from equation 4.30, we write,

$$\nabla \mathbf{u} = \mathbf{P} \bar{\mathbf{u}}, \quad \text{where, } \mathbf{P} \text{ is learnt from 4.17} \quad (4.31)$$

the reader may verify the accuracy of this statement. This enables the construction of the partial derivatives over the physical domain Ω_k from the reference domain K , such that,

$$\begin{aligned} \frac{\partial u_x}{\partial x} &= \frac{\partial \bar{u}_\xi}{\partial \xi} & \frac{\partial u_y}{\partial x} &= -0.1(3+\eta) \frac{\partial \bar{u}_\xi}{\partial \xi} \\ \frac{\partial u_x}{\partial y} &= \frac{\partial \bar{u}_\xi}{\partial \eta} - 0.1(3+\eta) \frac{\partial \bar{u}_\xi}{\partial \xi} & \frac{\partial u_y}{\partial y} &= -0.1 \bar{u}_\xi - 0.1(3+\eta) \left[\frac{\partial \bar{u}_\xi}{\partial \eta} - 0.1(3+\eta) \frac{\partial \bar{u}_\xi}{\partial \xi} \right] \end{aligned} \quad (4.32)$$

The field distribution computed over the physical shear deformed domain Ω_k is shown in the Figure 4.12 following the distribution $\mathbf{u}(x,y)$ as in equation 4.23. The velocity strength over the physical domain is shown in the Figure 4.13a, and the transformation of the component u_x to the distribution \bar{u}_ξ in the Figure 4.13b. Figures 4.14 and 4.15 show the reconstruction of the components u_x and u_y from the reference components \bar{u}_ξ and \bar{u}_η . The derivatives over the physical domain are shown in the figures 4.16, 4.17, 4.18 and 4.19.

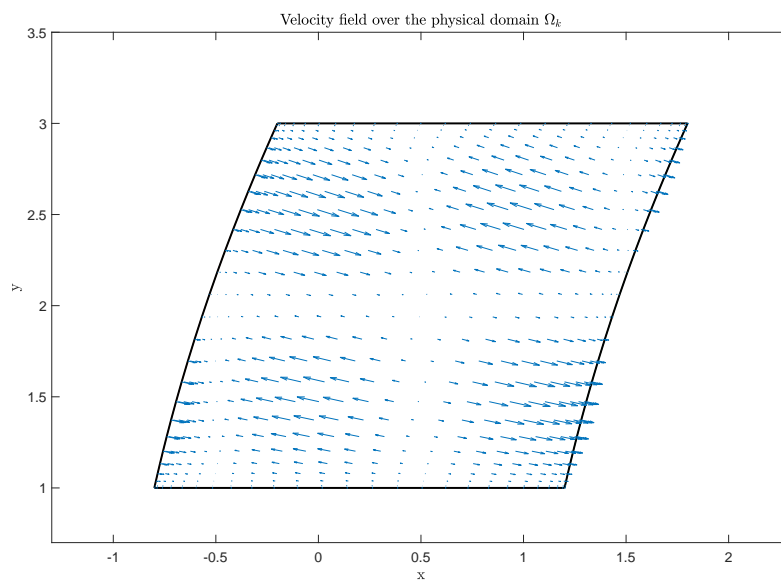
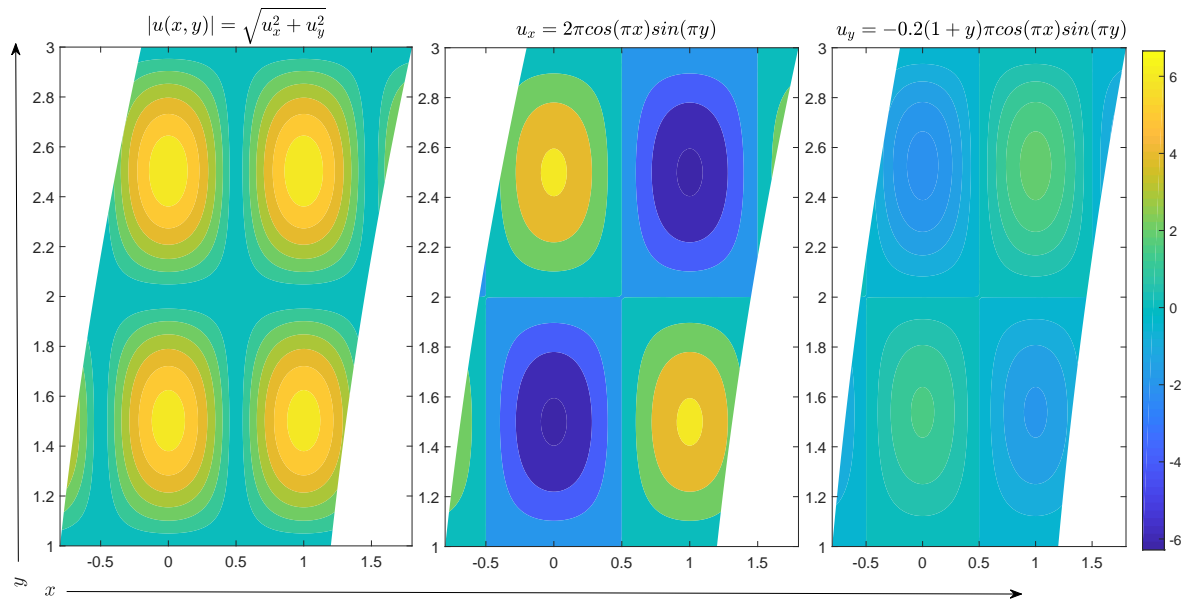
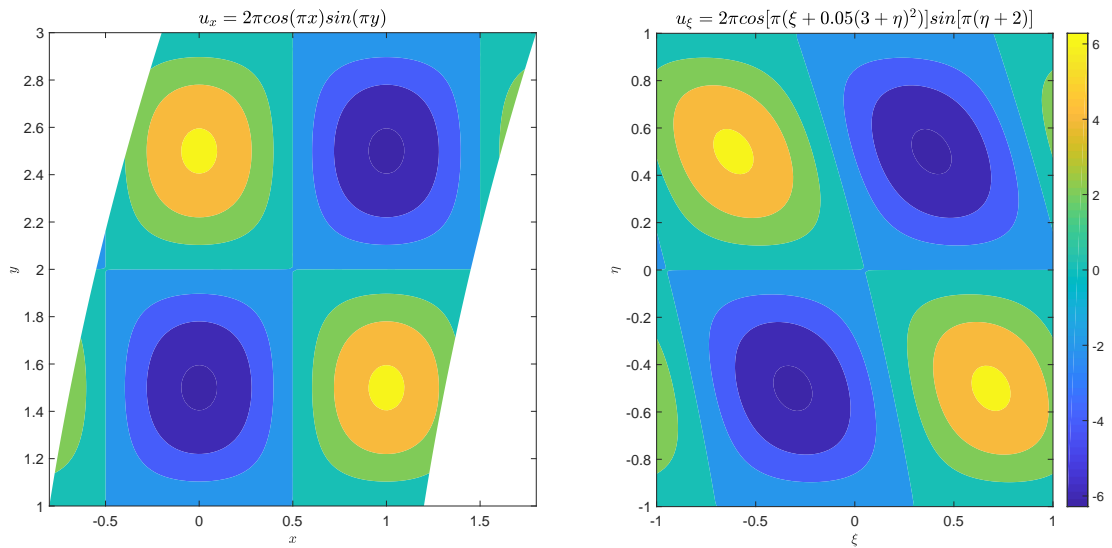


Figure 4.12: Vector field $\mathbf{u}(x,y)$ displayed over the physical domain Ω_k with a quiver plot, polynomial order of 15



(a) Filled contour plots showing the field strengths for the total co-vector field (left), the x -component (centre) and the y -component (right)



(b) Transformation of the scalar-valued x -component of the co-vector field u_x to the reference domain K , component u_ξ

Figure 4.13: Analytical distribution of co-vector field $\mathbf{u}(x, y)$ over both reference domain K as well as physical domain Ω_k

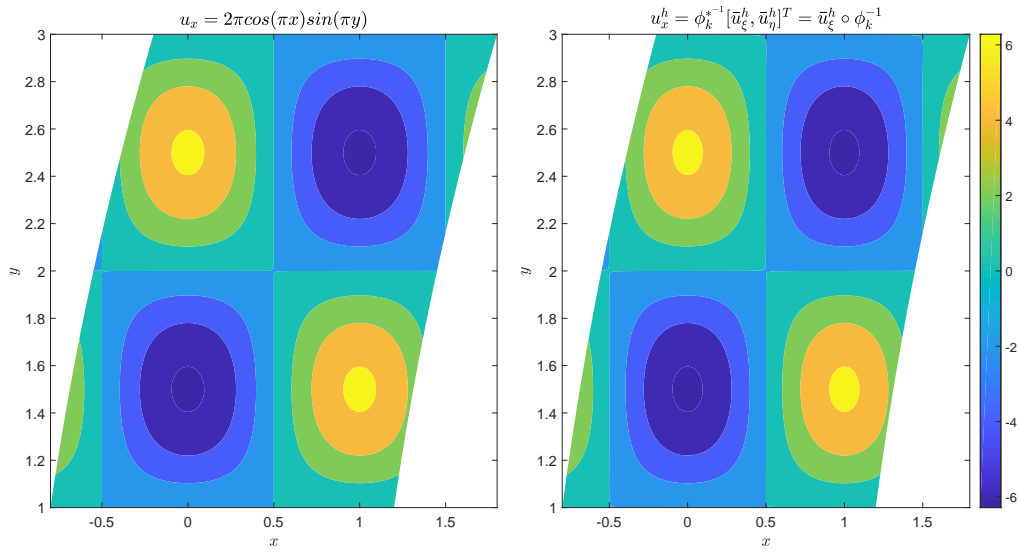


Figure 4.14: Exact function $u_x(x,y)$ (left) and reconstructed function $u_x^h(x,y)$ computed as a result of a pullback $(\phi_k^*)^{-1}[\bar{u}_\xi^h, \bar{u}_\eta^h]^T = \bar{u}_\xi^h \circ \phi_k^{-1}$ interpolated with primal and algebraic dual nodal functions (right). The results are plotted over the shear deformed domain Ω_k . Polynomial order, $p = 9$.

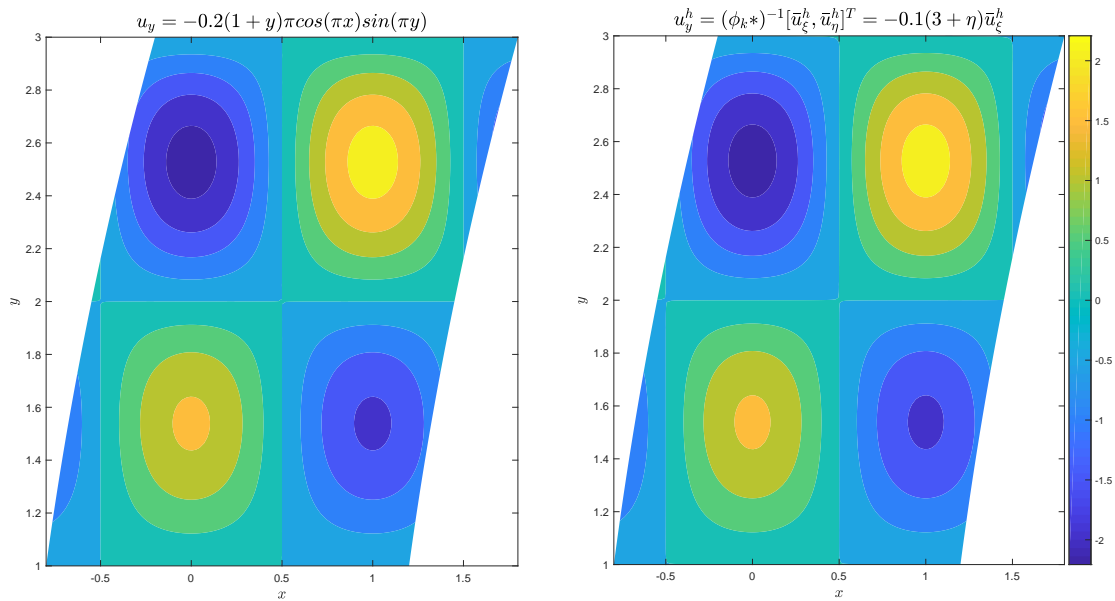


Figure 4.15: Exact function $u_y(x,y)$ (left) and reconstructed function $u_y^h(x,y)$ computed as a result of a pullback $(\phi_k^*)^{-1}[\bar{u}_\xi^h, \bar{u}_\eta^h]^T = -0.1(3+\eta)\bar{u}_\xi^h \circ \phi_k^{-1}$ interpolated with primal and algebraic dual nodal functions (right). The results are plotted over the shear deformed domain Ω_k . Polynomial order, $p = 9$.

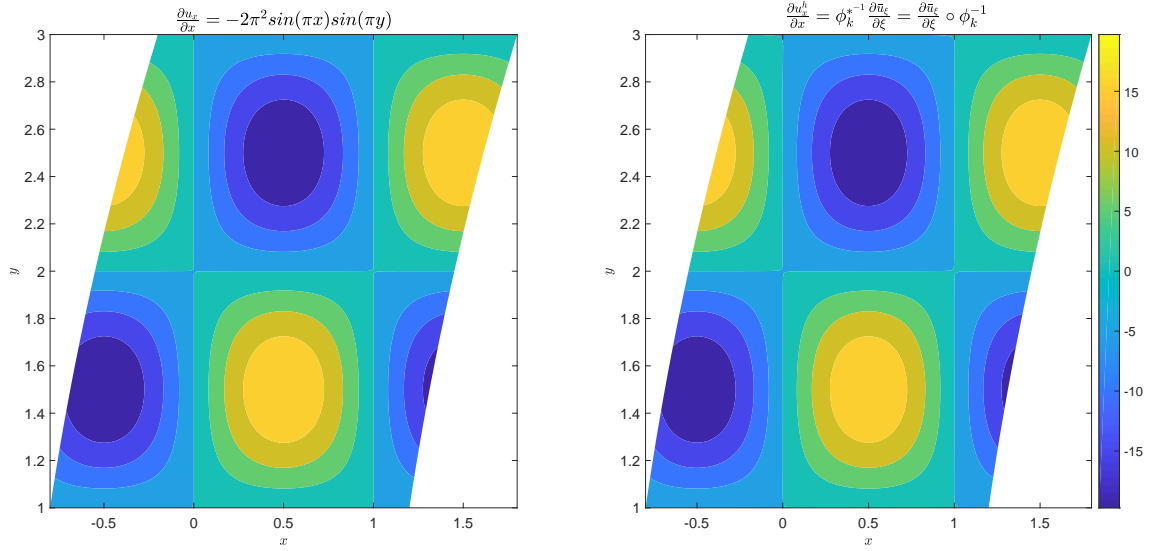


Figure 4.16: Exact function $\frac{\partial u_x}{\partial x}(x,y)$ (left) and reconstructed function $\frac{\partial u_x^h}{\partial x}(x,y)$ computed as a result of a pullback $(\phi_k^*)^{-1} \left[\frac{\partial \bar{u}_x^h}{\partial \xi}, \frac{\partial \bar{u}_x^h}{\partial \eta} \right]^T = \frac{\partial \bar{u}_x^h}{\partial \xi} \circ \phi_k^{-1}$ interpolated with primal and algebraic dual nodal functions (right). The results are plotted over the shear deformed domain Ω_k . Polynomial order, $p = 9$.

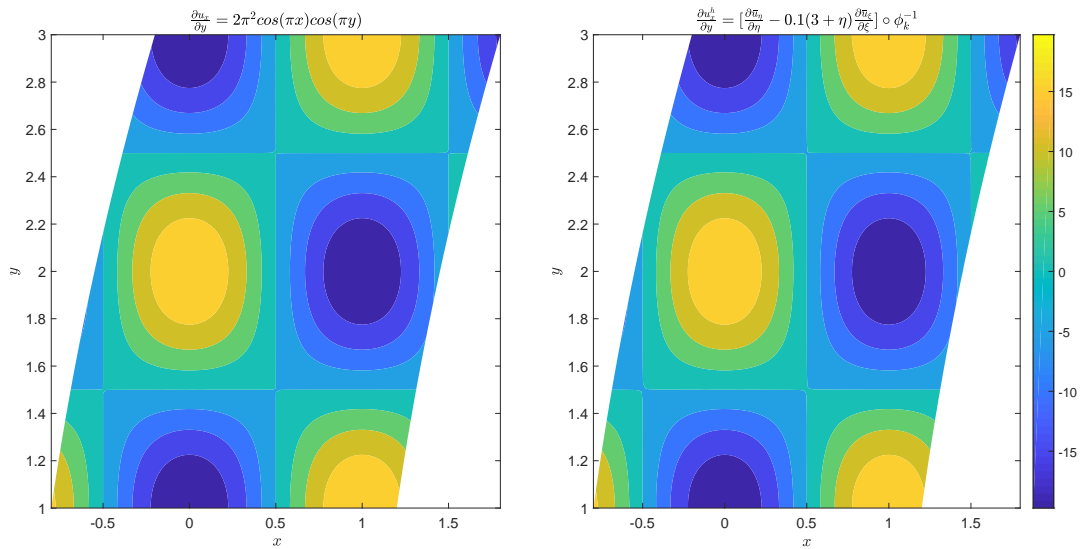


Figure 4.17: Exact function $\frac{\partial u_x}{\partial y}(x,y)$ (left) and reconstructed function $\frac{\partial u_x^h}{\partial y}(x,y)$ computed as a result of a pullback $(\phi_k^*)^{-1} \left[\frac{\partial \bar{u}_x^h}{\partial \xi}, \frac{\partial \bar{u}_x^h}{\partial \eta} \right]^T = \left[\frac{\partial \bar{u}_x}{\partial \eta} - 0.1(3 + \eta) \frac{\partial \bar{u}_x}{\partial \xi} \right] \circ \phi_k^{-1}$ interpolated with primal and algebraic dual nodal functions (right). The results are plotted over the shear deformed domain Ω_k . Polynomial order, $p = 9$.

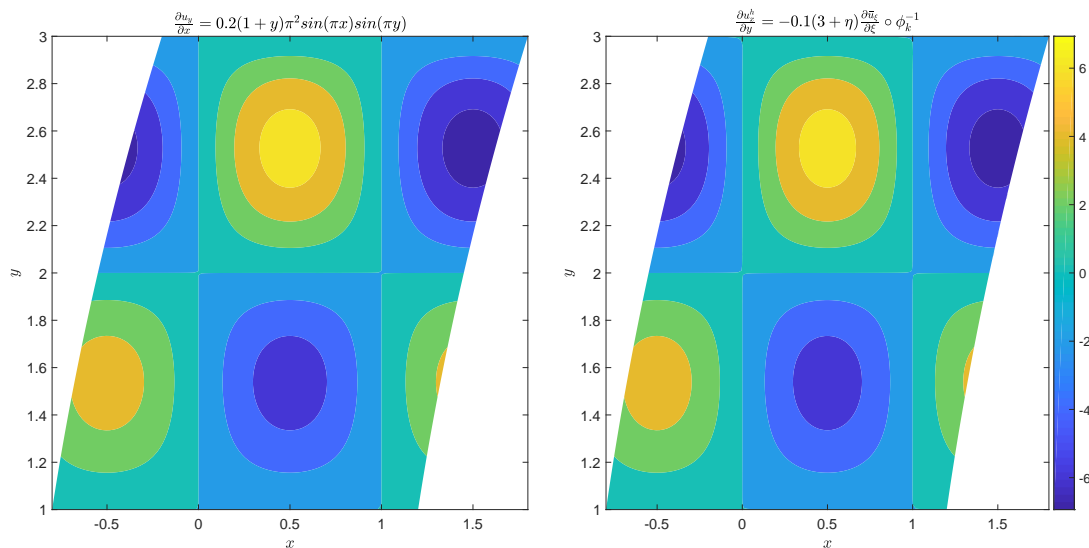


Figure 4.18: Exact function $\frac{\partial u_v}{\partial x}(x,y)$ (left) and reconstructed function $\frac{\partial u_v^h}{\partial x}(x,y)$ computed as a result of a pullback $(\phi_k^*)^{-1} \left[\frac{\partial \bar{u}_\xi^h}{\partial \xi}, \frac{\partial \bar{u}_\eta^h}{\partial \eta} \right]^T = [-0.1(3+\eta) \frac{\partial \bar{u}_\xi^h}{\partial \xi}] \circ \phi_k^{-1}$ interpolated with primal and algebraic dual nodal functions (right). The results are plotted over the shear deformed domain Ω_k . Polynomial order, $p = 9$.

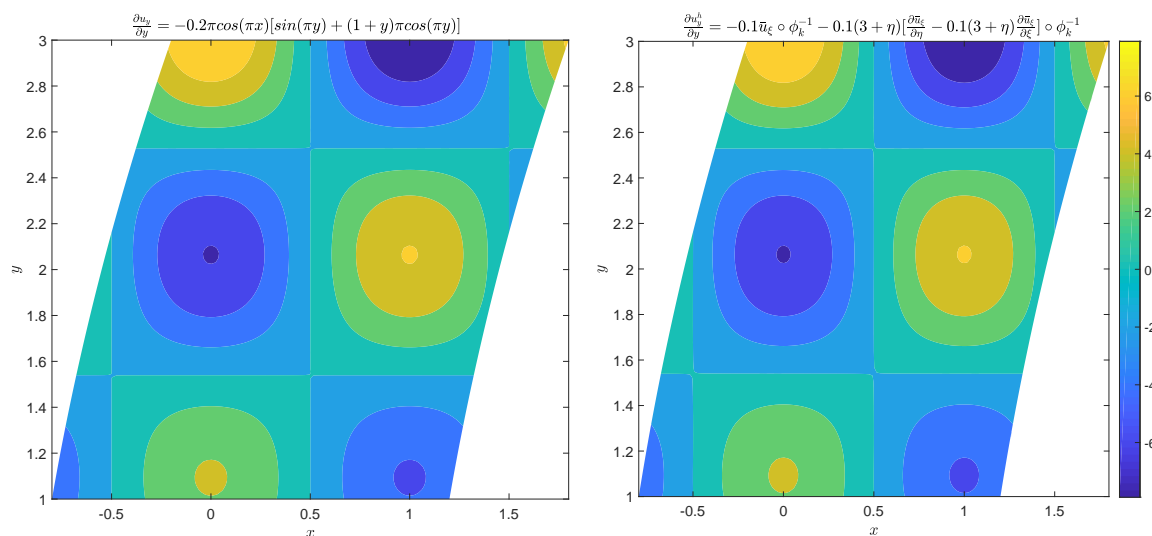


Figure 4.19: Exact function $\frac{\partial u_w}{\partial y}(x,y)$ (left) and reconstructed function $\frac{\partial u_w^h}{\partial y}(x,y)$ computed as a result of a pullback $(\phi_k^*)^{-1} \left[\frac{\partial \bar{u}_\xi^h}{\partial \xi}, \frac{\partial \bar{u}_\eta^h}{\partial \eta} \right]^T$ interpolated with primal and algebraic dual nodal functions (right). The results are plotted over the shear deformed domain Ω_k . Polynomial order, $p = 9$.

Error and convergence

We now compute the p-convergence behavior of this reconstruction for the covector-valued field function \mathbf{u} . The semi-log plot of the error with respect to the polynomial order of interpolation is shown in Figure 4.20. The p-convergence of the vector fields over the physical domain shows the exponential convergence with the increasing polynomial order.

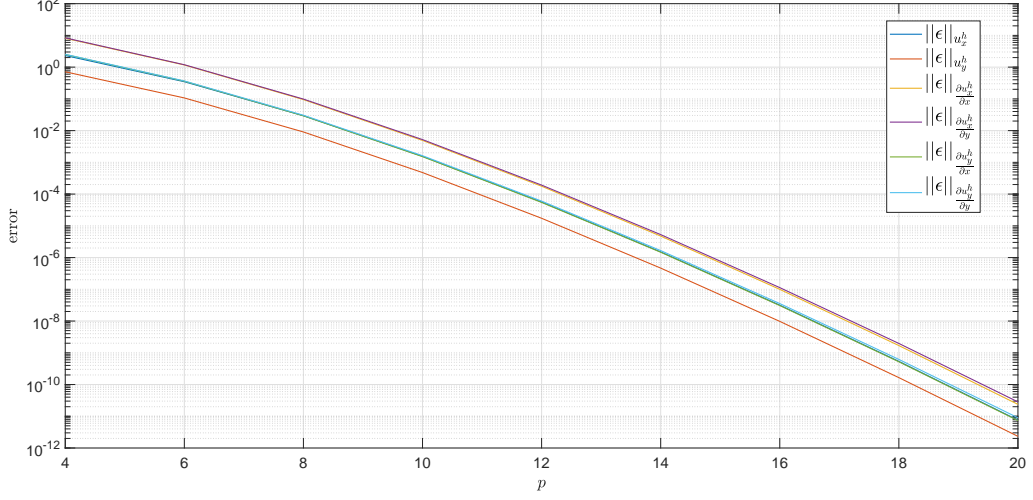


Figure 4.20: Spectral or p-refinement result for the covector field reconstruction $\mathbf{u}(x, y)$.

4.4.3. Example transformation: polar transformation (without origin)

We now consider another example case of a polar transformation without an origin point. For this example, we shall focus on purely covector field transformation to illustrate some physical applications, specifically for potential flows. The physical domain is a sector in the polar coordinate system such that the element under consideration does not contain the zero point, we will discuss the consequences of this choice soon. This transformed domain $\Omega_k \subset \mathbb{R}^2$ is morphed from the reference element $\mathbf{K} := [-1, 1]^2$ (see Figure 4.21 and for the discretization see Figure 4.22) using the following relationships:

$$\begin{aligned} r(\xi, \eta) &= \frac{1}{2} [r_2(1 + \xi) + r_1(1 - \xi)] \\ \theta(\xi, \eta) &= \delta + \varphi \cos \left[\frac{\pi}{4} \left(2 + \frac{\eta}{2} \right) \right] \end{aligned} \quad (4.33)$$

We now proceed with the same treatment as we observed previously for the shear domain, by calculating the connection coefficients for this mapping along with the requisite entities to establish the commutativity of the exterior derivative.

The Jacobian for this transformation is then given as:

$$\mathbf{J} \circ \Phi_k = \begin{bmatrix} \frac{r_2 - r_1}{2} & 0 \\ 0 & -\frac{\pi}{8} \varphi \sin \left[\frac{\pi}{4} \left(2 + \frac{\xi}{2} \right) \right] \end{bmatrix} \quad (4.34)$$

The Jacobian for the inverse of the transformation

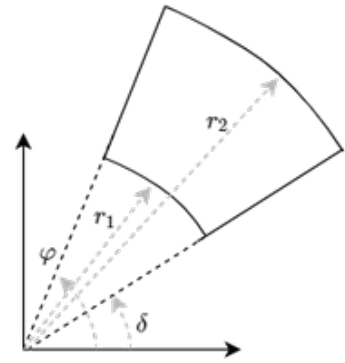


Figure 4.21: A transfinite mapping from Cartesian coordinate system to a modified Polar coordinate system as defined in equation 4.33.

is then computed as:

$$\mathbf{J} \circ \Phi_k^{-1} := \begin{bmatrix} -\frac{8}{\pi\varphi} \frac{1}{\sin[\frac{\pi}{4}(2+\frac{\xi}{2})]} & 0 \\ 0 & \frac{2}{r_2-r_1} \end{bmatrix} \quad (4.35)$$

Furthermore, the determinant is:

$$\begin{aligned} \det(\mathbf{J} \circ \Phi_k^{-1}) &:= \det \begin{pmatrix} -\frac{8}{\pi\varphi} \frac{1}{\sin[\frac{\pi}{4}(2+\frac{\xi}{2})]} & 0 \\ 0 & \frac{2}{r_2-r_1} \end{pmatrix} \\ \Rightarrow \det(\mathbf{J} \circ \Phi_k^{-1}) &:= -\frac{16}{\pi\varphi(r_2-r_1)} \frac{1}{\sin[\frac{\pi}{4}(2+\frac{\xi}{2})]} \end{aligned} \quad (4.36)$$

Note that unlike in the previous example of the shear transformation, the determinant does not yield a constant value, let alone unity. This implies that there is non-isotropic dilation of the domain volume under the mapping considered. We now take a look over the connection coefficients for this transformation.

Computing the Covariant Derivative

For the transformation in the equation 4.33, the following connections one-forms are obtained:

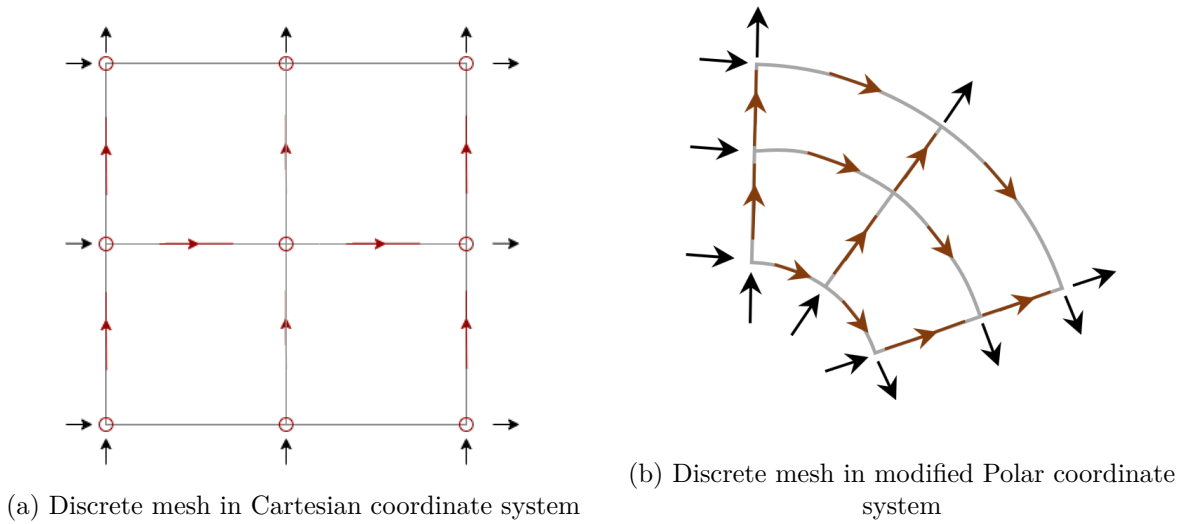


Figure 4.22: Discrete mesh systems in different coordinate systems with positive directions for flow assigned

$$\begin{cases} \frac{\partial}{\partial r} = \frac{\partial}{\partial \xi} \frac{\partial \xi}{\partial r} + \frac{\partial}{\partial \eta} \frac{\partial \eta}{\partial r} = \frac{2}{(r_2-r_1)} \frac{\partial}{\partial \xi} + 0 \frac{\partial}{\partial \eta} \\ \frac{\partial}{\partial \theta} = \frac{\partial}{\partial \xi} \frac{\partial \xi}{\partial \theta} + \frac{\partial}{\partial \eta} \frac{\partial \eta}{\partial \theta} = 0 \cdot \frac{\partial}{\partial \xi} - \frac{8}{\pi\varphi \sin[\frac{\pi}{4}(2+\frac{\xi}{2})]} \frac{\partial}{\partial \eta} \end{cases} \quad (4.37)$$

therefore we write that the matrix P as,

$$\left(\frac{\partial}{\partial r}, \frac{\partial}{\partial \theta} \right) = \left(\frac{\partial}{\partial \xi}, \frac{\partial}{\partial \eta} \right) \underbrace{\begin{pmatrix} \frac{2}{(r_2-r_1)} & 0 \\ 0 & -\frac{8}{\pi\varphi \sin[\frac{\pi}{4}(2+\frac{\xi}{2})]} \end{pmatrix}}_P \quad (4.38)$$

This then leads to the following terms,

$$\begin{aligned} dP &= \begin{pmatrix} 0 & 0 \\ 0 & \frac{\cos[\frac{\pi}{4}(2+\frac{\xi}{2})]}{\varphi \sin^2[\frac{\pi}{4}(2+\frac{\xi}{2})]} d\eta \end{pmatrix} \\ P^{-1} &= \begin{pmatrix} -\frac{\pi\varphi}{8} \sin[\frac{\pi}{4}(2+\frac{\xi}{2})] & 0 \\ 0 & \frac{(r_2-r_1)}{2} \end{pmatrix} \\ \omega' = P^{-1}dP &= \begin{pmatrix} 0 & 0 \\ 0 & -\frac{(r_2-r_1)\cos[\frac{\pi}{4}(2+\frac{\xi}{2})]}{2\sin^2[\frac{\pi}{4}(2+\frac{\xi}{2})]} d\eta \end{pmatrix} \end{aligned}$$

These terms are now used to evaluate transformation of function spaces such that the mapping of finite element spaces is mapped as shown in Figure 4.22, where the nodal and edge flow of velocities is shown.

Potential flow: line source of constant strength

Thus far we have identified the properties of the transformation seen above. Accordingly the ingredients for composing Cartan's structure equations have also been identified. We now consider an example case of covector field transformation that has conceivable application in physical flow approximations. For now, this example takes the form of a potential flow derived off of a line source of strength Q .

We consider the following velocity potential term, in the standard Cartesian coordinates (x,y) as,

$$\Phi(x,y) = \frac{Q}{2\pi} \log(\sqrt{x^2+y^2}) \quad (4.39)$$

such that, upon transformation into the polar coordinates using the relationships,

$$\begin{aligned} x &= r \cos\theta \\ y &= r \sin\theta \end{aligned} \quad (4.40)$$

we obtain,

$$\Phi(r,\theta) = \frac{Q}{2\pi} \log(r) \quad (4.41)$$

the velocity field thus obtained is given as:

$$\begin{aligned} u_r &= \frac{\partial \Phi}{\partial r}(r,\theta) = \frac{Q}{2\pi r} \\ u_\theta &= \frac{\partial \Phi}{\partial \theta}(r,\theta) = 0 \end{aligned} \quad (4.42)$$

we also know that the partial derivatives for these velocities are given as⁶:

$$\begin{aligned} \frac{\partial \mathbf{u}_r}{\partial r} &= -\frac{Q}{2\pi r^2} & \text{and} & & \frac{\partial \mathbf{u}_\theta}{\partial r} &= 0 \\ \frac{\partial \mathbf{u}_r}{\partial \theta} &= 0 & & & \frac{\partial \mathbf{u}_\theta}{\partial \theta} &= 0 \end{aligned} \quad (4.43)$$

⁶the boldface typeface denotes a vector, whereas the regular typeface denotes the scalar magnitude of the vector as in, $\mathbf{u}(r,\theta) = u_r \mathbf{d}\mathbf{r} + u_\theta \mathbf{d}\theta = u_r + u_\theta$

we know that,

$$\begin{pmatrix} u_\xi \\ u_\eta \end{pmatrix} = \mathbf{P} \begin{pmatrix} u_r \\ u_\theta \end{pmatrix} = \begin{pmatrix} \frac{2}{(r_2-r_1)} u_r \\ -\frac{8}{\pi\varphi \sin\alpha} u_\theta \end{pmatrix}, \quad \text{where, } \alpha = \left[\frac{\pi}{4} \left(2 + \frac{\eta}{2} \right) \right]$$

upon transformation of the scalar components along with the 1-forms, we observe the following scalar components of the velocity field over the reference element K ,

$$\begin{Bmatrix} \bar{u}_\xi \\ \bar{u}_\eta \end{Bmatrix} = \begin{Bmatrix} \frac{2Q}{\pi(r_2-r_1)[(r_2+r_1)+(r_2-r_1)\xi]} \\ 0 \end{Bmatrix}, \quad \text{where, } \xi, \eta \in K \quad (4.44)$$

Furthermore, computing the derivatives with respect to reference coordinates gives us,

$$\begin{aligned} \frac{\partial \bar{u}_\xi}{\partial \xi} &= -\frac{2Q}{\pi[(r_2+r_1)+(r_2-r_1)\xi]^2} & \frac{\partial \bar{u}_\eta}{\partial \xi} &= 0 \\ \frac{\partial \bar{u}_\xi}{\partial \eta} &= 0 & \frac{\partial \bar{u}_\eta}{\partial \eta} &= 0 \end{aligned} \quad (4.45)$$

Now the exercise becomes the construction of the physical domain vector fields using the results computed on the reference domain (where computationally, exterior differentiation operations are being performed). Accordingly, the reader may verify that, indeed the commutativity of the transformation with the derivative holds true as seen below:

in reference coordinates, the covariant derivative is written as:

$$\nabla \bar{\mathbf{u}} = \begin{pmatrix} \frac{\partial \bar{u}_\xi}{\partial \xi} d\xi + \frac{\partial \bar{u}_\xi}{\partial \eta} d\eta \\ \frac{\partial \bar{u}_\eta}{\partial \xi} d\xi + \frac{\partial \bar{u}_\eta}{\partial \eta} d\eta \end{pmatrix} = \begin{pmatrix} d\bar{u}_\xi \\ d\bar{u}_\eta \end{pmatrix} \quad (4.46)$$

whereas in the modified polar coordinates, we write:

$$\nabla \mathbf{u} = \begin{pmatrix} \frac{\partial u_r}{\partial r} dr + \frac{\partial u_r}{\partial \theta} d\theta \\ \frac{\partial u_\theta}{\partial r} dr + \frac{\partial u_\theta}{\partial \theta} d\theta \end{pmatrix} + \omega' \begin{pmatrix} u_r \\ u_\theta \end{pmatrix} = \begin{pmatrix} d\mathbf{u}_r \\ d\mathbf{u}_\theta \end{pmatrix} + \omega' \begin{pmatrix} u_r \\ u_\theta \end{pmatrix} \quad (4.47)$$

thus the commutative derivative is written as:

$$\mathbf{P} \nabla \mathbf{u} = \mathbf{P} \begin{pmatrix} d\mathbf{u}_r \\ d\mathbf{u}_\theta \end{pmatrix} + \mathbf{P} \omega' \begin{pmatrix} u_r \\ u_\theta \end{pmatrix} = \begin{pmatrix} d\bar{u}_\xi \\ d\bar{u}_\eta \end{pmatrix}$$

that is,

$$\mathbf{P} \nabla \mathbf{u} = \mathbf{P} \begin{pmatrix} d\mathbf{u}_r \\ d\mathbf{u}_\theta \end{pmatrix} + d\mathbf{P} \begin{pmatrix} u_r \\ u_\theta \end{pmatrix} = \begin{pmatrix} d\bar{u}_\xi \\ d\bar{u}_\eta \end{pmatrix}$$

substituting the values gives us,

$$\begin{aligned}
& \begin{pmatrix} \frac{2}{(r_2-r_1)} & 0 \\ 0 & \frac{8}{\pi\varphi\sin\alpha} \end{pmatrix} \begin{pmatrix} d\mathbf{u}_r \\ d\mathbf{u}_\theta \end{pmatrix} + \begin{pmatrix} 0 & 0 \\ 0 & \frac{\cos\alpha}{\varphi\sin^2\alpha}d\eta \end{pmatrix} \begin{pmatrix} u_r \\ u_\theta \end{pmatrix} = \begin{pmatrix} d\bar{u}_\xi \\ d\bar{u}_\eta \end{pmatrix} \\
\Rightarrow & \begin{pmatrix} \frac{2}{(r_2-r_1)}d\mathbf{u}_r \\ \frac{8}{\pi\varphi\sin\alpha}d\mathbf{u}_\theta \end{pmatrix} + \begin{pmatrix} 0 \\ \frac{u_\theta\cos\alpha}{\varphi\sin^2\alpha}d\xi \end{pmatrix} = \begin{pmatrix} d\bar{u}_\xi \\ d\bar{u}_\eta \end{pmatrix} \\
\therefore & \begin{pmatrix} d\left(\frac{2}{(r_2-r_1)}u_r\right) \\ d\left(-\frac{8}{\pi\varphi\sin\alpha}u_\theta\right) \end{pmatrix} = \begin{pmatrix} d\bar{u}_\xi \\ d\bar{u}_\eta \end{pmatrix} \tag{4.48}
\end{aligned}$$

and since we can express the matrix on the left hand side in terms of sum of partial derivatives as shown in equation 4.47, we can compare individual partial derivative fields. Thus, we obtain the following relationships,

$$\begin{aligned}
\frac{\partial \mathbf{u}_r}{\partial r} &= \frac{\partial \bar{u}_\xi}{\partial \xi} & \frac{\partial \mathbf{u}_\theta}{\partial r} &= 0 \\
\frac{\partial \mathbf{u}_r}{\partial \theta} &= 0 & \frac{\partial \mathbf{u}_\theta}{\partial \theta} &= 0
\end{aligned} \tag{4.49}$$

We now look at the reconstructed solutions of the velocity components on the reference element K , a unit strength line source is taken and the reference element maps a section of the radial sector portion with a maximum radius of 5 units and a minimum radius of 2 units, that is $r_2 = 5$ and $r_1 = 2$; the angular parameters are taken as $\delta = \frac{\pi}{12}$ and $\varphi = \frac{\pi}{3}$. The reconstruction of the ξ -component, \bar{u}_ξ^h and its derivative with $\frac{\partial \bar{u}_\xi}{\partial \xi}$ in figures 4.23 and 4.24. The reconstruction is shown for the polynomial order $p = 9$. Figures 4.25 and 4.26 show the velocity field distribution over the physical domain Ω_k . The covector field is later visualized through a quiver plot of the polar velocity 1-form, showing the radial outward flow from the source (placed over the origin of the original polar coordinates) in Figure 4.27.

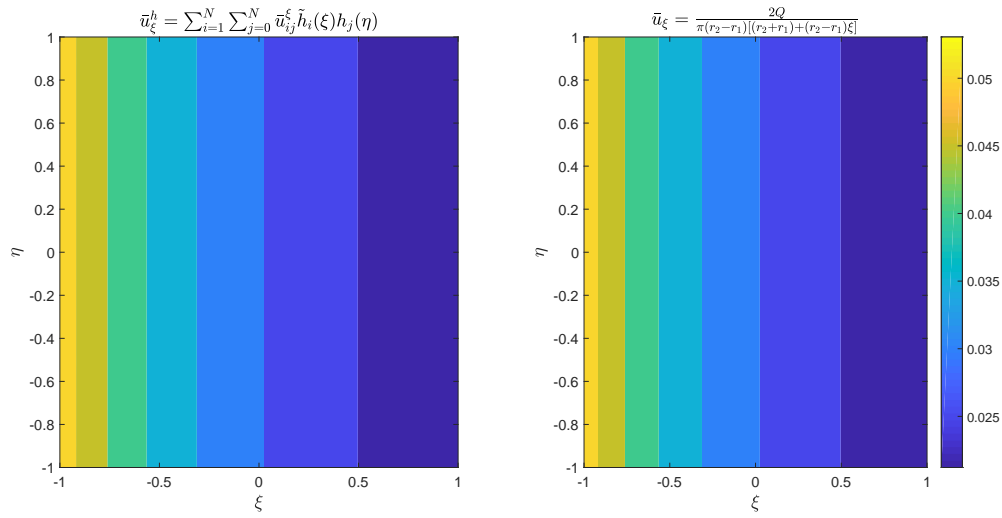


Figure 4.23: Exact function \bar{u}_ξ (right) and reconstructed function \bar{u}_ξ^h , using mixed basis functions, interpolated with primal and algebraic dual nodal functions (left). The results are plotted over the reference domain K. Polynomial order, $p = 9$.

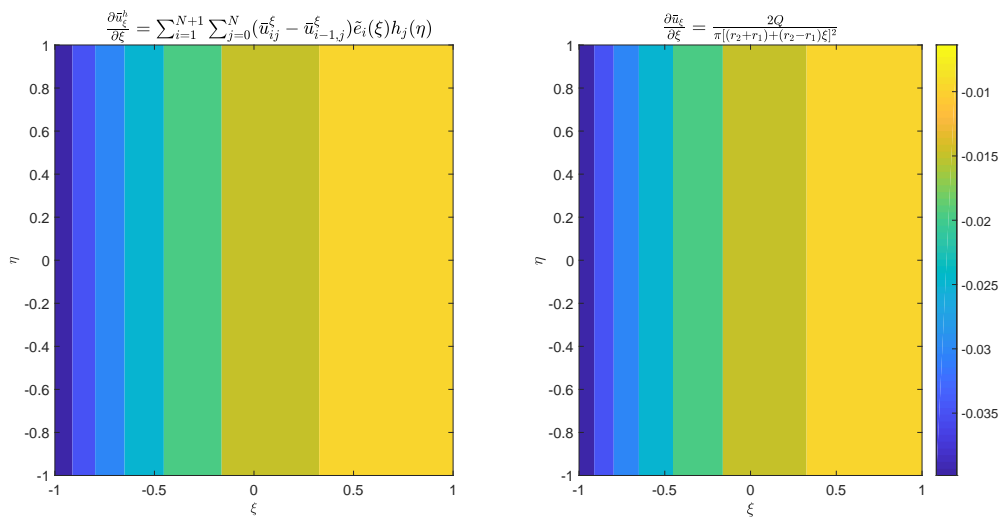


Figure 4.24: Exact function $\frac{\partial \bar{u}_\xi}{\partial \xi}$ (right) and reconstructed function $\frac{\partial \bar{u}_\xi^h}{\partial \xi}$ using mixed basis functions, interpolated with primal and algebraic dual nodal functions (left). The results are plotted over the reference domain K. Polynomial order, $p = 9$.

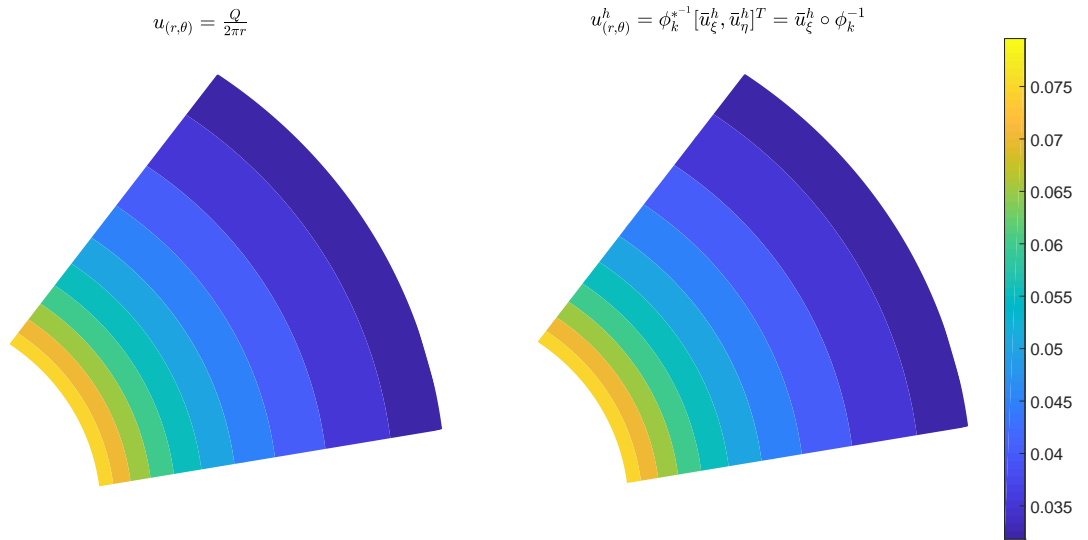


Figure 4.25: Exact function $u_\xi(r, \theta)$ (left) and reconstructed function $u_\xi^h(r, \theta)$ computed as a result of a pullback $(\phi_k^*)^{-1} [\bar{u}_\xi^h, \bar{u}_\eta^h]^T = \frac{(r_2 - r_1)}{2} \bar{u}_\xi^h \circ \phi_k^{-1}$ interpolated with primal and algebraic dual nodal functions (right). The results are plotted over the modified polar domain Ω_k . Polynomial order, $p = 9$.

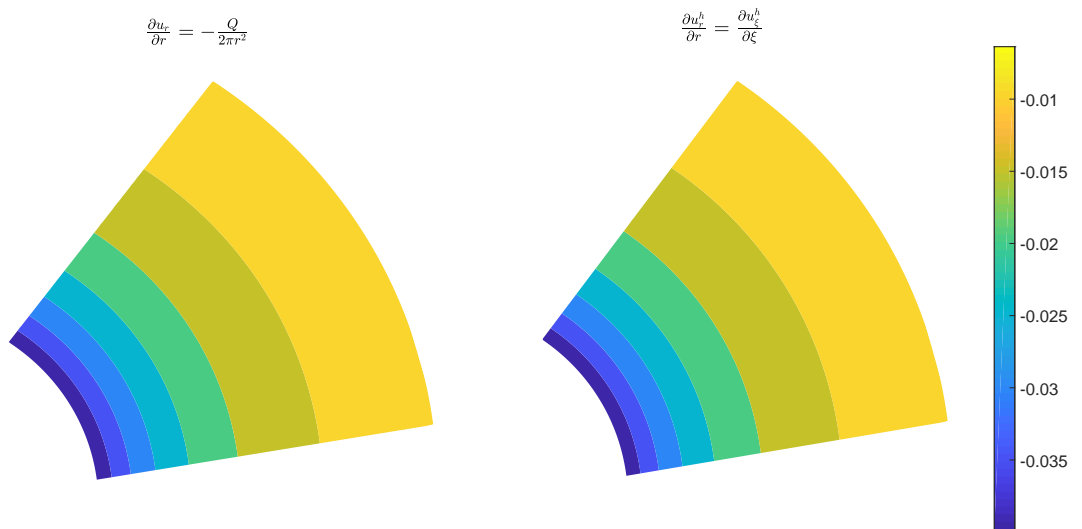


Figure 4.26: Exact function $\frac{\partial u_r}{\partial r}(r, \theta)$ (left) and reconstructed function $\frac{\partial u_r^h}{\partial r}(r, \theta)$ computed as a result of a pullback $(\phi_k^*)^{-1} [\frac{\partial u_\xi^h}{\partial \xi}, \frac{\partial u_\eta^h}{\partial \eta}]^T = \frac{\partial u_\xi^h}{\partial \xi} \circ \phi_k^{-1}$ interpolated with primal and algebraic dual nodal functions (right). The results are plotted over the modified polar domain Ω_k . Polynomial order, $p = 9$.

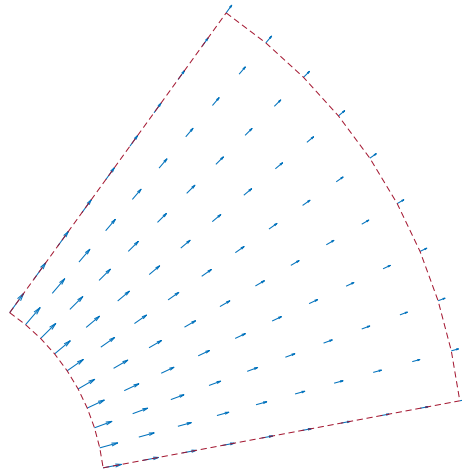


Figure 4.27: Velocity field over the modified polar domain Ω_k showing radially outward flow emanating from a unit strength line source, computed from the reconstructed solution (after transformation) for a polynomial order = 9.

Potential flow: line vortex of constant strength

We consider another example case, that of a line vortex of constant strength Γ , such that the following velocity potential term, in the standard polar coordinates (r, θ) holds,

$$\Phi(r, \theta) = \frac{\Gamma}{2\pi} \theta \quad (4.50)$$

the velocity field thus obtained is given as:

$$\begin{aligned} u_r &= \frac{\partial \Phi}{\partial r}(r, \theta) = 0 \\ u_\theta &= \frac{\partial \Phi}{\partial \theta}(r, \theta) = \frac{\Gamma}{2\pi r} \end{aligned} \quad (4.51)$$

we also know that the partial derivatives for these velocities are given as:

$$\begin{aligned} \frac{\partial u_r}{\partial r} &= 0 & \frac{\partial u_\theta}{\partial r} &= -\frac{\Gamma}{2\pi r^2} \\ \frac{\partial u_r}{\partial \theta} &= 0 & \frac{\partial u_\theta}{\partial \theta} &= 0 \end{aligned} \quad \text{and} \quad (4.52)$$

similar to the previous case, we obtain,

$$\left\{ \begin{array}{c} \bar{u}_\xi \\ \bar{u}_\eta \end{array} \right\} = \left\{ \begin{array}{c} 0 \\ 8 \Gamma \\ \frac{8 \Gamma}{\pi^2 \varphi \sin \alpha [(r_2 + r_1) + (r_2 - r_1) \xi]} \end{array} \right\}, \quad \text{where, } \xi, \eta \in K \quad (4.53)$$

Furthermore, computing the derivatives with respect to reference coordinates gives us,

$$\begin{aligned} \frac{\partial \bar{u}_\xi}{\partial \xi} &= 0 & \frac{\partial \bar{u}_\eta}{\partial \xi} &= \frac{8 \Gamma (r_2 - r_1)}{\pi^2 \varphi \sin \alpha [(r_2 + r_1) + (r_2 - r_1) \xi]^2} \\ \frac{\partial \bar{u}_\xi}{\partial \eta} &= 0 & \frac{\partial \bar{u}_\eta}{\partial \eta} &= \frac{\Gamma \cos \alpha}{\pi \varphi \sin^2 \alpha [(r_2 + r_1) + (r_2 - r_1) \xi]} \end{aligned} \quad \text{and} \quad (4.54)$$

Following similar treatment as seen in the previous section, we write:

$$\begin{aligned} \frac{\partial \mathbf{u}_r}{\partial r} &= 0 & \frac{\partial \mathbf{u}_\theta}{\partial r} &= -\frac{\pi \varphi \sin \alpha}{4(r_2 - r_1)} \frac{\partial \bar{u}_\eta}{\partial \xi} \\ \frac{\partial \mathbf{u}_r}{\partial \theta} &= 0 & \frac{\partial \mathbf{u}_\theta}{\partial \theta} &= \frac{\partial \bar{u}_\eta}{\partial \eta} - \frac{u_\theta \cos \alpha}{\varphi \sin^2 \alpha} = 0 \end{aligned} \quad \text{and} \quad (4.55)$$

Similar to the previous case, we now take a look at the reconstructed solutions over the reference element K , with the similar set of parameters, except instead of a unit strength source, we take a unit strength vortex such that a constant circulation of unity holds over the domain flow. The reconstruction of the analytical solutions \bar{u}_η , $\frac{\partial \bar{u}_\eta}{\partial \xi}$ and $\frac{\partial \bar{u}_\eta}{\partial \eta}$ is shown in figures 4.28, 4.29 and 4.30 respectively. Accordingly, its transformation towards the modified polar domain Ω_k is shown in the figures 4.31 ($u_{(r, \theta)} = u_\theta$), 4.32 ($\frac{\partial u_\theta}{\partial r}$) and 4.33 ($\frac{\partial u_\theta}{\partial \theta}$). The quiver plot showing the vector field is also illustrated in the Figure 4.34.

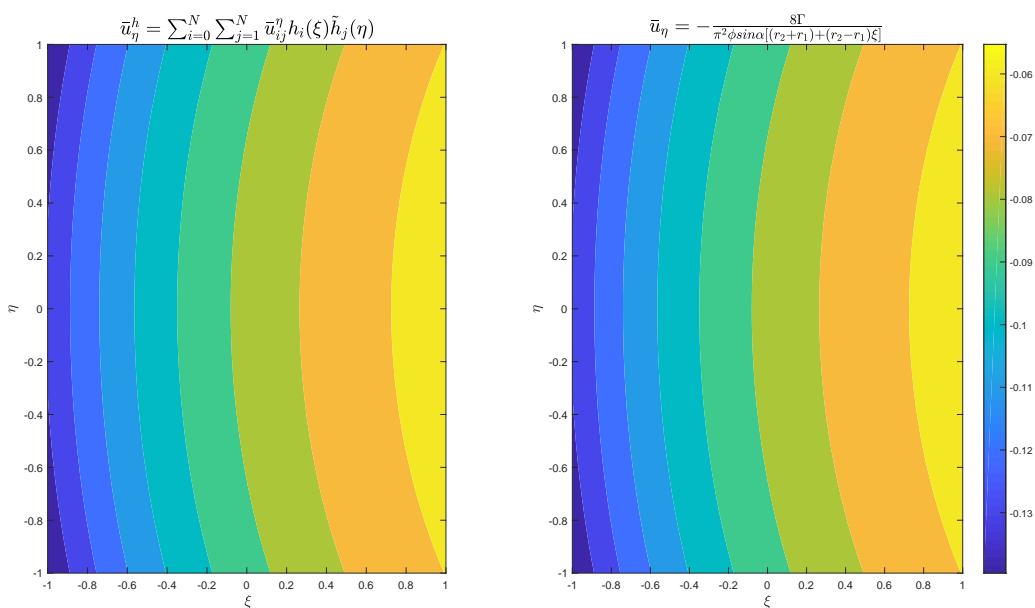


Figure 4.28: Exact function \bar{u}_η (right) and reconstructed function \bar{u}_η^h using mixed basis functions, interpolated with primal and algebraic dual nodal functions (left). The results are plotted over the reference domain K. Polynomial order, $p = 9$.

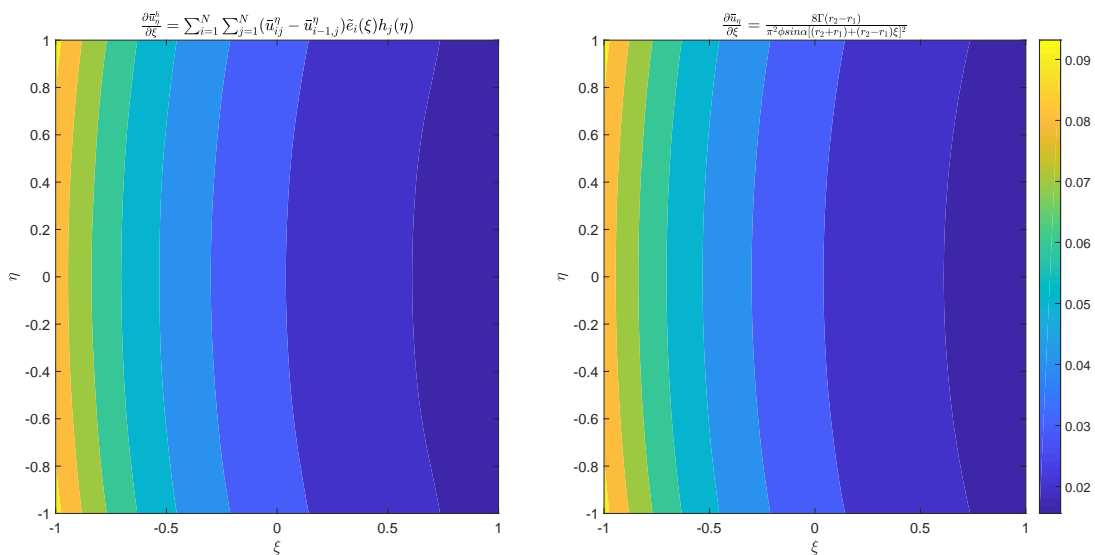


Figure 4.29: Exact function $\frac{\partial \bar{u}_\eta}{\partial \xi}$ (right) and reconstructed function $\frac{\partial \bar{u}_\eta^h}{\partial \xi}$ using mixed basis functions, interpolated with primal and algebraic dual nodal functions (left). The results are plotted over the reference domain K. Polynomial order, $p = 9$.

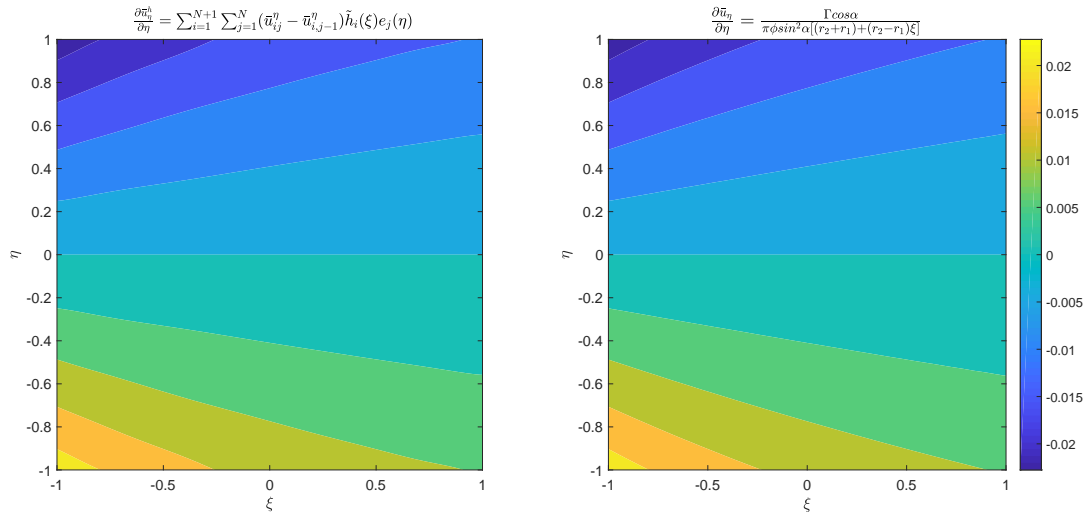


Figure 4.30: Exact function $\frac{\partial \bar{u}_\eta}{\partial \eta}$ (right) and reconstructed function $\frac{\partial \bar{u}_\eta^h}{\partial \eta}$ using mixed basis functions, interpolated with primal and algebraic dual nodal functions (left). The results are plotted over the reference domain K . Polynomial order, $p = 9$.

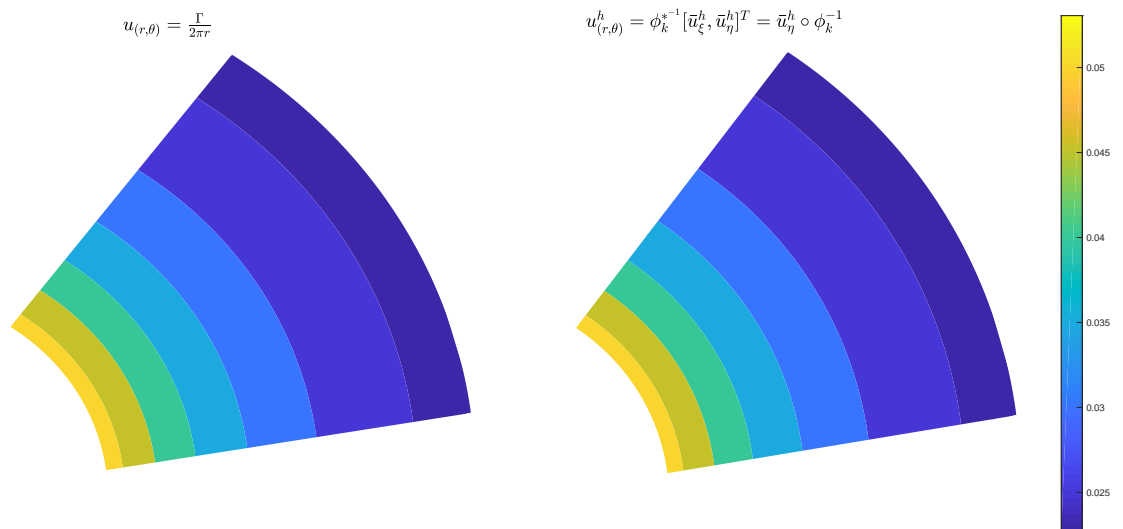


Figure 4.31: Exact function $u(r, \theta)$ (left) and reconstructed function $u^h(r, \theta)$ computed as a result of a pullback $(\phi_k^*)^{-1} [\bar{u}_\xi^h, \bar{u}_\eta^h]^T = \frac{2}{(r_2 - r_1)} \bar{u}_\eta^h \circ \phi_k^{-1}$ interpolated with primal and algebraic dual nodal functions (right). The results are plotted over the shear deformed domain Ω_k . Polynomial order, $p = 9$.

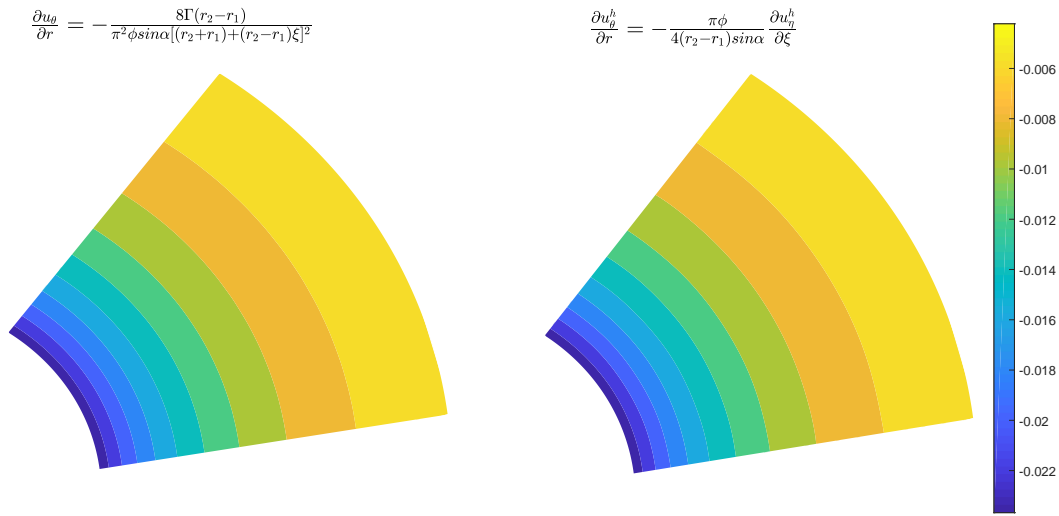


Figure 4.32: Exact function $\frac{\partial u_a}{\partial r}$ (left) and reconstructed function $\frac{\partial u_a^h}{\partial r}$ computed as a result of a pullback $(\phi_k^*)^{-1}[\bar{u}_\xi^h, \bar{u}_\eta^h]^\Gamma = \frac{2}{(r_2-r_1)} \bar{u}_\eta^h \circ \phi_k^{-1}$ interpolated with primal and algebraic dual nodal functions (right). The results are plotted over the shear deformed domain Ω_k . Polynomial order, $p = 9$.

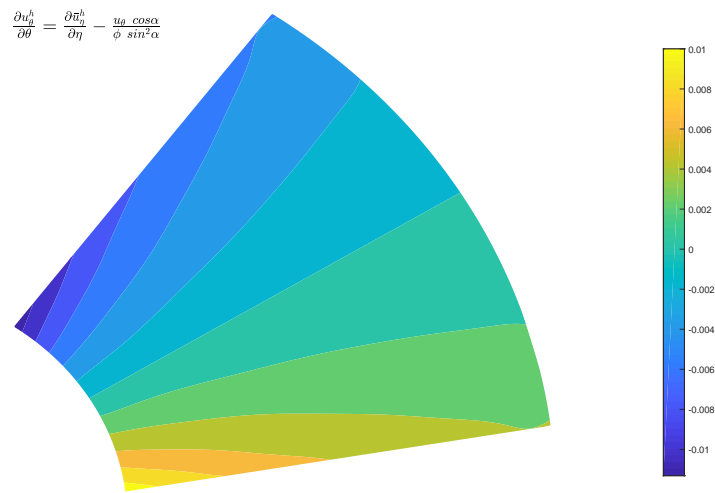


Figure 4.33: Reconstructed function $\frac{\partial u_a^h}{\partial \theta} = \frac{\partial \bar{u}_\eta^h}{\partial \theta} - \frac{u_a}{\phi} \cos\alpha \sin\alpha$ computed as a result of a pullback $(\phi_k^*)^{-1}[\bar{u}_\xi^h, \bar{u}_\eta^h]^\Gamma = \frac{2}{(r_2-r_1)} \bar{u}_\eta^h \circ \phi_k^{-1}$ interpolated with primal and algebraic dual nodal functions. The results are plotted over the shear deformed domain Ω_k . Note that as polynomial order increases and accuracy of approximation increases this distribution should vanish. Plotted with a low polynomial order, $p = 5$.

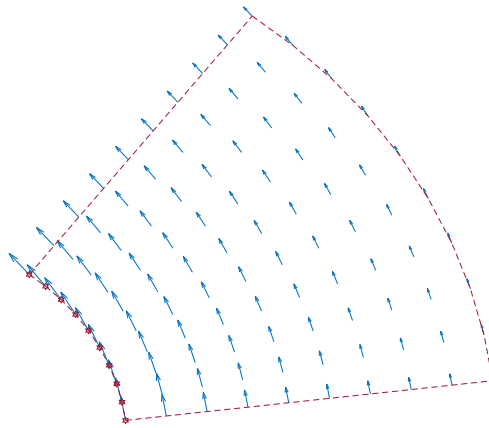


Figure 4.34: Velocity field over the modified polar domain Ω_k showing rotational flow emanating from a unit strength line vortex, computed from the reconstructed solution (after transformation) for a polynomial order $n = 9$.

Error and Convergence

For both the cases of potential flow problems, the spectral convergence results display exponential convergence as expected in figures 4.35 for the potential flow with line source and in 4.36 for potential flow with line vortex. Furthermore, the interpolation errors for the two problems and their reconstructed fields are shown in figures 4.37 for the potential flow with line source and in 4.38.

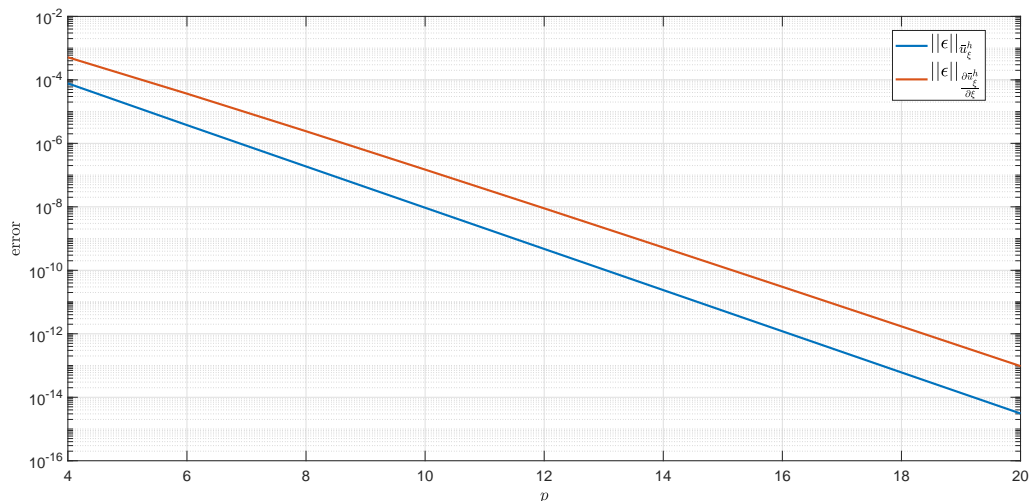


Figure 4.35: Spectral or p-refinement result for the covector field reconstruction $\mathbf{u}(x,y)$.

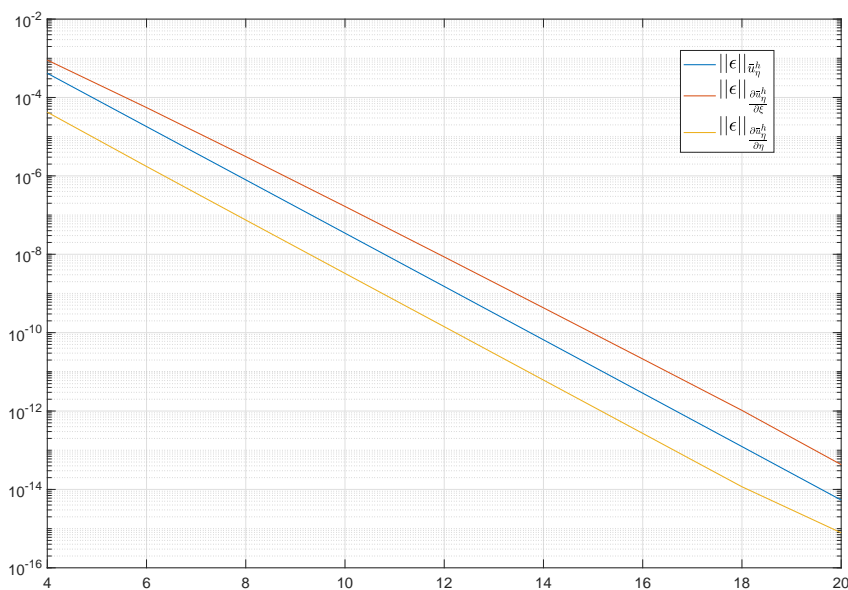
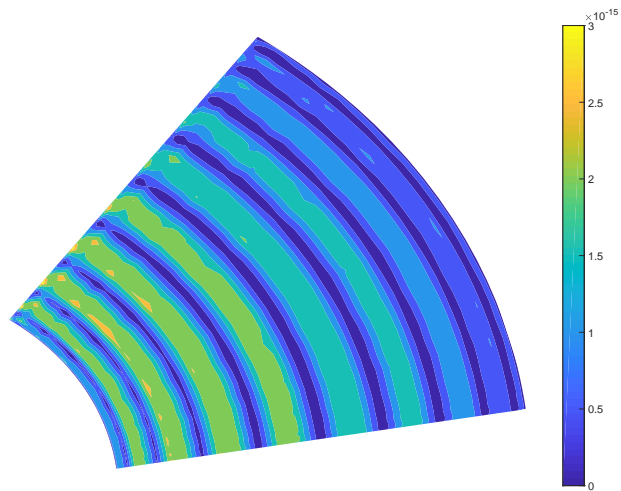
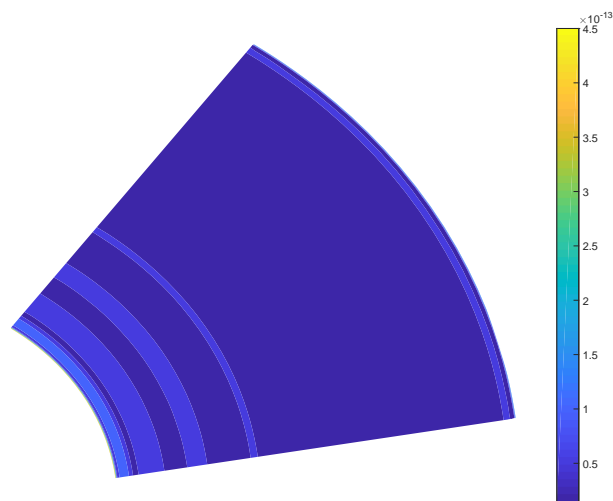


Figure 4.36: Spectral or p-refinement result for the covector field reconstruction $\mathbf{u}(x,y)$.

As a result of these examples, the use of covariant derivatives as a means to obtain commutative exterior derivative properties across curvilinear frames is established both mathematically and numerically for 0-forms and 1-forms. It is expected that this principle scales towards higher dimensions, that is for (n-1) forms in an ambient space of n-dimensions.

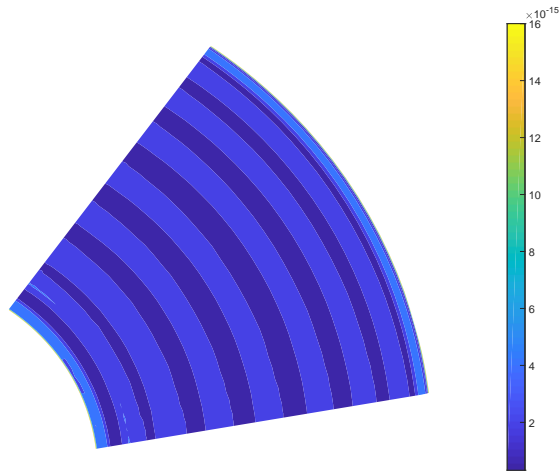


(a) Error on reference mesh $K := [-1, 1]^2$, polynomial order $p = 20$ for \bar{f}

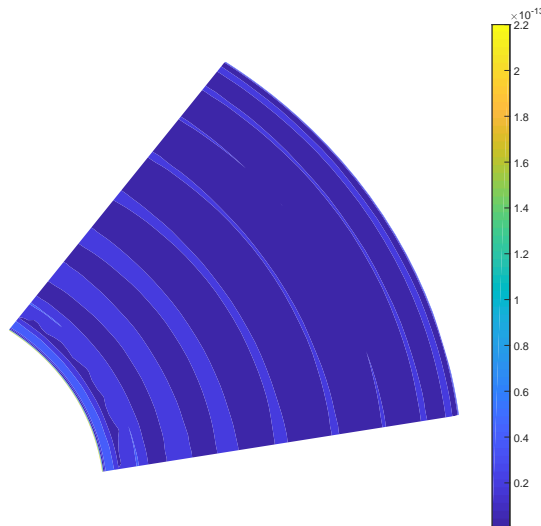


(b) Error on reference mesh $K := [-1, 1]^2$, polynomial order $p = 20$ for $\frac{\partial \bar{f}}{\partial \xi}$

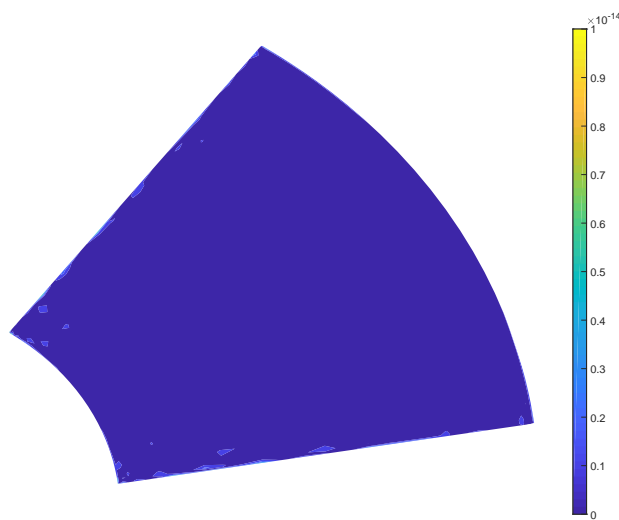
Figure 4.37: Error distribution over physical element for polynomial order, $p = 20$



(a) Error on reference mesh $K := [-1, 1]^2$, polynomial order $p = 20$ for \bar{f}



(b) Error on reference mesh $K := [-1, 1]^2$, polynomial order $p = 20$ for $\frac{\partial \bar{f}}{\partial \xi}$



(c) Error on reference mesh $K := [-1, 1]^2$, polynomial order $p = 20$ for $\frac{\partial \bar{f}}{\partial \eta}$

Figure 4.38: Error distribution over physical element for polynomial order, $p = 20$

4.5. Application towards stress tensors

Thus far, we have seen the application of the covariant exterior derivatives over the field of 0-forms (scalars) and 1-forms (co-vectors). Applications to continuum mechanics however, requires a broader integration of this covariant derivative approach to include stress tensors. Consider for example, the stress tensor τ defined in the reference Cartesian coordinates as:

$$\underline{\tau}(\xi, \eta) = d\xi \otimes (\tau_{\xi\xi}d\eta - \tau_{\eta\xi}d\xi) + d\eta \otimes (\tau_{\xi\eta}d\eta - \tau_{\eta\eta}d\xi)$$

It can be shown that the commutativity of the exterior covariant derivative approach shown previously can be extended to the divergence of this stress tensor, in any other transformation (calculation for the divergence of the stress tensor is shown in Appendix A). Similar derivations for other differential operators require considerations of symmetry and enforcing of conservation properties. For instance, Fisser [29] proposed a new linear elasticity formulation using mixed mimetic methods, wherein the stresses make use of the mixed mimetic formulation and occupy the same polynomial spaces (for the same order of dual and primal polynomials, for example the primal nodal and the algebraic dual of an nodal polynomial) and thus, can be set equal to one another. This allows for strong conservation of symmetry (required for angular momentum) alongside mass and linear momentum conservation [29, p. 69].

Note however, that another key consideration with Fisser' work (this research belonging to the same class of methods) makes use of co-vector valued stress tensor instead of a traditional notion of vector-valued stress tensors. Which is why the commutative nature of the covariant exterior derivative becomes more relevant as it has been shown to be applicable to 0-forms and 1-forms (for 2-D) and is mathematically expected to scale upto n-dimensional spaces and their respective (n-1) forms as well.

Conclusions and Future Scope

5.1. Summary of Work Done

The current research presents a mimetic spectral implementation that enables covariant discretization of covector-valued fields over curvilinear geometry. The underlying principle enabling this exercise was the formulation of the discrete field using mixed mimetic spectral basis functions, that is using primal and algebraic dual functions in the reduction-reconstruction cycle as shown in chapter 3. Further an application of boundary value substitution using the metric-independent mimetic approach is seen through the use of topological operators such as the incidence and inclusion matrices.

Furthermore, the use of connection coefficients for Levi-Civita connections, that is the Christoffel symbols, are bypassed through the use of covariant exterior derivatives, where the principal of invariance under the general coordinate transformation is used. Using this covariant derivative, we are able to discretize scalar, co-vector and potentially, tensor fields over curved geometries by defining a diffeomorphism to an orthogonal reference frame where the mixed spectral implementation is used. The application of the exterior derivative proves commutative with respect to the transformation.

Case studies of this curvature-compatible mixed mimetic method are presented using two analytical examples of scalar and co-vector fields, and later with potential flow applications for constant line source and line vortex flows. The transformation for analytical scalar and co-vector fields was realized over a physical domain that modeled a horizontally sheared domain with non-linear skew, the second transformation case (for potential flows) made use of a modified polar coordinate transformation.

Finally, a qualitative overview is provided that outlines extension of this method towards a new mixed mimetic formulation of elasticity, building on the concept of a covariant elasticity, that admits into itself strong conservation of mass, linear momentum and angular momentum. This discussion however, remains qualitative and is not addressed fully in the current scope.

5.2. Conclusions

This work aimed at implementing a curvature compatible discretization scheme using mixed mimetic methods using covariant exterior derivatives. The traditional change of frame requires the use of connections to redefine the new differential forms and over the transformed manifold, however, through the use of covariant derivatives, we are able to bypass the computation of these connection coefficients and are able to compute the transformed differential forms (in this case 0-forms and 1-forms) over curved domains.

5.3. Future Scope of Research

The current scope of work is very limited since an implementation of the mixed mimetic methods should be extended first to a multi-element setting wherefore, it becomes possible to observe better approximation and convergence behavior. This multi-element implementation would then serve as a template to implementing a novel linear elasticity formulation that allows

for strong conservation of mass, linear and angular momentum. Thus, a broader application of mimetic methods towards continuum mechanics becomes possible. The use of Lagrangian approach of studying flow invariance becomes possible with time-dependent problems when this approach is used within the mixed mimetic space-time integration algorithm.

Appendices

A

Covariant Divergence of Stress Tensor

Consider the mapping described in the equation 4.12, between the reference Cartesian frame (ξ, η) and the physical deformed domain (x, y) . We may write, the stress tensor as:

$$\underline{\underline{\tau}}(\xi, \eta) = d\xi \otimes (\tau_{\xi\xi} d\eta - \tau_{\eta\xi} d\xi) + d\eta \otimes (\tau_{\xi\eta} d\eta - \tau_{\eta\eta} d\xi)$$

upon transformation of co-vectors to the physical domain (x, y) , we get:

$$\begin{aligned} \underline{\underline{\tau}}(x, y) &= -d\mathbf{x} \otimes \tau_{\eta, \xi} d\mathbf{x} \\ &\quad + d\mathbf{y} \otimes [0.1(1+y)\tau_{\eta\xi} - \tau_{\eta\eta}] d\mathbf{x} \\ &\quad + d\mathbf{x} \otimes [\tau_{\xi\xi} + 0.1(1+y)\tau_{\eta, \xi}] d\mathbf{y} \\ &\quad + d\mathbf{y} \otimes [\tau_{\xi\eta} + 0.1(1+y)\tau_{\eta\eta} + \tau_{\xi\xi} + 0.1(1+y)\tau_{\eta\xi}] d\mathbf{y} \end{aligned}$$

which allows us to write:

$$\underline{\underline{\tau}}(x, y) = d\mathbf{x} \otimes (\tau_{xx} d\mathbf{y} - \tau_{yx} d\mathbf{x}) + d\mathbf{y} \otimes (\tau_{xy} d\mathbf{y} - \tau_{yy} d\mathbf{x})$$

where, we write:

$$\begin{aligned} \tau_{xx} &= 0.1(1+y)\tau_{\eta, \xi} - \tau_{\xi\xi} \\ \tau_{yx} &= \tau_{\eta\xi} \\ \tau_{xy} &= [\tau_{\xi\eta} + 0.1(1+y)\tau_{\eta\eta} - 0.1(1+y)\tau_{\xi\xi} + 0.01(1+y)^2\tau_{\eta\xi}] \\ \tau_{yy} &= 0.1(1+y)\tau_{\eta\xi} - \tau_{\eta\eta} \end{aligned}$$

The divergence of this stress tensor in both the frames is now computed. In the reference domain, we write:

$$\nabla \cdot \underline{\underline{\tau}}(\xi, \eta) = d\xi \otimes \left(\frac{\partial \tau_{\xi\xi}}{\partial \xi} + \frac{\partial \tau_{\eta\xi}}{\partial \eta} \right) d\xi d\eta + d\eta \otimes \left(\frac{\partial \tau_{\xi\eta}}{\partial \xi} + \frac{\partial \tau_{\eta\eta}}{\partial \eta} \right) d\xi d\eta$$

upon transformation of the second leg into the physical domain, we obtain,

$$\begin{aligned} \nabla \cdot \underline{\underline{\tau}}_{\phi_k \circ}(\xi, \eta) &= d\xi \otimes \left(\frac{\partial \tau_{\xi\xi}}{\partial x} + 0.1(1+y) \frac{\partial \tau_{\xi\xi}}{\partial y} + \frac{\partial \tau_{\eta\xi}}{\partial y} \right) d\mathbf{x} d\mathbf{y} \\ &\quad + d\eta \otimes \left\{ \frac{\partial \tau_{\xi\eta}}{\partial x} + [1 + 0.1(1+y)] \left[\frac{\partial \tau_{\eta\eta}}{\partial x} + \frac{\partial \tau_{\xi\xi}}{\partial x} + 0.1(1+y) \frac{\partial \tau_{\eta, \xi}}{\partial x} \right] \right\} d\mathbf{x} d\mathbf{y} \end{aligned}$$

the first leg, when transformed, now gives:

$$\begin{aligned} \nabla \cdot \underline{\underline{\tau}}[\phi_k \circ(\xi, \eta)] &= d\mathbf{x} \otimes \left(-\frac{\partial \tau_{\xi\xi}}{\partial x} + 0.1(1+y) \frac{\partial \tau_{\eta\xi}}{\partial x} + \frac{\partial \tau_{\eta\xi}}{\partial y} \right) d\mathbf{x} d\mathbf{y} \\ &\quad + d\mathbf{y} \otimes \left(-\frac{\partial \tau_{\eta\eta}}{\partial y} + 0.1(1+y) \frac{\partial \tau_{\eta, \xi}}{\partial y} - 0.1\tau_{\eta\xi} \right) d\mathbf{x} d\mathbf{y} \\ &\quad + d\mathbf{y} \otimes \left(-\frac{\partial \tau_{\eta\eta}}{\partial y} + 0.1(1+y) \frac{\partial \tau_{\eta, \xi}}{\partial y} - 0.1\tau_{\eta\xi} \right) d\mathbf{x} d\mathbf{y} \end{aligned}$$

$$\begin{aligned}
\nabla \cdot \underline{\underline{\tau}} [\varphi_k \circ (\xi, \eta)] &= \mathbf{dx} \otimes \left(\frac{\partial}{\partial x} [0.1(1+y)\tau_{\eta\xi} - \tau_{\xi\xi}] + \frac{\partial \tau_{\eta\xi}}{\partial y} \right) \mathbf{dx dy} \\
&+ \mathbf{dy} \otimes \left(\frac{\partial}{\partial x} [\tau_{\xi\eta} + 0.1(1+y)\tau_{\eta\eta} - 0.1(1+y)\tau_{\xi\xi} + 0.01(1+y)^2\tau_{\eta\xi}] \right) \mathbf{dx dy} \\
&+ \mathbf{dy} \otimes \left(\frac{\partial}{\partial y} [0.1(1+y)\tau_{\eta\xi} - \tau_{\eta\eta}] - 0.1\tau_{\eta\xi} \right) \mathbf{dx dy}
\end{aligned}$$

where, we may now write:

$$\nabla \cdot \underline{\underline{\tau}} [\varphi_k \circ (\xi, \eta)] = \mathbf{dx} \otimes \left(\frac{\partial \tau_{xx}}{\partial x} + \frac{\partial \tau_{yx}}{\partial y} \right) \mathbf{dx dy} + \mathbf{dy} \otimes \left(\frac{\partial \tau_{xy}}{\partial x} + \frac{\partial \tau_{yy}}{\partial y} - 0.1\tau_{\eta\xi} \right) \mathbf{dx dy}$$

Note that this description differs from that of the divergence in the physical domain, which is given as:

$$\nabla \cdot \underline{\underline{\tau}} (x, y) = \mathbf{dx} \otimes \left(\frac{\partial \tau_{xx}}{\partial x} + \frac{\partial \tau_{yx}}{\partial y} \right) \mathbf{dx dy} + \mathbf{dy} \otimes \left(\frac{\partial \tau_{xy}}{\partial x} + \frac{\partial \tau_{yy}}{\partial y} \right) \mathbf{dx dy}$$

This difference occurs due to the non-commutative nature of the regular exterior derivative, that does not take into account the connection coefficients. The exterior covariant derivative on the other hand is given as:

$$\nabla \cdot \underline{\underline{\tau}} (x, y) = \mathbf{dx} \otimes [d\tau_x - \omega_x^i \wedge \tau_i] \mathbf{dx dy} + \mathbf{dy} \otimes [d\tau_y - \omega_y^i \wedge \tau_i] \mathbf{dx dy}$$

where, τ_x and τ_y are the (n-1) forms described as $(\tau_{xx}\mathbf{dy} - \tau_{yx}\mathbf{dx})$ and $(\tau_{xy}\mathbf{dy} - \tau_{yy}\mathbf{dx})$ respectively. Recall from Equation 4.17, the connection coefficients are defined as:

$$\omega' = P^{-1}dP = \begin{pmatrix} 0 & 0.1 \mathbf{dy} \\ 0 & 0 \end{pmatrix}$$

using these results, we may write:

$$\begin{aligned}
\omega_x^i \wedge \tau_i &= \omega_x^x \wedge (\tau_{xx}\mathbf{dy} - \tau_{yx}\mathbf{dx}) + \omega_x^y (\tau_{xy}\mathbf{dy} - \tau_{yy}\mathbf{dx}) = 0 \\
\omega_y^i \wedge \tau_i &= \omega_y^x \wedge (\tau_{xx}\mathbf{dy} - \tau_{yx}\mathbf{dx}) + \omega_y^y (\tau_{xy}\mathbf{dy} - \tau_{yy}\mathbf{dx}) = 0.1\mathbf{dy} \wedge (\tau_{xy}\mathbf{dy} - \tau_{yy}\mathbf{dx}) = -0.1\tau_{yy}\mathbf{dy} \wedge \mathbf{dx}
\end{aligned}$$

Thus, we see that the covariant exterior derivative equals the transformed value of the divergence of the reference stress tensor, $\nabla \cdot \underline{\underline{\tau}} [\varphi_k \circ (\xi, \eta)]$.

Bibliography

- [1] Akio Arakawa. Computational design for long-term numerical integration of the equations of fluid motion: Two-dimensional incompressible flow. part i. *Journal of computational physics*, 1(1):119–143, 1966.
- [2] Douglas N Arnold, Richard S Falk, and Ragnar Winther. Finite element exterior calculus, homological techniques, and applications. *Acta numerica*, 15:1–155, 2006.
- [3] Douglas N Arnold, Pavel B Bochev, Richard B Lehoucq, Roy A Nicolaides, and Mikhail Shashkov. *Compatible spatial discretizations*, volume 142. Springer Science & Business Media, 2007.
- [4] Vladimir I Arnold and Boris A Khesin. *Topological methods in hydrodynamics*, volume 125. Springer Science & Business Media, 1999.
- [5] Ivo Babuška. The finite element method with lagrangian multipliers. *Numerische Mathematik*, 20(3):179–192, 1973.
- [6] John Baez and Javier P Muniain. *Gauge fields, knots and gravity*, volume 4. World Scientific Publishing Company, 1994.
- [7] Markus Berndt, Konstantin Lipnikov, David Moulton, and Mikhail Shashkov. Convergence of mimetic finite difference discretizations of the diffusion equation. *Journal of Numerical Mathematics*, 9(4):265–284, 2001.
- [8] Markus Berndt, Konstantin Lipnikov, Mikhail Shashkov, Mary F Wheeler, and Ivan Yotov. A mortar mimetic finite difference method on non-matching grids. *Numerische Mathematik*, 102(2):203–230, 2005.
- [9] Markus Berndt, Konstantin Lipnikov, MIKHAIL Shashkov, Mary F Wheeler, and Ivan Yotov. Superconvergence of the velocity in mimetic finite difference methods on quadrilaterals. *SIAM Journal on Numerical Analysis*, 43(4):1728–1749, 2005.
- [10] Alain Bossavit. Mixed finite elements and the complex of whitney forms. *The mathematics of finite elements and applications VI*, pages 137–144, 1988.
- [11] Alain Bossavit. Whitney forms: A class of finite elements for three-dimensional computations in electromagnetism. *IEE Proceedings A (Physical Science, Measurement and Instrumentation, Management and Education, Reviews)*, 135(8):493–500, 1988.
- [12] Alain Bossavit. Differential forms and the computation of fields and forces in electromagnetism. *Eur. J. Mech. B*, 10(5):474–488, 1991.
- [13] Alain Bossavit. *Computational electromagnetism: variational formulations, complementarity, edge elements*. Academic Press, 1998.
- [14] Alain Bossavit. On the geometry of electromagnetism. *J. Japan Soc. Appl. Electromagn. & Mech.*, 6:17–28, 1998.

-
- [15] F Brezzi, D Boffi, L Demkowicz, RG Durán, RS Falk, and M Fortin. *Mixed finite elements, compatibility conditions, and applications*. Springer, 2008.
- [16] Franco Brezzi. On the existence, uniqueness and approximation of saddle-point problems arising from lagrangian multipliers. *Publications mathématiques et informatique de Rennes*, (S4):1–26, 1974.
- [17] Franco Brezzi and Michel Fortin. *Mixed and hybrid finite element methods*, volume 15. Springer Science & Business Media, 2012.
- [18] William L Burke. *Applied differential geometry*. Cambridge University Press, 1985.
- [19] Richard Courant et al. *Variational methods for the solution of problems of equilibrium and vibrations*. Verlag nicht ermittelbar, 1943.
- [20] Michel Crouzeix and P-A Raviart. Conforming and nonconforming finite element methods for solving the stationary stokes equations i. *Revue française d'automatique informatique recherche opérationnelle. Mathématique*, 7(R3):33–75, 1973.
- [21] Mathieu Desbrun, Anil N Hirani, Melvin Leok, and Jerrold E Marsden. Discrete exterior calculus. *arXiv preprint math/0508341*, 2005.
- [22] AA Dezin. Method of orthogonal expansions. *Siberian Mathematical Journal*, 9(5):788–797, 1968.
- [23] AA Dezin. Some models related to the euler equations. *Differ. Equ*, 6(1):12–20, 1970.
- [24] AA Dezin. Combination model of euclidean space and difference operators. *Siberian Mathematical Journal*, 16(4):536–545, 1975.
- [25] Aleksei Alekseevich Dezin. Natural differential operators and the separation of variables. *Differentsial'nye Uravneniya*, 9(1):25–31, 1973.
- [26] Richard S Falk and John E Osborn. Error estimates for mixed methods. *RAIRO. Analyse numérique*, 14(3):249–277, 1980.
- [27] A Favorskii, M Shashkov, and V Tishkin. The usage of topological methods in the discrete models construction. *Preprint Keldysh Institute of Applied Mathematics of the USSR Academy of Sciences*, 96, 1983.
- [28] Desmond Fearnley-Sander. Hermann grassmann and the creation of linear algebra. *The American Mathematical Monthly*, 86(10):809–817, 1979.
- [29] Joël Fisser. Advancing the mimetic spectral element method: Towards continuum mechanics applications. 2019.
- [30] Harley Flanders. *Differential Forms with Applications to the Physical Sciences by Harley Flanders*, volume 11. Elsevier, 1963.
- [31] Michel Fortin. An analysis of the convergence of mixed finite element methods. *RAIRO. Analyse numérique*, 11(4):341–354, 1977.
- [32] Theodore Frankel. *The geometry of physics: an introduction*. Cambridge university press, 2011.

- [33] M Maurice Fréchet. Sur quelques points du calcul fonctionnel. *Rendiconti del Circolo Matematico di Palermo (1884-1940)*, 22(1):1–72, 1906.
- [34] Marc Gerritsma. An introduction to a compatible spectral discretization method. *Mechanics of Advanced Materials and Structures*, 19(1-3):48–67, 2012.
- [35] Marc Gerritsma, Varun Jain, Yi Zhang, and Artur Palha. Algebraic dual polynomials for the equivalence of curl-curl problems. *arXiv preprint arXiv:1805.00114*, 2018.
- [36] Ralf Hiptmair. Higher order whitney forms. *Progress in Electromagnetics Research*, 32:271–299, 2001.
- [37] Alexander Hrennikoff. Solution of problems of elasticity by the framework method. *J. appl. Mech.*, 1941.
- [38] James Hyman, Mikhail Shashkov, and Stanly Steinberg. The effect of inner products for discrete vector fields on the accuracy of mimetic finite difference methods. *Computers & Mathematics with Applications*, 42(12):1527–1547, 2001.
- [39] James M Hyman and Mikhail Shashkov. Adjoint operators for the natural discretizations of the divergence, gradient and curl on logically rectangular grids. *Applied Numerical Mathematics*, 25(4):413–442, 1997.
- [40] James M Hyman and Mikhail Shashkov. Natural discretizations for the divergence, gradient, and curl on logically rectangular grids. *Computers & Mathematics with Applications*, 33(4):81–104, 1997.
- [41] James M Hyman and Mikhail Shashkov. Approximation of boundary conditions for mimetic finite-difference methods. *Computers & Mathematics with Applications*, 36(5):79–99, 1998.
- [42] James M Hyman and Mikhail Shashkov. Mimetic discretizations for maxwell’s equations. *Journal of Computational Physics*, 151(2):881–909, 1999.
- [43] James M Hyman and Mikhail Shashkov. Mimetic finite difference methods for maxwell’s equations and the equations of magnetic diffusion. *Progress in Electromagnetics Research*, 32:89–121, 2001.
- [44] James M Hyman and Stanly Steinberg. The convergence of mimetic discretization for rough grids. *Computers & Mathematics with Applications*, 47(10-11):1565–1610, 2004.
- [45] Varun Jain, Yi Zhang, Artur Palha, and Marc Gerritsma. Construction and application of algebraic dual polynomial representations for finite element methods on quadrilateral and hexahedral meshes. *arXiv preprint arXiv:1712.09472*, 2017.
- [46] Varun Jain, Yi Zhang, Joël Fisser, Artur Palha, and Marc Gerritsma. A conservative hybrid method for darcy flow. *arXiv preprint arXiv:1904.11909*, 2019.
- [47] Eva Kanso, Marino Arroyo, Yiyong Tong, Arash Yavari, Jerrold G Marsden, and Mathieu Desbrun. On the geometric character of stress in continuum mechanics. *Zeitschrift für angewandte Mathematik und Physik*, 58(5):843–856, 2007.
- [48] Jasper Kreeft and Marc Gerritsma. Mixed mimetic spectral element method for stokes flow: A pointwise divergence-free solution. *Journal of Computational Physics*, 240:284–309, 2013.

- [49] Jasper Jonas Kreeft. *Mimetic spectral element method: a discretization of geometry and physics*. PhD thesis, Delft University of Technology, The Netherlands, 2013.
- [50] Aleksandr L'vovich Krylov. Difference approximation to differential operators of mathematical physics. In *Doklady Akademii Nauk*, volume 178, pages 535–538. Russian Academy of Sciences, 1968.
- [51] Yu Kuznetsov and S Repin. New mixed finite element method on polygonal and polyhedral meshes. *Russian Journal of Numerical Analysis and Mathematical Modelling rnam*, 18(3):261–278, 2003.
- [52] Yu Kuznetsov and S Repin. Convergence analysis and error estimates for mixed finite element method on distorted meshes. *Journal of Numerical Mathematics jnma*, 13(1):33–51, 2005.
- [53] Yuri Kuznetsov, Konstantin Lipnikov, and Mikhail Shashkov. The mimetic finite difference method on polygonal meshes for diffusion-type problems. *Computational Geosciences*, 8(4):301–324, 2004.
- [54] Vyacheslav Ivanovich Lebedev. Method of orthogonal projections for a finite difference analogue of a system of equations. In *Doklady Akademii Nauk*, volume 113, pages 1206–1209. Russian Academy of Sciences, 1957.
- [55] Vyacheslav Ivanovich Lebedev. Difference analogues of orthogonal decompositions, basic differential operators and some boundary problems of mathematical physics. i. *USSR Computational Mathematics and Mathematical Physics*, 4(3):69–92, 1964.
- [56] Vyacheslav Ivanovich Lebedev. Difference analogues of orthogonal decompositions, basic differential operators and some boundary problems of mathematical physics. ii. *USSR Computational Mathematics and Mathematical Physics*, 4(4):36–50, 1964.
- [57] John M Lee. Smooth manifolds. In *Introduction to Smooth Manifolds*, pages 1–31. Springer, 2013.
- [58] Zhen Lei and Thomas Y Hou. On the stabilizing effect of convection in three-dimensional incompressible flows. *Communications on Pure and Applied Mathematics: A Journal Issued by the Courant Institute of Mathematical Sciences*, 62(4):501–564, 2009.
- [59] Konstantin Lipnikov, Gianmarco Manzini, and Mikhail Shashkov. Mimetic finite difference method. *Journal of Computational Physics*, 257:1163–1227, 2014.
- [60] Louis Melville Milne-Thomson. *Theoretical aerodynamics*. Courier Corporation, 1973.
- [61] Brian J Moritz. Vector difference calculus. 2001.
- [62] Roy A Nicolaides and Kathryn A Trapp. Covolume discretization of differential forms. In *Compatible spatial discretizations*, pages 161–171. Springer, 2006.
- [63] Dmitry Pavlov, Patrick Mullen, Yiyang Tong, Eva Kanso, Jerrold E Marsden, and Mathieu Desbrun. Structure-preserving discretization of incompressible fluids. *Physica D: Nonlinear Phenomena*, 240(6):443–458, 2011.
- [64] Giuseppe Peano. *Calcolo geometrico secondo l'Ausdehnungslehre di H. Grassmann*. Bocca, 1888.

-
- [65] Norman A Phillips. An example of non-linear computational instability. *The atmosphere and the sea in motion*, 501:504, 1959.
- [66] Henri Poincaré. *Analysis situs*. Gauthier-Villars, 1895.
- [67] W Schwalm, B Moritz, M Giona, and M Schwalm. Vector difference calculus for physical lattice models. *Physical Review E*, 59(1):1217, 1999.
- [68] Andrej N Tikhonov and Aleksandr A Samarskii. Homogeneous difference schemes. *USSR Computational Mathematics and Mathematical Physics*, 1(1):5–67, 1962.
- [69] Enzo Tonti. *On the formal structure of physical theories*. Istituto di matematica del Politecnico di Milano, 1975.
- [70] Enzo Tonti. The reason for analogies between physical theories. *Applied Mathematical Modelling*, 1(1):37–50, 1976.
- [71] Enzo Tonti. The reason of the analogies in physics. 1977.
- [72] Hassler Whitney. *Geometric integration theory*. Courier Corporation, 2012.
- [73] Arash Yavari. On geometric discretization of elasticity. *Journal of Mathematical Physics*, 49(2):022901, 2008.